12-9-2011 12:00 AM

Quantum Coherence and Interference in Metallic Photonic Crystals and Hybrid Systems

Ali Hatef, *The University of Western Ontario*

Supervisor: Prof. Mahi Singh, *The University of Western Ontario*

A thesis submitted in partial fulfillment of the requirements for the Doctor of Philosophy degree in Physics

Recommended Citation

Hatef, Ali, "Quantum Coherence and Interference in Metallic Photonic Crystals and Hybrid Systems" (2011). *Electronic Thesis and Dissertation Repository*. 358.
https://ir.lib.uwo.ca/etd/358

Quantum Coherence and Interference in Metallic Photonic Crystals and Hybrid Systems

(Spine title: Quantum Coherence and Interference in MPCs and Hybrid Systems)

(Thesis format: Monograph)

by

A. Hatef

Graduate Program in Physics

A thesis submitted in partial fulfillment
of the requirements for the degree of
Doctor of Philosophy

The School of Graduate and Postdoctoral Studies
The University of Western Ontario
London, Ontario, Canada

THE UNIVERSITY OF WESTERN ONTARIO
School of Graduate and Postdoctoral Studies

CERTIFICATE OF EXAMINATION

Supervisor	Examiners
Dr. Mahi R. Singh	Dr. Silvia Mittler
Supervisory Committee	Dr. Lyudmila Goncharova
Dr. Silvia Mittler	Dr. John F. Corrigan
Dr. Michael G. Cottam	Dr. Xun Li

The thesis by

Ali Hatef

entitled:

Quantum Coherence and Interference in Metallic Photonic Crystal and Hybrid Systems

is accepted in partial fulfillment of the
requirements for the degree of
Doctor of Philosophy

Date	Chair of the Thesis Examination Board

Abstract

Quantum Coherence and Interference in Metallic Photonic Crystals Hybrid Systems

by

A. Hatef

Department of Physics and Astronomy

The University of Western Ontario

In this thesis, we study the absorption coefficient of quantum dots doped in metallic photonic crystals under different circumferences. The quantum dots are considered as an ensemble of three-level energy systems, containing two excited states and a ground state.

We study numerically the temporal evolution of the absorption coefficient profile where a probe field is applied to monitor the absorption process in two cases, when quantum dots are embedded lightly and densely. It is found that the absorption profile shows more oscillations and system goes towards the transparent state.

We also studied the effect of a changing plasma frequency on the absorption profile of quantum dots two possible field configurations. In the first configuration, a single probe field couples with the ground state and the two excited states. In this case it is found that the position of the transparent peak is moved, due to a slight change in the plasma energy. This means that the transparent state becomes an absorbing state. In the second configuration, a pump field couples with only one excited state, while the probe field couples to the other. In this case, we found that a peak in the absorption profile appears due to plasmon coupling, and this peak splits into two peaks when the plasma energy is decreased. This change in plasma energy can also take the system from the absorption region to the gain region.

We developed an analytical theory for the photonic band structure and density of states of two-dimensional rectangular metallic photonic crystals. We found that the location of the photonic band gap can be controlled by modifying the plasma energy of either metal. We showed that by changing the plasma energy one can control the spontaneous emission in the metallic photonic crystal.

Finally, I studied hybrid systems (quantum dot - metallic nanoparticle). In such hybrid systems, it is possible to control spontaneous emission in the semiconductor nanocrystals. Significant applications of this include the development of chemical and biological nanosensors, electrical DNA switches, and nanoscale devices as biosensors. The main advantage of hybrid systems when compared with other nano-optical systems is the possibility for direct energy and quantum information transfer between nanoparticles. In this project, we investigate the control of thermal energy loss in metallic nanoparticles, an effect which could destroy the quality of transformed information if not properly controlled.

Keywords

Quantum dot, quantum coherence, quantum interference, metallic photonic crystals, plasma frequency, dipole-dipole interaction, hybrid systems, metallic nanoparticles, plasmonic.

To My Beloved Wife

Acknowledgments

I would like to express my deeply-felt thanks to my supervisor, Prof. Mahi R. Singh whose expertise, understanding, and patience, added considerably to my graduate experience. With his enthusiasm, his inspiration, and his great efforts to explain things clearly and simply, he helped to make my research very smooth. Throughout my thesis-writing period, he provided encouragement, sound advice, good teaching, good company, and lots of good ideas. I would have been lost without him.

I want to thank my beloved wife Raziyeh. The encouragement and support from her was a powerful source of inspiration and energy.

I am deeply indebted to my fellow PhD student Joel D. Cox for helpful discussions and for proofreading the thesis.

Finally, I’d like to thank Nicole Bindseil, for final proofreading my thesis.

List of Abbreviations

PC	Photonic crystals
MPC	Metallic photonic crystal
HSQ	Hydrogen silsesquioxane
DDI	Dipole-dipole interaction
RWA	Rotating wave approximations
PWM	Plane wave method
TMM	Transfer matrix method
FDTD	Finite difference time domain method
EP	Electron photon
EM	Electro magnetic
TE	Transverse electric
PBG	Photonic band gap
QD	Quantum dot
MP	Metallic particle
EIT	Exciton induced transparency

Contents

List of Figures

List of Tables

Chapter 1

Introduction

1.1 Metallic Photonic Crystal

In the past few decades there has been a growing interest in the development of artificial nanoscale materials. With unique properties, photonic crystals (PCs) are one of the noteworthy categories of these synthetically produced materials. PCs are optical nanomaterial structures characterized by their periodically modulating dielectric constant, which may vary in one, two or three spatial dimensions. Due to multiple reflections at the interfaces between regions with different dielectric constants in the structure, electromagnetic waves of a certain frequency range cannot propagate through a photonic crystal; this range of frequencies is referred to as the photonic band gap. Generally, the wavelengths of light which fall within the photonic band gap are on the order of the crystal's lattice constant, while the width of the photonic band gap is proportional to the crystal's dielectric contrast.

The photonic band gap of a one-dimensional photonic crystal, which is fabricated by depositing two dielectric materials in alternating layers, lies in only one direction, whereas for a two- or three-dimensional photonic crystal photonic band gap varies for different photon propagation directions. The existence of the photonic band gap has inspired the design of various nano-optical and optoelectronic devices [1]. The photonic band gap controls the propagation of electromagnetic waves in PCs in the same manner that the electronic band gap controls electrons in semiconductors.

It is well-known that in a dielectric photonic crystal, high dielectric contrast is required to have a complete photonic band gap [2][3][4]. For example, inverse opal photonic crystals made from ordinary dielectric materials require that the contrast be greater than eight to have a complete photonic band gap in the optical regime [5].

In terms of fabrication, this restriction causes a great deal of difficulty. To exhibit a noticeable photonic band gap with fewer periodicities it is much better to use impenetrable materials. When comparing ordinary dielectric or semiconducting materials for selection, metals are one of the best options due to their large refractive index and high reflectivity over a broad range of frequencies. Therefore, these nanoscale metal-based structures are more likely to possess a complete photonic band gap than their dielectric counterparts [6][7][8].

Recently, intensive experimental and theoretical research has been done on metallic photonic crystals (MPCs) and metallo-dielectric photonic crystals due to their ability of controlling electronic and photonic resonances simultaneously [9][10]. Furthermore, this photonic band gap will be effective for crystals with fewer lattice periods, even if the total thickness of metal in the MPC is hundreds of skin depths in length [11] [12]. The photonic band gap that is formed by a MPC is the result of a combination of plasma screening effects and Brag scattering. On the other hand, photons interact much more strongly with metals than dielectrics, making MPCs more useful for developing integrated photonic devices. Devices may be designed with fewer lattice constants, making elements simpler to fabricate and easier to pack densely. Such structures may also present further remarkable possibilities for investigating light-matter interactions [13][14]. MPCs also have many applications in the field of telecommunications, as antennas [15] , all-optical switches [16] , biosensors [17] and solar cells[18].

MPCs can also provide strong simultaneous coupling between electronic and photonic resonances in the same range of the frequencies, which gives them interesting optical properties [19], and can lead to well-pronounced spectral features [9][19]. One of the promising features of MPCs is their capability of tailoring thermal emission spectra. Theoretical analysis has shown that the existence of the photonic band gap and modification of the photon density of states in these structures can lead to significant enhancement and suppression of thermal radiation near and within the photonic band gap, respectively[20][21][22][23].

Initially, studies on MPCs were focused within the range of microwave and far-infrared frequencies, owing to the fact that the metallic layers are strong reflectors in these frequency ranges

[6][24][25], however, due to the improvement in micro-fabrication techniques, several samples of MPCs that operate in the visible or near-infrared frequency range have been fabricated. These MPCs may consist of silver, nickel, copper, etc., despite the fact that these metals are dispersive and absorptive in these frequency ranges [14][8][26][27].

The following provide several theoretical and experimental examples of novel achievements regarding MPC.

Scalora *et al.* [11][28] have investigated numerically the transmission of light passing through a one-dimensional MPC composed of a stack of alternating layers of silver (metal) and MgF2 (dielectric component). Their results showed that the structure remains transparent over a tunable range of frequencies, including the ultraviolet, visible, and infrared.

Wang et al. [7] have theoretically studied the optical properties of a three-dimensional self-assembled MPC consisting of spherical metal nanoparticles. They showed the formation of photonic band gaps within the near-infrared to optical regime, even when absorption is taken into account, for silver spheres band-structure calculations.

Kuo et al. [26] fabricated opaline gold photonic crystals possessing complete photonic band gaps in the optical regime. Chang et al. [27] constructed a 5-layer modified-woodpile 3-D MPC structure composed of gold, immersed in a dielectric material known as hydrogen silsesquioxane (HSQ) that exhibits characteristics of a 3-D complete photonic band gap extending from near-infrared down to visible wavelengths at around 650 nm.

Yang et al. [14] have fabricated a 3-D all-copper photonic crystal with a feature size of 0.20 μm by using electron-beam lithography with the photoresist of hydrogen silsesquioxane (HSQ), which can open a photonic band edge located at a wavelength of around 0.80 μm in normal incidence.

1.2 Hybrid Quantum-Dot/Metal Nanoparticle System

In recent years, researchers have exploited the unique optical properties of metallic nanoparticles for a wide range of fundamental research such as nanoscale optical devices, biophotonics and biomedical applications [29][30]. Enhanced local fields in the vicinity of the metallic nanoparticle provide strong coupling to the neighboring particles such as semiconductor quantum dots, dye molecules, antibodies and human cells. Theses interesting properties arise from the coupling of the excitation of metallic nanoparticles (plasmon) and the excitation of semiconductor quantum dot (exciton). This coupling will enable us to probe and control the optical and thermal modification of these particles. One of the latest projects on this field is the study of the plasmonic induced transparency in the hybrid structures composed of semiconductor quantum dot and metallic nanoparticle [31][32]. In this case, the sharp optical response of the discrete excitons in semiconductor quantum dots coupled with the strong optical response of the plasmons in metallic nanoparticle (plasmonic resonance) will allow for the appearance of excitonic hybrid states and signatures for the optical response. The main objective of this study was to control the thermal energy absorption rate in metallic nanoparticles when they are in the vicinity of the semiconductor quantum dot. For example, the reduction of the thermal energy absorption rate in metallic nanoparticle controls the quality of the transmission of the energy and quantum information between nanoparticles [29][33]. In the case of biomedical application controlling the energy absorption by metallic nanoparticles in the biological media plays a key role in avoiding extreme heating which could lead to cell fragmentation and death [34].

1.3 Nanoparticles Embedded in Photonic Crystal

Recently, considerable effort has also been devoted to the investigation of the quantum optics of PCs and MPCs doped with a nano-sized active medium such as dye molecules, impurity atoms or quantum dots. According to Fermi's 'Golden Rule' the decay rate is proportional to the density of states which counts the number of electromagnetic modes available to the photons for emission into the environment. Therefore any modification in the density of states would lead to a change in the decay rate.

A photonic crystal can alter the density of states surrounding the active medium. It has been shown that the radiation behavior of an active medium can be drastically altered as the density of states in space changes. The inhibition, enhancement, and quantum interference effects of spontaneous emission from the quantum dots doped in 3D–PCs have been widely studied, both experimentally and theoretically [35][36][37][38][39].

Controlling spontaneous emission by using quantum optics would lead to several interesting effects, such as optical gain enhancement [40] and photoluminescence enhancement [41] , optical switching [42][43], quantum information processing [44][45] and electromagnetically induced transparency [46].

One of the other unique properties of photonic band gaps is that they can provide the means for strong confinements of light in PCs. The control of confined light can be achieved using photonic crystals possessing tunable photonic band gaps by applying a coherent control energy [47]. It is also possible to control the photonic band gaps of MPCs by changing the metallic dielectric function. For instance, the presence of a static magnetic field can greatly change the dielectric response of a free electron in the metal [48] or change the plasma energy by altering the surface charge density on each metallic particle [49][50].

Quantum interference in a three- or multi-level atomic system can arise from the superposition of spontaneous emissions when electron transitions take place between the upper and lower levels. Under certain circumstances the initially excited atomic system may not decay to its ground level due to a cancellation of spontaneous emission by quantum interference between atomic transition levels. The maximum value of quantum interference leads to dark states with zero absorption amplitude. This phenomenon causes the multi-level atomic system acts like a transparent medium, which has potential applications for optical switches and photonic devices [51][52]. Quantum interference of spontaneous emission can lead to many remarkable phenomena such as coherent population trapping [53], lasing without inversion [54], optical switches and photonic devices. [51][52].

1.4 Thesis Outline

The objective of the first four chapters of this thesis is to explore the optical response profile of an ensemble of nanoparticles which are doped in metallic photonic crystal (MPC). The novel research of this thesis is focused on controlling the absorption dynamics of these nanoparticles by modifying different parameters such as dipole-dipole interaction and the plasmon energy of the metal.

In chapter 2 we begin with a description of the basic physical and dynamic processes of the time evolution of the absorption coefficient of an ensemble of three-level nano-particles doped within metallic photonic crystals. These crystals are made from metallic spheres which are arranged equidistant and periodically in air. The refractive index of the metallic spheres depends on the plasma frequency. A probe field is applied to monitor the absorption process. The density matrix method has been used to calculate the steady state and transient behavior of the absorption coefficient in the system. We consider a situation where two absorbed photons interfere with each other (quantum interference). The following are two experimental possibilities which have been investigated.

In the first case, we consider that the concentration of the doped nanoparticles is very low so that they are not interacting with each other. It is found that when the resonance states lie away from the upper band edge of photonic band gap the system goes to transparent sate. It is also found when the difference between the electron resonance energy of the nanoparticle and the energy of the probe laser field (i.e. detuning parameter) is zero the system reaches to the steady state. However, when the parameter is not zero the absorption coefficient oscillates with time and then reaches the steady state.

In the second case, we consider the concentration of the dopant nanoparticles to be high and interacting with each other through the dipole-dipole interaction. Our calculations show that when the dipole-dipole interaction parameter increases the absorption shows an oscillatory behavior before reaching to the steady state. The number of oscillations and the required time to reach the steady state would also increase when increasing the dipole-dipole interaction parameter.

In chapter 3, we investigate the effect of plasma energy variation on the absorption coefficient profile in doped metallic photonic crystals. Two different field configurations are considered. In the first configuration a probe field couples the ground state and two closely excited states. Absorption occurs due to the transitions from ground state to the two excited states. It is found that the position of the transparent peak is moved due to the change of the plasma energy. In other words, changing the plasma energy causes the system to switch between a transparent and an absorbing state. The strong coupling between plasma and quantum dots is responsible for this phenomenon. In the second configuration the probe field couples only one excited state and the pump field couples the other excited state. The transition between excited states is dipole forbidden. We observed that the apparent peak in absorption profile splits into two peaks and the system also exhibits gain with inversion in response to the change of the plasma frequency resulting from the quantum interference and coherence. These are interesting results and can be used to make nano-scale plasma devices.

In chapter 4 we have developed an analytical theory for the photonic band structure and density of states of a two-dimensional metallic photonic crystal consisting of two different metallic pillars in an air background medium. Our calculations show that this structure forms a full two-dimensional photonic band gap when the appropriate size and type of metallic pillar are chosen. The advantage of using two metals is that the band structure and optical properties of these photonic crystals can be easily controlled by changing the plasma energies of two metals rather than one. We have chosen parameters for our metallic photonic crystal which present exact analytical expressions for the photonic dispersion relation. The analytical dispersion relation for the two-dimensional metallic photonic crystal is obtained using the transfer matrix method. From the dispersion relation we obtain the band structure, photonic density of states and the spontaneous decay rate. It is found that the density of states has singularities at energies near the edges of the photonic band gaps. Using the Schrödinger equation method and the photonic density of states, we calculated the linewidth broadening and the spectral function of radiation due to spontaneous emission for two-level quantum dots doped in the system. Our results show that by changing the plasma energies one can control spontaneous emission of quantum dots doped in the metallic photonic crystal.

Finally, in chapter 5 we investigate the exciton-induced transparency in hybrid systems (quantum-dot/metal nanoparticle) under different conditions. In this chapter the semiconductor quantum dot is considered as a three level quantized system when one of its excitonic transition energies matches with the plasmon resonance energy of the metallic nanoparticle. The hybrid system is drived by to probe and control field. We showed the behavior of the thermal energy absorption rate in metallic nanoparticles versus several variables such as the inter-particle distance, the metallic nanoparticle radius, the intensity of probe and the control field. In this project also for the first time, to our knowledge, we calculated the thermal energy absorption rate in metallic nanoparticles when the hybrid system is doped in an ordinary photonic crystal. We found several interesting results showing the capability of controlling the thermal energy absorption rate in metallic nanoparticles when the excitonic energy lies near the photonic crystal band gap.

Chapter 2

Time Evolution of Absorption Process

2.1 Introduction

In this chapter, we performed the numerical simulation to study the temporal evolution of the absorption coefficient of quantum dots doped in metallic photonic crystal (MPC)[1]. We assume that the MPC is made of metallic spheres embedded in air which acts as a reservoir. We consider the quantum dots are an ensemble of three-level systems with two upper excited states and one lower ground state where the resonant energies difference between states are small. This quantum dot configuration is called V configuration in quantum optics. A double quantum well system such as coupled GaAs /AlxGa1-xAs [55][56] can be motioned as a practical example of this configuration. The quantum interference is also considered in our calculations where the two decay pathways from the excited to the ground state are not independent.

To show the temporal evolution of the absorption process, we study a field configuration where the system is driven by a single probe laser field which is coupled with two transition energies simultaneously. This weak field facilitates the study of the absorption profile of the quantum dots.

---

[1] The work presented in this chapter has been published in:M. Singh and A. Hatef, "Time Evolution of Absorption Process in Nonlinear Metallic Photonic crystals", Phys. Status Solidi C 6, No. S1, S158–S161 (2009) and M. Singh and A. Hatef, "Quantum interference due to the spontaneous emission in nonlinear metallic photonic crystals" Microelectronics Journal 40, 854–856, (2009).

In our calculations two different cases are investigated. In the first case, we assume that the MPC is lightly doped and the concentration of quantum dots is low, therefore, the interactions between quantum dots are ignorable. In the second case, we consider a highly doped MPC where quantum dots interact with each other via dipole-dipole interaction.

The absorption coefficient is calculated using the density-matrix formalism. Interesting effects have been observed due to the quantum coherence and interference effects between two spontaneous emitted photons.

In the first case, where the dipole-dipole interaction is ignored, our results show that as the detuning of probe field increases the absorption profile exhibits an oscillatory behavior till reaches the steady state and the system goes towards the transparent state. In this case, we also see the same behavior for absorption profile when the resonant energy difference increases. In the second case, where the dipole-dipole interaction is taken into account, as the dipole-dipole interaction variable increases, the absorption profile again shows an oscillatory behavior till reaches the steady state and the system goes towards the transparent state. The number of oscillations and the required time to reach to the steady state also increases by increasing the dipole-dipole interaction variable.

2.2 Dispersion Relation in MPC

Photonic crystals (PCs) are periodic dielectric structures in which the refractive index varies periodically on a length scale of the order of the wavelength of light. In a PC, light of specific wavelengths is prohibited from propagating in certain directions. This effect is due to the influence of the Bragg diffraction when the reflected waves at each interface can destructively interfere. The behavior of light in PCs is similar to the behavior of electrons in an atomic structure. For this reason sometime the PCs are called semiconductor of light.

Depends on the application of PCs, different spatial periodic arrangements can be made in one-dimensional (1-D), two-dimensional (2-D) or three-dimensional (3-D) structures. Schematic representations of PCs in different dimensions are shown in Fig. 2-1.

One-dimensional PC, or the so called multilayer structure, consists of alternating layers of two materials with different refractive indices. As result the refractive index varies periodically

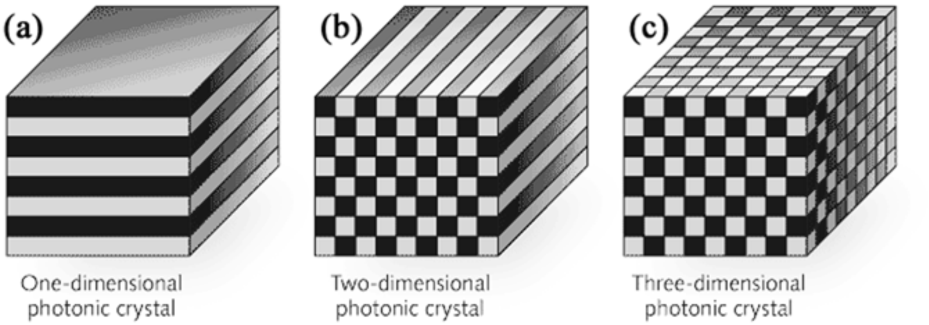

Figure 2-1: Example models for (a) a one-dimensional photonic crystal, (b) a two-dimensional photonic crystal and (c) a three-dimensional photonic crystal. In regions with dark colors, the index of refraction takes on different values

only in one-dimension.

In two-dimensional PC the refractive index alternates in two directions. In general, the 2-D photonic crystals can be made in two forms of hole-type and rod-type structures. The hole-type structures can be fabricated by drilling holes in a medium of high refractive index. These holes also can be filled by other materials with lower refractive index. On the other hand, the rod-type structures can be made by rods of high refractive index materials surrounded by a low refractive index. Both structures can have triangular or square symmetry.

Three-dimensional PCs are structures in which the refractive index varies in three dimensions. The fabrication of 3-D PCs is much more challenging task as compared to 1-D and 2-D PCs. Among different process of fabricating 3-D PCs, self-assembly process is a very promising approach. The 3-D PCs which are fabricated with this process are in the form of opal or inverse opal.

As motioned before in MPC the refractive index depends on the energy of the incident light beam. Drude model is one of the most common expression for refractive index function for metallic materials which offers an excellent fit to measured data over a wide energy ranges. This model has been used in almost all calculations related to MPCs. Using this model, the refractive index for a metallic material is expressed as[57]:

$$n_m(\varepsilon_k) = \sqrt{(1 - \frac{\varepsilon_p^2}{\varepsilon_k^2}) + \frac{\hbar\varepsilon_p^2}{\varepsilon_k^3\tau}i} \tag{2.1}$$

where ε_k, ε_p and τ are the energy of the incident electromagnetic wave, the plasma energy and the relaxation time of the conduction-band electrons, respectively. The plasma energy is defined by

$$\varepsilon_p^2 = \hbar^2 N e^2 / \epsilon_0 m_{eff} \tag{2.2}$$

where N is the electron density, m_{eff} is the effective mass of the electron, e is the electron charge and ϵ_0 is the permittivity of the free space.

Eqn. 2.1 shows that when the energy of the incident light approaches the plasma energy, the real part of the dielectric function becomes infinitesimally small. This would imply that regardless of the magnitude of the dielectric constant of the background medium, the contrast is large enough to meet the requirement for the creation of a complete photonic band gap. If we choose a proper metal which satisfies the $\varepsilon_k \tau / \hbar \gg 1$ for large values of ε_p (in the range of visible light), the imaginary part of the dielectric function becomes small, and therefore the absorption can be negligible. Among all metals, only silver, copper and gold meets this criterion, since they have plasma energies within the optical regime due to d-electron band resonance as well as relaxation times on the order of a few tens of femtoseconds [26].

The range of light energy can also be less than the plasma energy when the real part of the dielectric function becomes negative. In this case, the radius of the metallic spheres can be chosen close to or smaller than the relevant skin depth of the corresponding metal, so that an electromagnetic wave in the visible energy range can be transmitted by tunneling through the structure [11][6].

Fig. 2-2 shows the refractive index for different metals as a function of energy. When the energy of incident light is less than the plasma energy of the metal the refractive index is pure imaginary number (See Fig. 2-2a). On the other hand, for the energies greater the plasma energy the imaginary part vanishes and the refractive index becomes a real number (See Fig. 2-2b).

The relation between the photon energy ε_k and the wave vector k is called the dispersion relation (i.e. $\varepsilon_k = \varepsilon_k(k)$). The dispersion relation for a wave propagating within a homogeneous material is given by $\varepsilon_k = \hbar k v$, where k is the magnitude of the wave vector and v is the velocity of the wave. In the case of an electromagnetic wave propagating within a PC the dispersion

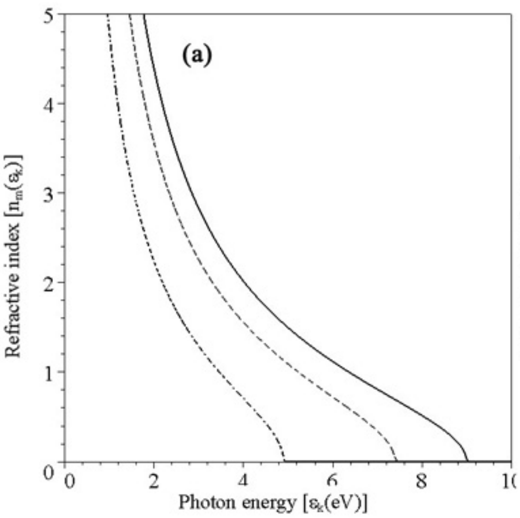

Figure 2-2: The refractive index of different metals versus photon energy ε_k . If photon energy is greater or less than the plasma energy the refractive index can be pure imaginary (a) or real (b). The solid line is for silver ($\varepsilon_p = 9$ eV), the dashed line is for copper ($\varepsilon_p = 7.4$ eV) and the dash-dot line is for nickel ($\varepsilon_p = 4.9$ eV).

relation can be calculated analytically or numerically depends on the PC configuration. In the case of an isotropic PC, the dispersion relation can be calculated by considering the Maxwell's and Bloch wave equations as following [58]:

$$\cos(kL) = F\left(\varepsilon_k\right) \tag{2.3}$$

where,

$$F\left(\varepsilon_k\right) = \sum_{\pm}\left[\pm\left(\frac{\left[n_m\left(\varepsilon_k\right) \pm n_b\right]^2}{4n_m\left(\varepsilon_k\right) n_b}\right)\cos\left(\frac{2\varepsilon_k\left[n_m\left(\varepsilon_k\right) r_s \pm n_b b\right]}{\hbar c}\right)\right] \tag{2.4}$$

in the above equations, $L = 2r_s + 2b$ is lattice constant, $2b$ is the spacing between the spheres and r_s are the radius of the metallic spheres , ε_k is the energy and k is the wave vector of the photons. $n_m\left(\varepsilon_k\right)$ and n_b are the refractive index of the metal spheres and background dielectric material, respectively. Note that background material can be considered as a dielectric material or air.

The graph of the dispersion relation (Eqn. 2.3) as a function of the wave vector k is called the band diagram or the band structure of the PC. Fig. 2-3 shows the band structure for

Metal	$\varepsilon_p\,(eV)$	$\varepsilon_l\,(eV)$	$\varepsilon_u\,(eV)$	$\Delta\varepsilon/\varepsilon_m\,(\%)$
Silver	9.0	1.8	2.5	32.5
Copper	7.4	1.5	2.0	28.6
Nickel	4.9	1.0	1.4	16.7

Table 2.1: The values of the plasma energy ε_p, the maximum energy of the lower energy band ε_l, the minimum energy of the upper energy band ε_u and Gap to mid-gap ratio $\Delta\varepsilon/\varepsilon_m$ for different types of metals.

an isotropic PC made by a periodic structure of metallic spheres embedded in a dielectric background ($n_b = 1.5$). The radius of the metallic spheres and lattice constant of the PC in reduced units are chosen as $r_s = 0.25\ \hbar c/\varepsilon_p$ and $L = 10.5\ \hbar c/\varepsilon_p$, respectively. In Fig. 2-3, the horizontal axis is shown in a unit of $\varepsilon_k/\varepsilon_p$, therefore, one can compare the photonic band structure of MPC made by different metals. In our calculation a band gap arises between point $\varepsilon_l/\varepsilon_p = 0.2$ and $\varepsilon_u/\varepsilon_p = 0.28$ which are the maximum normalized energy of the lower energy band and the minimum normalized energy of the upper energy band, respectively. The band gap implies an energy region where there is no allowed mode for light propagating along the k direction. Table 2.1 shows the plasma energy (ε_p), the maximum energy of the lower energy band (ε_u), the minimum energy of the upper energy band (ε_v) and gap to mid-gap ratio ($\Delta\varepsilon/\varepsilon_m = 2(\varepsilon_u - \varepsilon_l)/((\varepsilon_u + \varepsilon_l))$ for different type of metals. Note that the photonic band gap lies in the optical energy range, which shows that our theoretical model is in good agreement with recent experimental results [59][60].

2.3 Density of State and Decay Rate in MPC

In this chapter, we consider a metallic photonic crystal (MPC) doped with an ensemble of three-level quantum dots called V-configuration (See Fig. 2-5). These quantum dots consist of two upper $|b\rangle$ and $|c\rangle$, and one ground sate $|a\rangle$. We consider that spontaneous emission is allowed from the upper states to the ground state (i.e. $|b\rangle \longrightarrow |a\rangle$ and $|c\rangle \longrightarrow |a\rangle$ transitions), whereas the $|b\rangle \longrightarrow |c\rangle$ transition is inhibited in the electric dipole approximation. We also consider that the maximum quantum interference between spontaneous emission pathways from the transitions $|b\rangle \longrightarrow |a\rangle$ and $|c\rangle \longrightarrow |a\rangle$. To show a better picture of the system, a schematic representation of an ensemble of quantum dots doped in a three dimensional metallic photonic

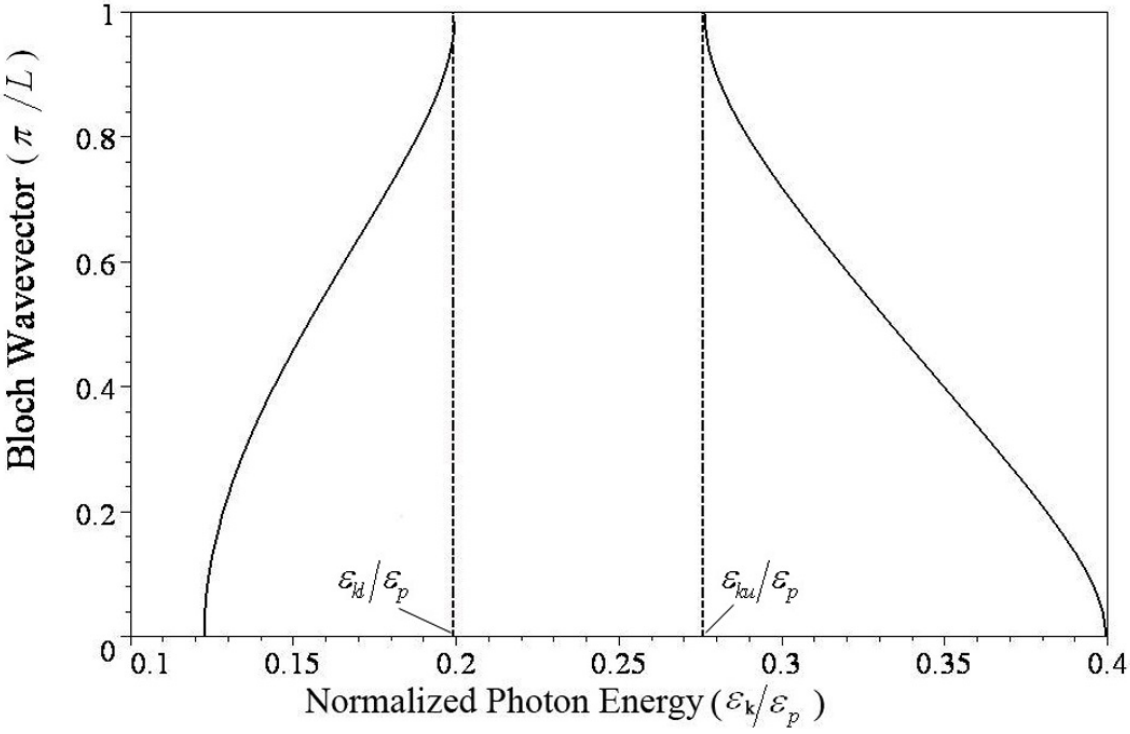

Figure 2-3: Plot of the Bloch wavevector k as a function of the normalized photon energy for a metallic PBG. The vertical dashed lines show, $\varepsilon_l/\varepsilon_p = 0.2$ and $\varepsilon_u/\varepsilon_p = 0.28$ which are the maximum normalized energy of the lower energy band and the minimum normalized energy of the upper energy band, respectively. The refractive index of background is $n_b = 1.5$.

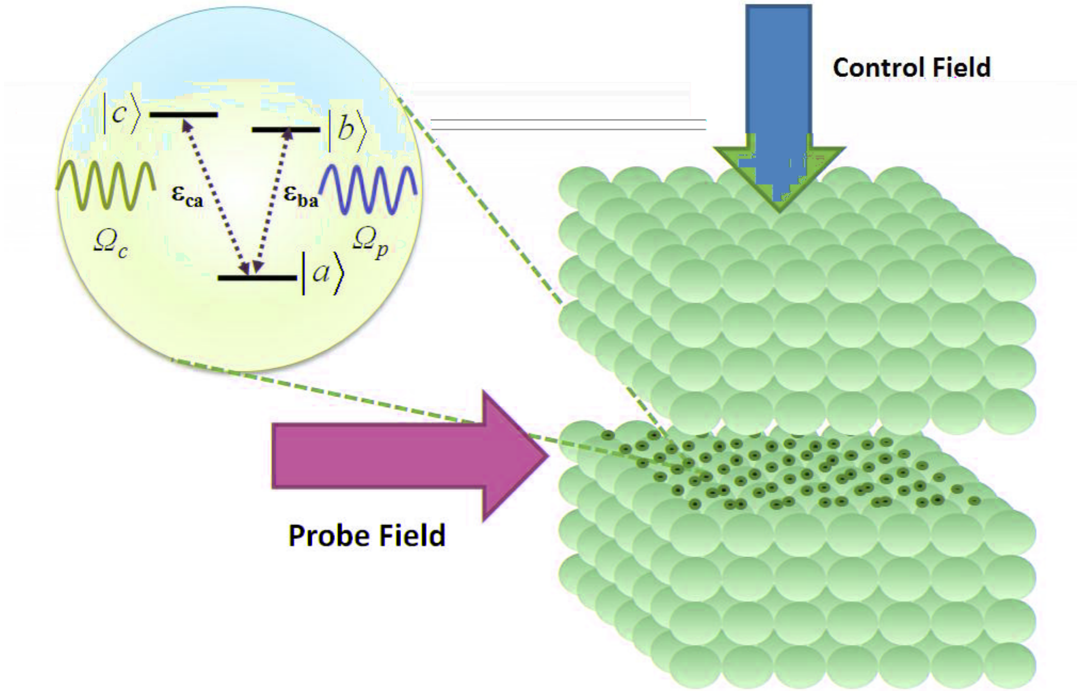

Figure 2-4: Schematic representation of an ensemble of quantum dots (QDs) embedded in metallic photonic crystal (MPC). The quantum dots are considered to be three level quantized particles. The system can be driven by a probe and a pump field, simultaneously.

crystal is illustrated in Fig. 2-4.

A quantum dot can be excited when an electron jumps to upper state by absorbing a specific amount of energy equal to the energy difference between the transition states. The excited quantum dot interacts with reservoir and spontaneously decays to the ground state by emitting a photon with energy equal to the difference between the two states. The reservoir (MPC) can be modeled as a quantized three-dimensional multimode electromagnetic field. The reservoir plays an important role on controlling the spontaneous emission, therefore, any manipulation in reservoir causes the decay of emitted light to be accelerated or slowed down. Using the second-quantization quantum mechanics theory and several reasonable approximations such as Wigner-Weisskopf approximation [61] the radiative decay rate for transition $|i\rangle \longrightarrow |a\rangle$ can be described through Fermi-golden rule [62] as following:

$$\Gamma_i(\varepsilon_{ia}) = \frac{2\pi}{\hbar}\int d\varepsilon_k D(\varepsilon_k)\left|g_{ia}(\varepsilon_k)\right|^2 \delta(\varepsilon_k - \varepsilon_{ia}) \tag{2.5}$$

in Eqn. 2.5 , $g_{ia}(\varepsilon_k)$ is the atom-field coupling constant and is written as:

$$g_{ia}(\varepsilon_k) = \sqrt{\frac{\varepsilon_k}{2\hbar^2\epsilon_0 V}}(\boldsymbol{\mu}_{ia}.\mathbf{e}_{k\lambda}) \tag{2.6}$$

where V is the is the mode volume of the field, $\boldsymbol{\mu}_{ia}$ is the electronic dipole moment induced by the transition $|i\rangle \leftrightarrow |a\rangle$ $(i = b, c)$ and $\mathbf{e}_{k\lambda}$ $(\lambda = 1, 2)$ is the unit polarization vector of the field.

The density of states of the reservoir is obtained by replacing the summation over k in the Golden rule by the integration

$$\sum_k = \int d\varepsilon_k D(\varepsilon_k) \tag{2.7}$$

where $D(\varepsilon)$ is the density of states of photons which counts the available number of electromagnetic modes provided by reservoir. As one can see the role of the reservoir on decay rate appears in the form of density of states in Eqn. 2.5.

The calculations of density of states and the experimental results have proved that the 3-D PCs can be used for tailoring spontaneous emission through modifying the density of states [37][63]. For certain photon energies at the edges of the bandgap (lower and upper energy band), the density of states are significantly enhanced whereas inside the bandgap is strongly reduced or, ideally vanished.

The main equation for density of states of the photons in k-space can be written as:

$$D(\varepsilon_k) = \frac{Vk^2}{3\pi^2}\frac{dk}{d\varepsilon_k} \tag{2.8}$$

The density of states can be expressed in terms of another parameter which is called the form factor $Z(\varepsilon_k)$ by manipulating the Eqn. 2.8 as [64][65]:

$$D(\varepsilon_k) = \frac{V\varepsilon_k^2}{\pi^2\hbar^3c^3}Z^2(\varepsilon_k) \tag{2.9}$$

As one can see for free space where $\varepsilon_k = \hbar ck$ the form factor is one.

Using Eqn. 2.3, the following expression can be obtained for the Form factor

$$Z(\varepsilon_k) = \left[\frac{\hbar^3 c^3}{V} \left(\frac{\xi(\varepsilon_k)(\arccos[F(\varepsilon_k)])^2}{\varepsilon_k^2 \sqrt{1 - F^2(\varepsilon_k)}} \right) \right]^{1/2} \tag{2.10}$$

where $F(\varepsilon_k)$ is given in Eqn. 2.4 and $\xi(\varepsilon_k)$ is

$$\xi(\varepsilon_k) = \frac{1}{4}\varepsilon_k^2 \left[\kappa(\cos(\varepsilon_k\theta_+) - \cos(\varepsilon_k\theta_-)) + \kappa_+\theta_+ \sin(\varepsilon_k\theta_+) - \kappa_-\theta_- \sin(\varepsilon_k\theta_-)\right] \tag{2.11}$$

The other parameters in Eqn. 2.11 are defined as:

$$\kappa = \left(\frac{\varepsilon_p^2}{\varepsilon_k^2}\right) \left(\frac{1}{n_b(1 - \varepsilon_p^2/\varepsilon_k^2)^{1/2}} - \frac{1}{n_m(1 - \varepsilon_p^2/\varepsilon_k^2)^{1/2}} \right) \tag{2.12}$$

$$\kappa_\pm = \left(\frac{1}{n_b}(1 - \varepsilon_p^2/\varepsilon_k^2)^{1/2} - n_b(1 - \varepsilon_p^2/\varepsilon_k^2)^{1/2} \pm 2 \right) \tag{2.13}$$

$$\theta_\pm = \frac{1}{\hbar c} \left(a(1 - \varepsilon_p^2/\varepsilon_k^2)^{-1/2} \pm n_b b \right) \tag{2.14}$$

We have used the Fermi-Golden rule in Eqn. 2.5 to calculate the transition decay rates from the final to initial (upper to lower) state for each transition. For example the transition decay rate for $|b\rangle \longrightarrow |a\rangle$ can be calculated as following:

$$\Gamma_b(\varepsilon_{ba}) = \gamma_0 Z(\varepsilon_{ba})^2 \tag{2.15a}$$

where γ_0 the decay rate of the excited atom in the free space and is defined as:

$$\gamma_0 = \frac{\mu_{ba}^2 \varepsilon_{ba}^3}{3\pi\hbar^3 c^3 \epsilon_0} \tag{2.16}$$

here, ϵ_0 is permittivity of vacuum, $\mu_{ba} = \langle b| \mu |a\rangle = \langle a| \mu |b\rangle$ and ε_{ba} are the electric dipole moments induced by the transition $|b\rangle \leftrightarrow |a\rangle$ and the energy difference between levels, respectively.

Similarly we can also calculate the decay rate for the transition $|c\rangle \leftrightarrow |a\rangle$ as:

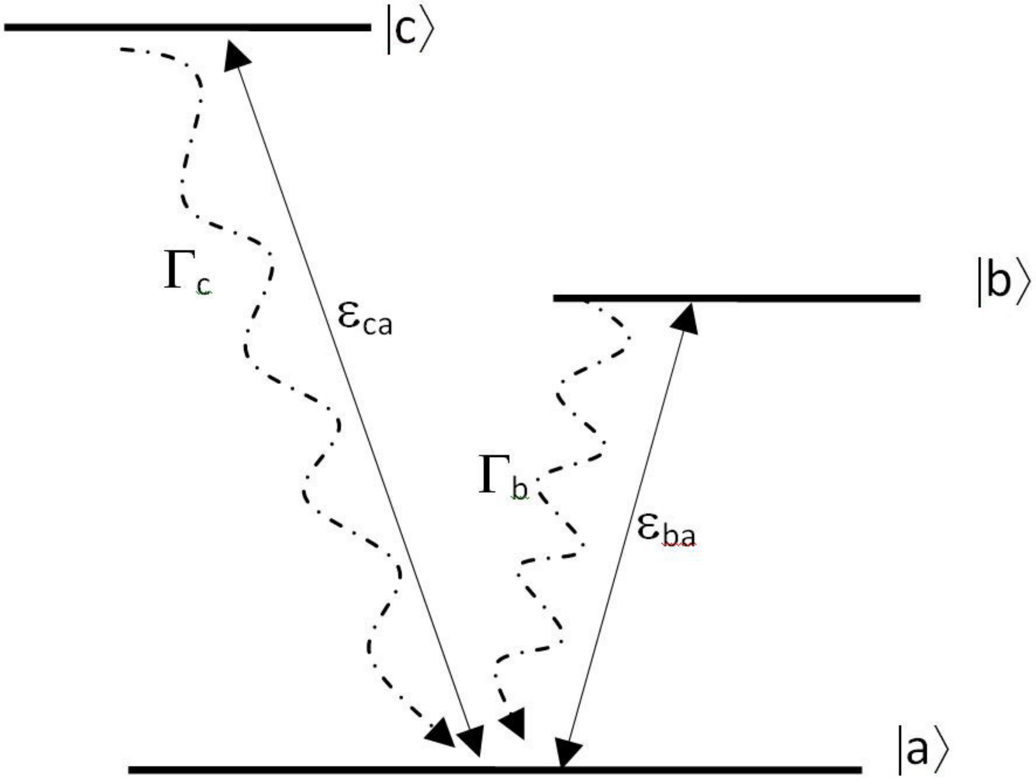

Figure 2-5: Three level quantum dot in V-configuration with two upper close levels $|c\rangle$ and $|b\rangle$ and ground sate $|a\rangle$. The energy difference between levels $|b\rangle \longrightarrow |a\rangle$ and $|c\rangle \longrightarrow |a\rangle$ are denoted as ε_{ba} and ε_{ca}, respectively. Γ_b and Γ_c are the decay rates from the exited states to ground state.

$$\Gamma_c(\varepsilon_{ca}) = \gamma_0 Z(\varepsilon_{ca})^2 \tag{2.17a}$$

Note that in our calculation the γ_0 is considered the same for each transition since the resonant energies difference between levels are small.

2.4 The system Hamiltonian

In this section we investigate the Hamiltonian of our three-level quantum dots doped in a photonic band gap reservoir, where two probe and pump fields with slowly varying amplitudes will drive the system. The total Hamiltonian of the system in the interaction picture can be written as :

$$H = H_Q + H_{QF} + H_R + H_{QR}. \tag{2.18}$$

The first term in Eqn. 2.18 is the Hamiltonian of the three-level quantum dot and is given by:

$$H_Q = \varepsilon_a \sigma_{aa} + \varepsilon_b \sigma_{bb} + \varepsilon_c \sigma_{cc} \tag{2.19}$$

here, ε_i denotes the energy of state $|i\rangle$ and operator $\sigma_{ii} = |i\rangle \langle i|$, where $i = a$, b and c.

The second term in Eqn. 2.18 denotes the interaction semi-classical Hamiltonian between the quantum dot and the two laser fields. It is given by:

$$H_{QF} = -\hbar\gamma_0(\Omega_b \sigma_{ab} e^{-i\Delta_b t} + \Omega_c \sigma_{ac} e^{-i\Delta_c t}) + H.C. \tag{2.20}$$

where, Δ_c and Δ_b the detuning of the energy transitions defined as:

$$\Delta_c = (\varepsilon_{ca} - \varepsilon_k)/\hbar \tag{2.21a}$$

$$\Delta_b = (\varepsilon_{ba} - \varepsilon_k)/\hbar \tag{2.21b}$$

The quantities ε_{ba} and ε_{ca} are the transition energies corresponding to the $|b\rangle \leftrightarrow |a\rangle$ and $|c\rangle \leftrightarrow |a\rangle$ transitions, respectively. H.C., stands for the Hermitian Conjugate.

In Eqn. 2.20, Ω_b and Ω_c, the normalized Rabi frequencies of the transitions $|b\rangle \leftrightarrow |a\rangle$ and

$|c\rangle \leftrightarrow |a\rangle$, are defined as following:

$$\Omega_b = \frac{\boldsymbol{\mu}_{ba}.\mathbf{E}_b}{2\hbar\gamma_0} \tag{2.22a}$$

$$\Omega_c = \frac{\boldsymbol{\mu}_{ca}.\mathbf{E}_c}{2\hbar\gamma_0} \tag{2.22b}$$

where $\mathbf{E}_b$ and $\mathbf{E}_c$ are the slowly varying amplitudes of the two laser beams. $\boldsymbol{\mu}_{ba} = \langle b|\, \boldsymbol{\mu}\, |a\rangle = \langle a|\, \boldsymbol{\mu}\, |b\rangle$ and $\boldsymbol{\mu}_{ca} = \langle c|\, \boldsymbol{\mu}\, |a\rangle = \langle a|\, \boldsymbol{\mu}\, |c\rangle$ are induced electric dipole moments for the energy transitions $|b\rangle \leftrightarrow |a\rangle$ and $|c\rangle \leftrightarrow |a\rangle$, respectively. These induced dipole moments are created in quantum dots because of the presence of the external electromagnetic fields.

The third term in Eqn. 2.18 represents the Hamiltonian of the MPC reservoir. It can be written as [66]:

$$H_R = \int_C \frac{d\varepsilon_k}{2\pi} \varepsilon_k p^+(\varepsilon_k)\ p(\varepsilon_k) \tag{2.23}$$

where, the operator $p(\varepsilon_k)$ and $p^+(\varepsilon_k)$ are the annihilation and creation operators, respectively. The integration contour C consists of two intervals $-\infty \prec \varepsilon_k \preccurlyeq \varepsilon_l$ and $\varepsilon_u \prec \varepsilon_k \preccurlyeq +\infty$.

The last term in Eqn. 2.18 represents the quantum dot-MPC reservoir interaction Hamiltonian and is responsible for the decays from level $|b\rangle \to |a\rangle$ and $|c\rangle \to |a\rangle$.

$$H_{QR} = -\int_c \frac{d\varepsilon_k}{2\pi} \sqrt{\gamma_0} Z_{ba}(\varepsilon_k) p(\varepsilon_k) \sigma_{ab} e^{i\Delta_b t} - \int_c \frac{d\varepsilon_k}{2\pi} \sqrt{\gamma_0} Z_{ca}(\varepsilon_k) p(\varepsilon_k) \sigma_{ac} e^{i\Delta_c t} + H.C. \tag{2.24}$$

The first and second terms in Eqn. 2.24 represent interaction terms for the decay transitions $|b\rangle \to |a\rangle$ and $|c\rangle \to |a\rangle$ with photonic band gap reservoir, respectively. The operator ${\sigma_{ij}}^+$and σ_{ij} are called the raising and lowering operators, respectively. These operators can be defined as following:

$$\sigma_{ij}^+ = |i\rangle\langle j| \tag{2.25a}$$

$$\sigma_{ij} = |j\rangle\langle i| \tag{2.25b}$$

where $|i\rangle$ and $|j\rangle$ denote levels $|a\rangle$, $|b\rangle$ and $|b\rangle$. Note that to derive the interaction Hamiltonian given in Eqn. 2.20 the electric dipole and rotating wave approximations (RWA) is used [67][68][69].

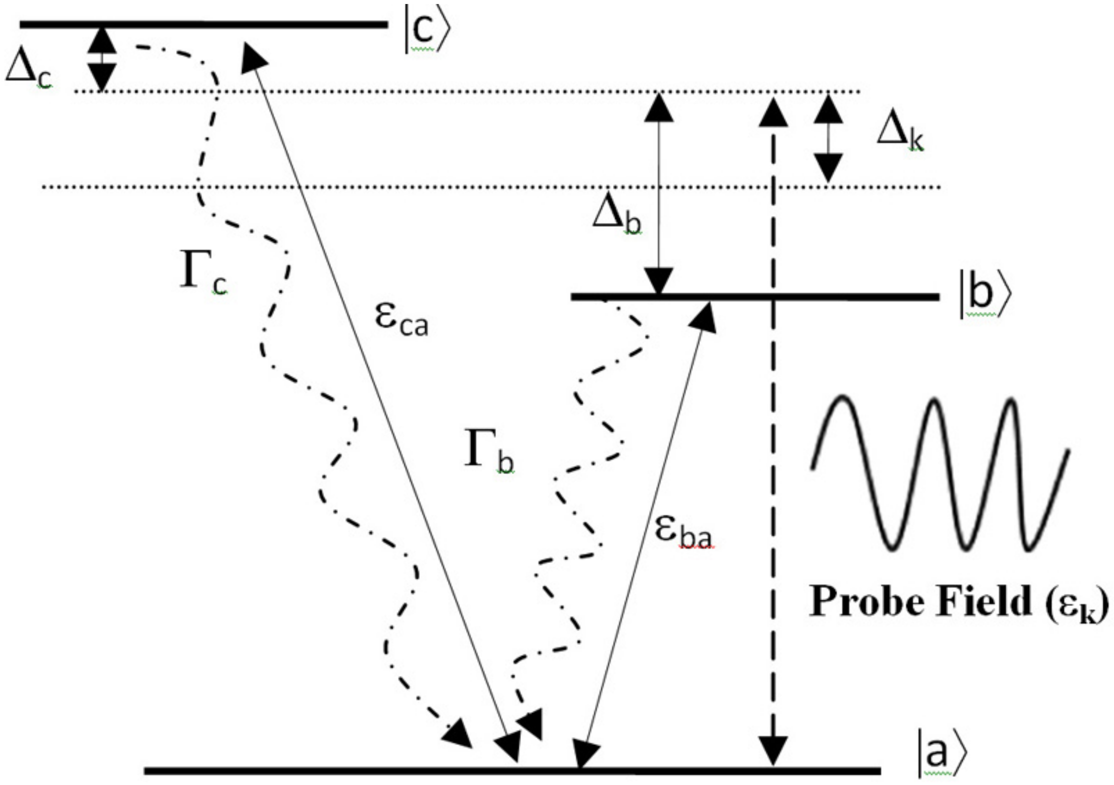

Figure 2-6: The three-level quantum dot driven by a probe laser field with energy ε_k. $\Delta_c = \varepsilon_{ca} - \varepsilon_k$, and $\Delta_b = \varepsilon_{ba} - \varepsilon_k$, are the detunings of the atomic transitions. Γ_b and Γ_c are the decay rates from the exited states to ground state. Δ_k is the detuning of the probe field with the central frequency which is the middle point of the two upper levels.

2.5 Linear Susceptibility and Absorption Coefficient

In this chapter in order to calculate the absorption coefficient of quantum dots doped in MPC we use the optical coherence on the atomic transition for a particular field configuration. In this configuration we assume that the two upper excited states of the quantum dot are close and the system is driven by a single probe field which couples simultaneously the ground state with two excited states (See Fig. 2-6).This configurations is already used in several studies in the gaseous state [70][71] as well.

Here the linear response with a single probe laser field can be shown by the absorption coefficient for the transitions $|b\rangle \rightarrow |a\rangle$ and $|c\rangle \rightarrow |a\rangle$ as following [72]:

$$a(t) = a_0 \, \mathrm{Im}([\widetilde{\rho}_{ba}(t) + \widetilde{\rho}_{ca}(t)] \, e^{-i\varepsilon_k t/\hbar}) \tag{2.26}$$

where α_0 is defined as

$$a_0 = \frac{N_0 \mu^2 \varepsilon_k}{\hbar^2 c \epsilon_0 \gamma_0 \Omega} \tag{2.27}$$

In Eqn. 2.27, N_0, Ω and ε_k are the quantum dots density, the normalized Rabi frequency and the energy of the of the probe laser beam, respectively. The evolving quantities in Eqn. 2.26 are coherences $\widetilde{\rho}_{ba}(t)$ and $\widetilde{\rho}_{ca}(t)$. These coherences are the elements of the reduced density matrix.

Note that in our calculation each transition has a corresponding induced dipole in atomic scale, however, the two upper energies are reasonably close to one another so it is totally a reasonable approximation if we consider the two dipoles equal (i.e. $\mu_{ab} \approx \mu_{ac} = \mu$). We also assume that $\Omega_b = \Omega_c = \Omega$.

2.6 Density Matrix Method and Equation of Motion

As mentioned in Eqn. 2.26 the absorption coefficient of the quantum dots doped in MPC is directly proportional to the quantum coherence associated with the transition energies which are coupled by probe field. We used the density matrix method in a proper rotating frame and the following master equation to find the quantum coherences.

$$\frac{d\rho}{dt} = -\frac{i}{\hbar}[H, \widetilde{\rho}\,(t)] \tag{2.28}$$

In Eqn. 2.28 H and $\widetilde{\rho}\,(t)$ are the Hamiltonian and the density matrix elements of the compound system in the interaction picture.

By introducing the normalized as $\tau = \gamma_0 t$, the evolution equations of the density matrix elements in the interaction picture in an appropriate rotating frame can be written as follows[65]:

$$\frac{d\rho_{ba}}{d\tau} = -d_{ba}\rho_{ba} - i(\Omega_c + \alpha_{ca}\rho_{ca})\rho_{bc} - i\Omega_b(\rho_{bb} - \rho_{aa}) - P\rho_{ca} \tag{2.29}$$

$$\frac{d\rho_{ca}}{d\tau} = -d_{ca}\rho_{ca} - i\Omega_b\rho_{cb} - i\Omega_c(\rho_{cc} - \rho_{aa}) - P\rho_{ba} \tag{2.30}$$

$$\frac{d\rho_{cb}}{d\tau} = -d_{cb}\rho_{cb} + i\Omega_c\rho_{ab} - i\Omega_b\rho_{ca} - P(\rho_{cc} + \rho_{bb}) \tag{2.31}$$

$$\frac{d\rho_{cc}}{d\tau} = -\frac{\Gamma_c}{\gamma_0}\rho_{cc} - i\Omega_c(\rho_{ca} - \rho_{ac}) - P(\rho_{cb} + \rho_{bc}) \tag{2.32}$$

$$\frac{d\rho_{bb}}{d\tau} = -\frac{\Gamma_b}{\gamma_0}\rho_{bb} - i\Omega_b(\rho_{ba} - \rho_{ab}) - P(\rho_{cb} + \rho_{bc}) \tag{2.33}$$

where

$$d_{ca} = \frac{1}{\gamma_0}(\frac{\Gamma_c}{2} + i\Delta_c) \tag{2.34a}$$
$$d_{ba} = \frac{1}{\gamma_0}(\frac{\Gamma_b}{2} + i\Delta_b) \tag{2.34b}$$
$$d_{cb} = \frac{1}{\gamma_0}(\frac{\Gamma_c + \Gamma_b}{2} + i(\Delta_c - \Delta_b)) \tag{2.34c}$$

Note that we used the following rotating frame to derive the evolution equations of the density matrix elements.

$$\rho_{ba}(t) = \widetilde{\rho}_{ba}(t)e^{-i\Delta_b t/\hbar} \tag{2.35a}$$
$$\rho_{ca}(t) = \widetilde{\rho}_{ca}(t)e^{-i\Delta_c t/\hbar} \tag{2.35b}$$
$$\rho_{cb}(t) = \widetilde{\rho}_{cb}(t)e^{-i(\Delta_c - \Delta_b)t/\hbar} \tag{2.35c}$$

In the above equations, Γ_b and Γ_c denote the decay rates (linewidths) related to the $|b\rangle \leftrightarrow |a\rangle$ and $|c\rangle \leftrightarrow |a\rangle$ transitions, respectively. These decay rates are obtained from Eqns.2.15a and 2.17a.

The effect of quantum interference resulting from the cross coupling between the $|b\rangle \leftrightarrow |a\rangle$ and $|c\rangle \leftrightarrow |a\rangle$ transitions is given by [73]:

$$P = P_0\frac{\sqrt{\Gamma_b\Gamma_c}}{2\gamma_0} \tag{2.36}$$

where

$$P_0 = \frac{\boldsymbol{\mu}_{ca} \cdot \boldsymbol{\mu}_{ba}}{\mu_{ca}\mu_{ba}} \tag{2.37}$$

Optimal quantum interference is achieved when the dipole moments are parallel.

Note that population conservation requires that:

$$\rho_{aa}(t) + \rho_{bb}(t) + \rho_{cc}(t) = 1 \tag{2.38}$$

and also

$$\rho_{ij} = \rho^*_{ji}. \tag{2.39}$$

2.7 Effect of Dipole-Dipole Interaction in Absorption Coefficient

As mentioned before the induced electric dipole moments are created in quantum dots due to the presence of the external electromagnetic fields. When the concentration of these nanoparticles is high, the role of the interaction between these dipole moments becomes important and needed to be taken into account in the calculations. In this section, we discuss the dipole-dipole interaction (DDI) effect between quantum dots. The dipole-dipole interaction in our model is calculated using mean field theory. According to mean field theory, the total interaction effect on a given dipole can be evaluated by the mean electric field created by all other dipoles.

In order to consider the effect of dipole-dipole interaction, we need to add another term to Eqn. 2.18. The dipole-dipole interaction Hamiltonian in the mean field approximation is written as [74] :

$$H_{DDI} = -\sum_{i=b,c} \Lambda_{ia}\sigma_{ia} + H.C. \tag{2.40}$$

where Λ_{ia} is the dipole-dipole interaction parameter defined as [75]:

$$\Lambda_{ia} = \sum_{j=b,c \text{ and } i\neq j} \left[C_{ia}\rho_{ia} + C_{ij}\rho_{ja} \right] \tag{2.41}$$

where ρ_{ia} and ρ_{ja} are the density matrix elements (coherences) associated with the transitions$|i\rangle \leftrightarrow |a\rangle$ and $|j\rangle \leftrightarrow |a\rangle$, respectively.

The variables C_{ab}, C_{ac} and C_{cb} are called the dipole-dipole interaction coupling constants which measure the strength of the interactions. These variables are directly proportional to the density of quantum dots and they are obtained as:

$$C_{ba} = \left(\frac{N_0}{3\hbar\epsilon_0}\right)\mu_{ba}^2 \tag{2.42a}$$

$$C_{ca} = \left(\frac{N_0}{3\hbar\epsilon_0}\right)\mu_{ca}^2 \tag{2.42b}$$

$$C_{cb} = \left(\frac{N_0}{3\hbar\epsilon_0}\right)\boldsymbol{\mu}_{ba}.\boldsymbol{\mu}_{ca} \tag{2.42c}$$

2.8 Density Matrix with Dipole-Dipole Interaction Effect

By substituting the total Hamiltonian (Eqn.2.18) to the master equation (Eqn.2.28), the evolution equations of the density matrix elements can be rewritten with consideration of the dipole-dipole interaction effect as following:

$$\begin{aligned}\frac{d\rho_{ba}}{d\tau} &= -\left[d_{ba} + i\alpha_{ba}(\rho_{bb}-\rho_{aa}) + i\alpha_{cb}\rho_{bc}\right]\rho_{ba} - i(\Omega_c + \alpha_{ca}\rho_{ca})\rho_{bc} \\ &\quad -i\Omega_b(\rho_{bb}-\rho_{aa}) - P[1 + i\sqrt{\alpha_{ba}\alpha_{ca}}(\rho_{bb}-\rho_{aa})]\rho_{ca}\end{aligned} \tag{2.43}$$

$$\begin{aligned}\frac{d\rho_{ca}}{d\tau} &= -\left[d_{ca} + i\alpha_{ca}(\rho_{cc}-\rho_{aa}) + i\alpha_{cb}\rho_{cb}\right]\rho_{ca} - i(\Omega_b + \alpha_{ba}\rho_{ba})\rho_{cb} \\ &\quad -i\Omega_c(\rho_{cc}-\rho_{aa}) - P[1 + i\sqrt{\alpha_{ba}\alpha_{ca}}(\rho_{cc}-\rho_{aa})]\rho_{ba}\end{aligned} \tag{2.44}$$

$$\begin{aligned}\frac{d\rho_{cb}}{d\tau} &= -d_{cb}\rho_{cb} + i\Omega_c\rho_{ab} - i\Omega_b\rho_{ca} - \frac{P}{2}(\rho_{cc}+\rho_{bb}) - i(\alpha_{ba}-\alpha_{ca})\rho_{ca}\rho_{ab} \\ &\quad + i\alpha_{cb}(|\rho_{ba}|^2 - |\rho_{ca}|^2)\end{aligned} \tag{2.45}$$

$$\frac{d\rho_{cc}}{d\tau} = -\frac{\Gamma_c}{\gamma_0}\rho_{cc} - i\Omega_c(\rho_{ca}-\rho_{ac}) - P(\rho_{cb}+\rho_{bc}) \ + i\alpha_{cb}(\rho_{ba}\rho_{ac} - \rho_{ab}\rho_{ca}) \tag{2.46}$$

$$\frac{d\rho_{bb}}{d\tau} = -\frac{\Gamma_b}{\gamma_0}\rho_{bb} - i\Omega_b(\rho_{ba}-\rho_{ab}) - P(\rho_{cb}+\rho_{bc}) + i\alpha_{cb}(\rho_{ab}\rho_{ca} - \rho_{ba}\rho_{ac}) \tag{2.47}$$

The normalized dipole-dipole interaction parameters are $\alpha_{ca} = C_{ca}/\gamma_0$, $\alpha_{ba} = C_{ba}/\gamma_0$ and $\alpha_{cb} = C_{cb}/\gamma_0$.

2.9 Results and Discussion

In this section, we calculate the temporal evolution of the absorption coefficient for an ensemble of three-level quantum dots with Vee configuration in two different cases. First, we assume that the concentration of the quantum dots is light and the dipole-dipole interaction is ignorable. Second, we consider the effect of dipole-dipole interaction when the concentration of quantum dots is high.

For the first case, we describe the temporal evolution of normalized absorption coefficient ($\mathrm{Im}(\rho_{ab}(t)+\rho_{ac}(t))$) versus dimensionless time (τ) for different values of δ_k (detuning from the resonance with the center of the excited levels) and ε_{cb} (the energy difference between two transitions).

Considering the energy scheme depicted in Fig. 2-6 the detuning of the atomic transitions can be defined as following:

$$\Delta_b = \Delta_k - \frac{1}{2}\varepsilon_{cb} \tag{2.48a}$$

$$\Delta_c = \Delta_k + \frac{1}{2}\varepsilon_{cb} \tag{2.48b}$$

Also the dimensionless laser detuning can be defined as:

$$\delta_k = \frac{(\Delta_b + \Delta_c)}{2\gamma_0} \tag{2.49}$$

We consider that the MPC structure consists of a three dimensional isotropic arrangement of silver spheres ($\varepsilon_p = 9.0$ eV) embedded in the air background ($n_b = 1.0$). The diameter of the metallic spheres and lattice constant of the MPC are chosen as $2r_s = 0.8L$ and $L = 2r_s + 2b = 320$ nm, respectively. Using Eqn. 2.9, the band structure for this particular type of MPC has been calculated. Our calculations show that this MPC opens a photonic band gap between the lower energy band ($\varepsilon_l = 10.12$ eV) and upper energy band ($\varepsilon_u = 11.41$ eV).

As mentioned before in this chapter we assume that the resonance energies of the quantum dots are close ($\varepsilon_{cb} = 0.5$ meV) and are driven by a single probe field ($\Omega_b = \Omega_c = \Omega$) .

The resonance energies are taken as $\varepsilon_{ba} = 11.45$ eV and $\varepsilon_{ca} = 11.455$ eV which lie close to the upper edge of the photonic band gap.

The corresponding decay rates of the energy levels of the quantum dots depend on the location of the resonance energies in relation to the band structure of the MPC. The decay rates can be evaluated by Eqn. 2.15a and Eqn. 2.17a as $\Gamma(\varepsilon_{ba}) = \gamma_0 Z^2(\varepsilon_{ba}) = 2.05\ \gamma_0$ and $\Gamma(\varepsilon_{ca}) = \gamma_0 Z^2(\varepsilon_{ca}) = 1.99\ \gamma_0$. In our calculation the normalized energy factor is γ_0, which is the decay rate of excited state in free space.

The normalized Rabi frequency of the probe field is taken as: $\Omega_b = \Omega_c = \Omega = 0.02$. In the calculations the quantum coherence is considered to be maximum ($P_0 = 1$).

The differential equations for the density matrix elements for this case are given in Eqns. 2.29 to 2.33.

To show the temporal evolution of normalized absorption coefficient, we have solved these equations numerically for a weak laser probe field using the dverk78 method (seventh-eighth order continuous Runge–Kutta) provided by Maple. Our results show that the dverk78 method has a rather higher precision in comparison to other available methods. The following set has been considered as the initial conditions: $\rho_{aa}(0) = 1$, $\rho_{bb}(0) = \rho_{cc}(0) = 0$ and $\rho_{ij}(0) = 0 (i \neq j)$. This initial conditions imply that the electron is in ground state at t=0.

In Fig. 2-7 the temporal evolution of normalized absorption coefficient $(\mathrm{Im}(\rho_{ab}(t) + \rho_{ac}(t)))$ is plotted as a function of the normalized time (τ) for different values of normalized detuning parameter (δ_k). In our calculation we change the normalized detuning parameter from $\delta_k = 0$ to $\delta_k = 5$. Fig. 2-7 shows that as the detuning parameter increases the number of oscillations increases and the absorption decreases which means the system will tend toward a transparent state.

In Fig. 2-8 the temporal evolution of the normalized absorption coefficient $(\mathrm{Im}(\rho_{ab}(t) + \rho_{ac}(t)))$ is plotted as a function of the normalized time (τ) for different values of resonance energy difference (ε_{cb}). Here to show the effect of the resonance energy difference (ε_{cb}) better we consider a fix value for $\varepsilon_{ba} = 11.415$ eV which is closer to the upper edge of the bang gap. The decay rate for this transition energy is calculated by Eqn. 2.15a as $\Gamma(\varepsilon_{ba}) = \gamma_0 Z^2(\varepsilon_{ba}) = 4.63\ \gamma_0$. The normalized detuning parameter is $\delta_k = 0$. We increase the resonance energy difference (ε_{cb}) from 5 meV to 50 meV. As ε_{cb} increases the transition energy (ε_{ca}) gets further from the upper edge of the bang gap and in result the decay rate associated with this transition decreases. Table 2.2 shows the calculated values of decay rates $\left(\Gamma(\varepsilon_{ca}) = \gamma_0 Z^2(\varepsilon_{ca})\right)$ using Eqn. 2.17a for

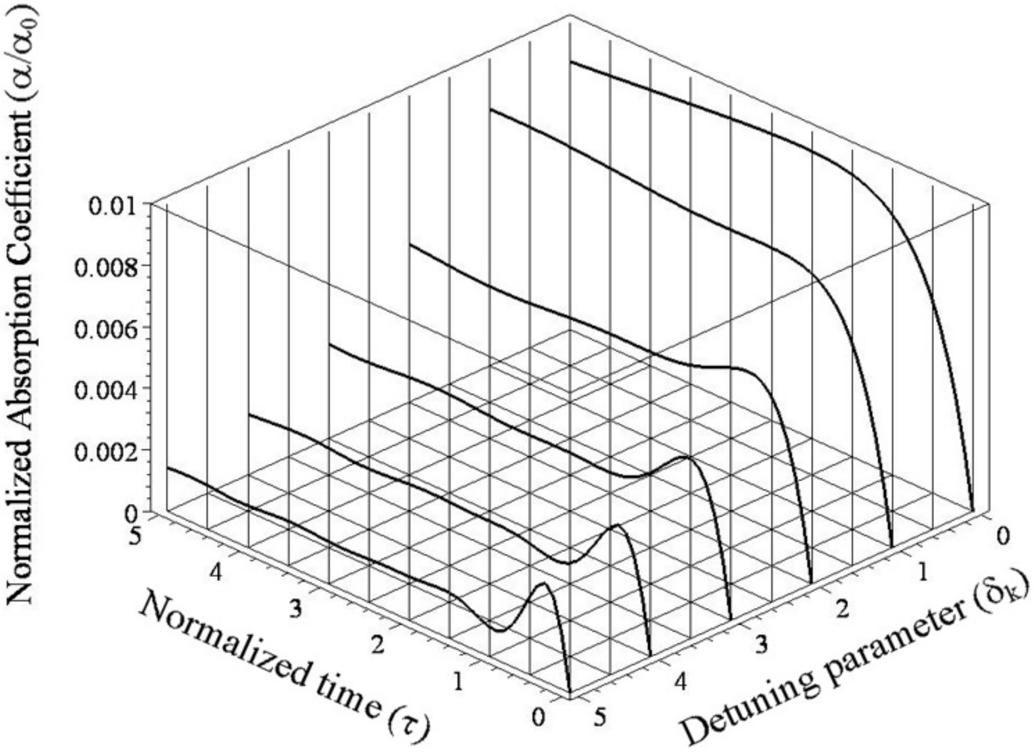

Figure 2-7: Numerical plots of the temporal evolution of the normalized absorption coefficient versus dimensionless time (τ) for different values of detuning parameter (δ_k) where the resonance energies are taken as $\varepsilon_{ba} = 11.45$ eV and $\varepsilon_{ca} = 11.455$ eV, the decay rates are $\Gamma(\varepsilon_{ba}) = 2.05\ \gamma_0$ and $\Gamma(\varepsilon_{ca}) = 1.99\ \gamma_0$, the resonance energy difference is $\varepsilon_{cb} = 0.5\ meV$, the Rabi frequency of the probe fields is $\Omega_a = \Omega_b = \Omega = 0.02$ and the quantum coherence is considered to be maximum ($P = 1$).

$\varepsilon_{cb}\times$ 5 (meV)	1	2	3	4	5	6	7	8	9	10
$\Gamma_b\,(\varepsilon_{ac})\,\times\,\gamma_0$	1.93	1.79	1.68	1.60	1.55	1.51	1.48	1.45	1.43	1.40

Table 2.2: The values of the resonance energy difference (ε_{cb}) and decay rates $\big(\Gamma(\varepsilon_{ca}) = \gamma_0 Z^2(\varepsilon_{ca})\big)$ using Eqn.2.17a for $|c\rangle \leftrightarrow |a\rangle$ transition energies (ε_{ca}).

different transition energies (ε_{ca}). The other variables are the same as Fig. 2-7.

Fig. 2-8 shows that as the transition energy difference between two levels increases the absorption profile shows more oscillatory behavior and its value decreases or the system will tend again toward a transparent state. The reduction in the absorption coefficient is due to quantum coherence between the two spontaneous emissions from transitions $|b\rangle \leftrightarrow |a\rangle$ and $|c\rangle \leftrightarrow |a\rangle$.

Now we perform the numerical calculations for the second case when the three-level quantum dots are doped densely. For this case, Eqns. 2.43 to 2.47 are used and we have considered that all dipole-dipole interaction parameters are equal (i.e. $\alpha_{ab} = \alpha_{ac} = \alpha_{cb} = \alpha$). In Fig. 2-9, we plot the scaled absorption coefficient ($\mathrm{Im}(\rho_{ab}(t) + \rho_{ac}(t))$) a function of dimensionless time (τ) for two values of dipole-dipole interaction parameter when the probe laser detuning is $\delta_k = 0$. The other variables are the same as Fig. 2-7 except the normalized Rabi frequency of the probe field which is taken as: $\Omega_b = \Omega_c = \Omega = 0.01$. In order to show the dipole-dipole interaction effect clearly the greater values of this parameter are considered ($\alpha = 5$ and 10).

Fig. 2-9 shows that the normalized absorption coefficient when dipole-dipole interaction parameter increases the absorption shows an oscillatory behavior before reaching to the steady state. The number of oscillations and the required time to reach to the steady state increases by increasing the dipole-dipole interaction parameter. Our results have a very good consistency with the achieved result in the case of gaseous sate where the decay rates are constant [76].

2.10 Conclusion

In this chapter, we study numerically the temporal evolution of the absorption coefficient profile of quantum dots doped in metallic photonic crystals where a probe field is applied to monitor the absorption process. The V field configuration is considered for quantum dots where the transition energy difference of the two upper levels is small. We consider two cases. First

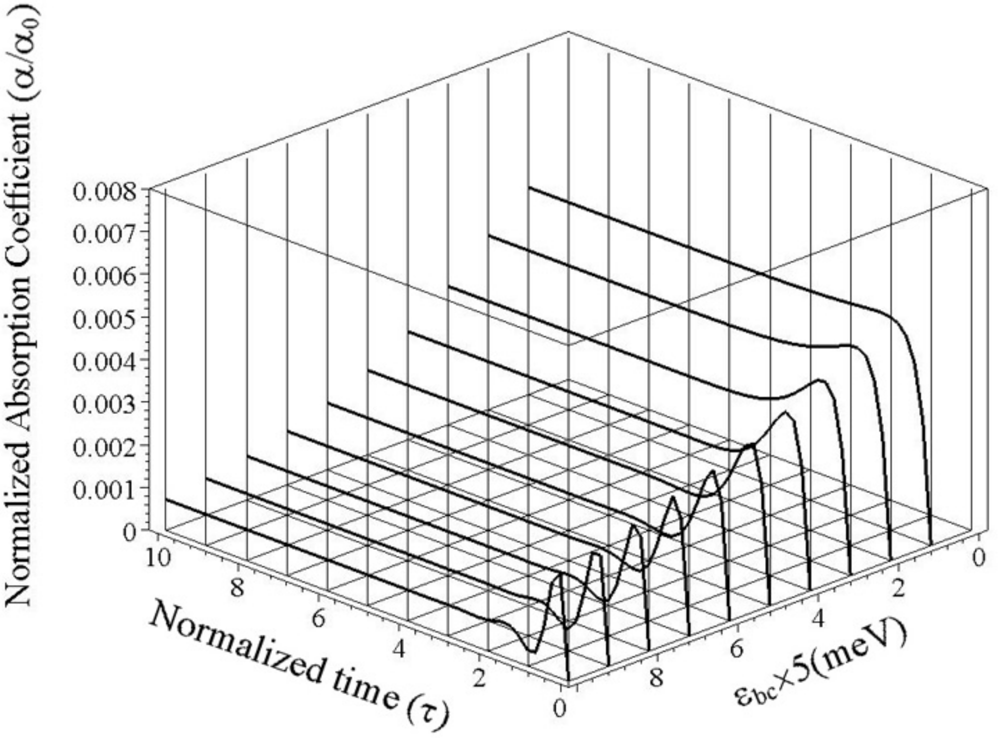

Figure 2-8: Numerical plots of the temporal evolution of the normalized absorption coefficient versus dimensionless time (τ) for different values of the resonance energy difference ($\varepsilon_{cb} = 5 - 50meV$). Here, the normalized detuning parameter is $\delta_k = 0$, the resonance energy $\varepsilon_{ba} = 11.415$ eV , the decay rates are $\Gamma(\varepsilon_{ba}) = 4.63\ \gamma_0$, the Rabi frequency of the probe fiels is $\Omega_a = \Omega_b = \Omega = 0.02$ and the quantum coherence is considered to be maximum ($P = 1$).

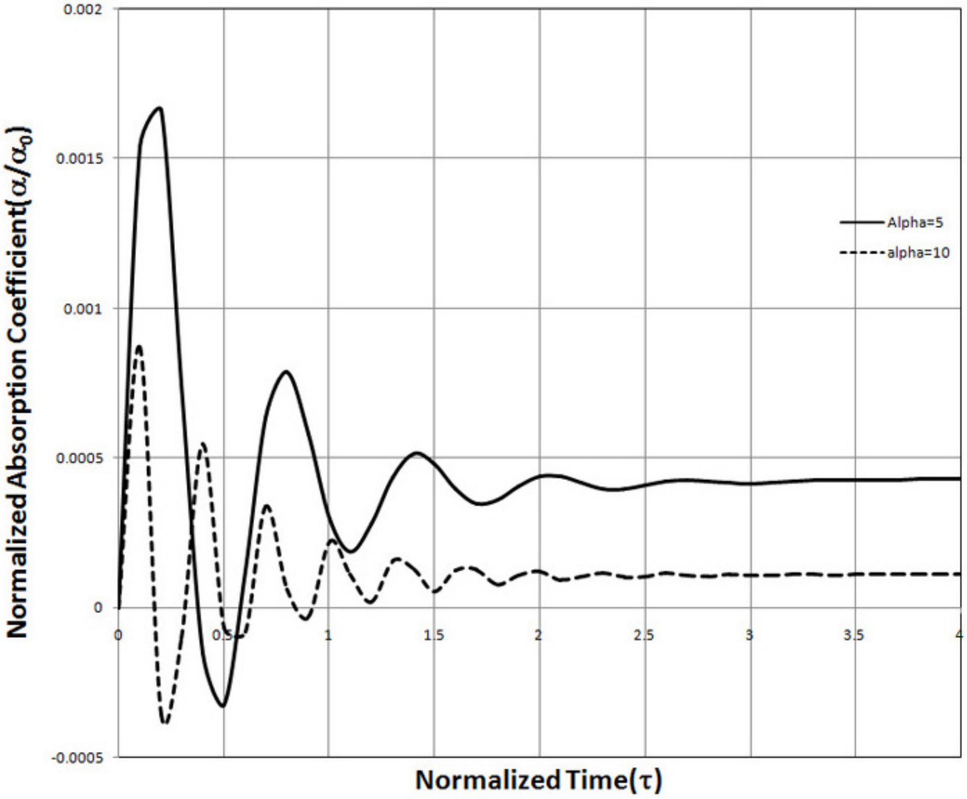

Figure 2-9: Numerical plots of the temporal evolution of the normalized absorption coefficient versus dimensionless time (τ) for two values of dipole-dipole ineraction parameter (α). The solid and dashed curves show when $\alpha = 5$ and $\alpha = 10$, respectively. Here, the normalized detuning parameter is $\delta_k = 0$, the resonance energies are taken as $\varepsilon_{ba} = 11.45$ eV and $\varepsilon_{ca} = 11.455$ eV, the decay rates are $\Gamma(\varepsilon_{ba}) = 2.05\ \gamma_0$ and $\Gamma(\varepsilon_{ca}) = 1.99\ \gamma_0$, the Rabi frequency of the probe fiels is $\Omega_a = \Omega_b = \Omega = 0.01$, the quantum coherence is considered to be maximum ($P = 1$) and the laser detuning is $\delta_k = 0$.

we consider that quantum dots are embedded lightly so that their interaction is ignorable. In this case, we describe the temporal evolution of normalized absorption coefficient versus dimensionless time for different values of detuning parameter and the energy difference between the two transitions. It is found that when these two parameters increase the absorption profile shows more oscillations and the system goes towards the transparent state. In the second situation we consider that quantum dots are doped densely so that they will interact with each other via the dipole-dipole interaction effect. It is found that when the dipole-dipole interaction increases the absorption coefficient decreases, shows more oscillatory behavior with time and then reaches the steady state.

Chapter 3

Plasmonic Effect on Quantum Coherence and Interference

3.1 Introduction

Confining and releasing light near the nano-sized active medium such as dye molecules, impurity atoms and quantum dots embedded in photonic crystals is one of the most important steps leading towards the development of optical switches [77] and optical transistors [78]. The control of confined light can be achieved using photonic crystals possessing tunable photonic band gaps, by applying a coherent control energy [47]. It is also possible to control the photonic band gaps of MPCs by changing the metallic dielectric function. For instance, the presence of a static magnetic field can greatly change the dielectric response of a free electron in the metal [48] or change the plasma energy by altering the surface charge density on each metallic particle [49][50].

Recently, considerable effort has been devoted to the investigation of the quantum optics of MPCs doped with an active medium. For example, Kaso and John [79] have demonstrated the occurrence of nonlinear Bloch waves in MPCs when 5-nm-diameter PbS close-packed quantum dots fill the void regions. Singh [80] has studied the effect of plasmas on the bound photon modes in metallic photonic nanowires. Yannopapas *et al.* [81] have investigated the electromagnetically induced transparency when light is absorbed by a two-dimensional lattice of metallic (gold) spherical nanoparticles mounted on an asymmetric dielectric (indium-tin-oxide) waveguide.

We also have studied the quantum optics of four-level quantum dots doped in metallic photonic crystals [82]. A probe field was applied between the first excited state and higher excited states to study the absorption coefficient of the system in its steady state configuration. It was considered that the first excited state decayed to the ground state. The density matrix method was used to calculate the absorption coefficient of the system. It was found that the height of the absorption peak can be controlled by changing the transition energy between the ground state and the first excited state.

In this chapter we have studied the effect of plasma energy on the absorption coefficient profile in doped metallic photonic crystals[1]. The crystal is doped with ensemble of three-level quantum dots of V-configuration which are interacting with each other via the dipole-dipole interaction. They are also interacting with coupled plasma photon modes present in the system. A probe laser field is applied to study the absorption coefficient. We consider quantum interference here as well. The density matrix method has been used to calculate the steady state and transient behavior of the absorption coefficient and population density in the system. Two different field configurations are considered. In the first configuration is the same configuration illustrated in chapter 2 (See Fig. 2-6) where a probe field couples the ground state and two closely excited states.

Absorption occurs due to the transitions from ground state to two excited states. It is found that position of the transparent peak is moved due to the change of the plasma energy. In other words, changing the plasma energy causes the system switches between a transparent and an absorbing state. The strong coupling between plasma and quantum dots is responsible for this phenomenon. In the second configuration the weak probe field couples only one excited state and a strong pump field couples to other excited state. The transition between excited states is dipole forbidden. This configuration is shown in Fig. 3-1. We observed that the appeared peak in absorption profile splits into two peaks and also the system can be switched from the absorption to the gain state due to the change of the plasma frequency due to the quantum interference and coherence. These are interesting results and can be used to make nano-scale

---

[1] The work presented in this chapter has been published in: A. Hatef and M. Singh, “The Study of Quantum Interference in Metallic Photonic Crystals Doped with Four-Level Quantum Dots” Nanoscale Research Letter 5, 464–468, (2010) and A. Hatef and M. Singh, "Plasmonic effect on quantum coherence and interference in metallic photonic crystals doped with quantum dots", Phys. Rev. A, 81, 063816 (2010).

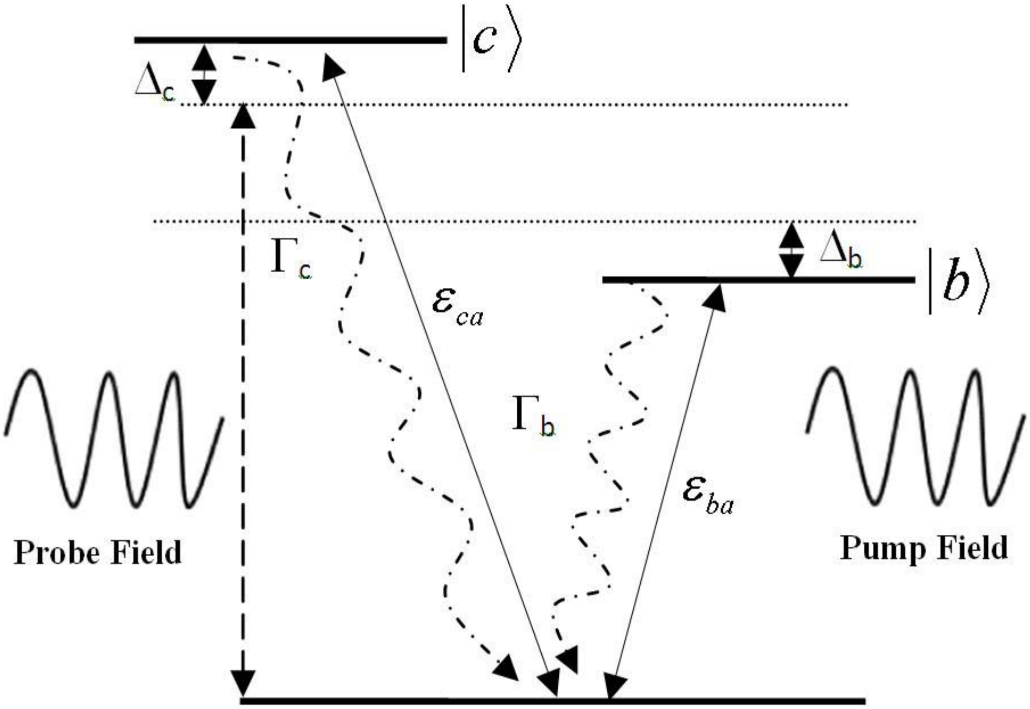

Figure 3-1: Three-level QD in the V-configuration with two upper levels ($|b\rangle$ and $|c\rangle$) and ground sate ($|a\rangle$). The strong pump field of frequency is coupled to the ground sate and the excited , while the weak probe field of frequency is coupled to the ground sate and the excited state . Here and are the transition energies, respectively, while and are the decay rates from the exited states to ground state. The parameters and are the detuning of the atomic transitions.

plasma devices.

3.2 Theory

To calculate the band gap structure we have used a dispersion for a three-dimensional isotropic photonic crystal model used in [58] [63]. We have considered that our MPC is fabricated from metallic spheres which are arranged in a periodic structure and embedded within a background dielectric material[6] . This dielectric background material can be taken as an ordinary dielectric material such as MgF_2 [11] , Stycast or Teflon [6], which have constant refractive indices. Here we take metallic spheres made of silver, as in [83] [84]. The lattice constant of the crystal and radii of the spheres are taken as L and r_s, respectively and the refractive index of the dielectric background material is denoted as n_b. As mentioned in chapter 2, almost in all photonic band gap calculation in MPCs, the Drude model is used to show the refractive index of a metal (See Eqn. 2.1).

Kee *et al.* [48] have shown that the refractive index of metallic nano-layers is modified in the presence of a large static magnetic field as:

$$n_m(\varepsilon_k) = \sqrt{1 - \frac{\varepsilon_p^2}{\varepsilon_k^2}} \tag{3.1}$$

where

$$\varepsilon_p = \frac{\varepsilon_p^0}{(1 \mp \hbar H_{ext}/8\pi\epsilon_0 c m_{eff}\varepsilon_k)} \tag{3.2}$$

In Eqn. 3.2, the plus/minus sign refers to left- or right-circularly polarized EM waves, c is the speed of light in a vacuum, and H_{ext} is the magnitude of the external static magnetic field in cgs units.

Rostalski *et al.* [50] have also shown that that an excess charge on the surface of a metal nano-particle would affect its plasma energy. Extra charge on the nano particles can be induced by friction, photoemission and ion adhesion/bombardment. For example, the modified plasma energy for a spherical silver cluster is obtained as:

$$\varepsilon_p(n) = \varepsilon_p(n_0)\sqrt{\frac{n_0 + n}{n_0}} \tag{3.3}$$

where n_0 is the number of atoms in a metallic sphere, corresponding to the number of free electrons , and n is the number of excess electrons. This means that the plasma energy is increased by stationary surface charge on the uncharged sphere.

We consider that the MPC is doped with an ensemble of three-level quantum dots. The quantum dots are interacting with the metallic crystal, which is acting as a reservoir. The electronic $|b\rangle \leftrightarrow |a\rangle$ and $|c\rangle \leftrightarrow |a\rangle$ transitions are interacting via electron-photon interaction in the dipole and rotating wave approximations. The above electronic transitions induce a dipole moment in the quantum dots, and therefore these quantum dots are also interacting with each other through dipole-dipole interaction [75]. The interaction Hamiltonian of the system is written as:

$$H = -\sum_{i=b,c}\left[\int_c \frac{d\varepsilon_k}{2\pi}\sqrt{\gamma_0}Z_{ia}(\varepsilon_k)p(\varepsilon_k)\sigma_{ai}^{+} + \Lambda_{ia}\sigma_{ai}^{+} + h.c.\right] \tag{3.4}$$

In Eqn. 3.4, *h.c.* stands for the hermitian conjugate. The first and second terms are the electron-photon interaction and the dipole-dipole interaction, respectively. The $\sigma_{ai}^{+} = |i\rangle\langle a|$ is called the electron raising operator, where $i = b$ or c, while $p(\varepsilon_k)$ is the photon annihilation operator. The integration contour C consists of two intervals due to the photonic band gap of the MPC, which are $-\infty < \varepsilon_k \leq \varepsilon_l$ and $\varepsilon_u < \varepsilon_k \leq \infty$ [66]. The quantities ε_l and ε_u are the lower and upper edges of the photonic band gap, respectively, while γ_0 is the vacuum decay rate, and is defined in [85]. The form factor function ($Z(\varepsilon_k)$) is given in Eqn. 2.10 in chapter 2. In Eqn. 3.4, Λ_{ia} is the dipole-dipole interaction parameter defined the same as Eqn. 2.41 :

$$\Lambda_{ia} = \sum_{j=b,c\ i\neq j}[C_{ia}\rho_{ia} + C_{ij}\rho_{ja}] \tag{3.5}$$

where ρ_{ia} and ρ_{ja} are the density matrix elements associated with the transitions $|i\rangle \leftrightarrow |a\rangle$ and $|j\rangle \leftrightarrow |a\rangle$, respectively. The parameters C_{ia} and C_{ij} are the dipole-dipole interaction coupling constants, which measure the strength of the dipole-dipole interaction interaction and shown in chapter 2 (See Eqns. 2.42a). The density matrix elements (coherences) are calculated using the density matrix method and master equation developed in references [75][86]. Using the interaction Hamiltonian given in Eqn. 3.4, one can obtain the following expressions for the density matrix elements of a three-level energy system driven by two external laser fields at steady state. The system is prepared in such a way that initially the quantum dots are in the ground state $|a\rangle$.

$$\begin{aligned}\frac{d\rho_{ba}}{d\tau} &= -\left[d_{ba} + i\alpha_{ba}(\rho_{bb}-\rho_{aa}) + i\alpha_{cb}\rho_{bc}\right]\rho_{ba} - i(\Omega_c + \alpha_{ca}\rho_{ca})\rho_{bc} - i\Omega_b(\rho_{bb}-\rho_{aa}) \\ &-\frac{P}{\Gamma_0}[1 + i\sqrt{\alpha_{ba}\alpha_{ca}}(\rho_{bb}-\rho_{aa})]\rho_{ca}\end{aligned} \tag{3.6}$$

$$\begin{aligned}\frac{d\rho_{ca}}{d\tau} &= -\left[d_{ca} + i\alpha_{ca}(\rho_{cc}-\rho_{aa}) + i\alpha_{cb}\rho_{cb}\right]\rho_{ca} - i(\Omega_b + \alpha_{ba}\rho_{ba})\rho_{cb} - i\Omega_c(\rho_{cc}-\rho_{aa}) \\ &-\frac{P}{\Gamma_0}[1 + i\sqrt{\alpha_{ba}\alpha_{ca}}(\rho_{cc}-\rho_{aa})]\rho_{ba}\end{aligned} \tag{3.7}$$

$$\frac{d\rho_{cb}}{d\tau} = -d_{cb}\rho_{cb} + i\Omega_c\rho_{ab} - i\Omega_b\rho_{ca} - P(\rho_{cc} + \rho_{bb}) - i(\alpha_{ba} - \alpha_{ca})\rho_{ca}\rho_{ab} + i\alpha_{cb}(|\rho_{ba}|^2 - |\rho_{ca}|^2) \quad (3.8)$$

$$\frac{d\rho_{cc}}{d\tau} = -2\frac{\Gamma_c}{\Gamma_0}\rho_{cc} - i\Omega_c(\rho_{ca} - \rho_{ac}) - P(\rho_{cb} + \rho_{bc}) + i\alpha_{cb}(\rho_{ba}\rho_{ac} - \rho_{ab}\rho_{ca}) \quad (3.9)$$

$$\frac{d\rho_{bb}}{d\tau} = -2\frac{\Gamma_b}{\Gamma_0}\rho_{bb} - i\Omega_b(\rho_{ba} - \rho_{ab}) - P(\rho_{cb} + \rho_{bc}) + i\alpha_{cb}(\rho_{ab}\rho_{ca} - \rho_{ba}\rho_{ac}) \quad (3.10)$$

where

$$d_{ca} = (\frac{\Gamma_c}{\Gamma_0} + \frac{2\Delta_c}{\Gamma_0}i) \quad (3.11a)$$

$$d_{ba} = (\frac{\Gamma_b}{\Gamma_0} + \frac{2\Delta_b}{\Gamma_0}i) \quad (3.11b)$$

$$d_{cb} = (\frac{\Gamma_c + \Gamma_b}{\Gamma_0} + \frac{2(\Delta_c - \Delta_b)}{\Gamma_0}i) \quad (3.11c)$$

In above equations all the parameters are defined in chapter 2. In our calculations, all energies have been normalized with respect to $\Gamma_0(\varepsilon_m)/2$, where ε_m lies far away from the photonic band gap of the MPC. The effect of quantum interference is defined as

$$P = \frac{P_0\sqrt{\Gamma_b\Gamma_c}}{\Gamma_0} \quad (3.12)$$

The normalized Rabi frequencies are

$$\Omega_b = \frac{\boldsymbol{\mu}_{ba}.\mathbf{E}_b}{\hbar\Gamma_0} \quad (3.13a)$$

$$\Omega_c = \frac{\boldsymbol{\mu}_{ca}.\mathbf{E}_c}{\hbar\Gamma_0} \quad (3.13b)$$

The normalized dipole-dipole interaction parameters are

$$\alpha_{ca} = \frac{2C_{ca}}{\Gamma_0} \quad (3.14a)$$

$$\alpha_{ba} = \frac{2C_{ba}}{\Gamma_0} \quad (3.14b)$$

$$\alpha_{cb} = \frac{2C_{cb}}{\Gamma_0} \quad (3.14c)$$

In the first configuration we assume that the two upper excited levels of the quantum dots ($|b\rangle$ and $|c\rangle$) are close to one another, so they are almost degenerate. Here the pump field is absent, and the transitions $|b\rangle \leftrightarrow |a\rangle$ and $|c\rangle \leftrightarrow |a\rangle$ are simultaneously driven by a weak tunable probe field of energy ε_c. For this configuration, the absorption due to the $|b\rangle \leftrightarrow |a\rangle$ and $|c\rangle \leftrightarrow |a\rangle$ transitions in the presence of the applied probe field is defined in Eqn. 2.26 as:

$$\alpha(t) = \alpha_0 \frac{\mathrm{Im}(\rho_{ab}(t) + \rho_{ac}(t))}{\Omega} \tag{3.15}$$

where α_0 is defined as:

$$a_0 = \frac{N_0 \Omega \mu^2}{2\hbar \epsilon_0 R} \tag{3.16}$$

here, Ω is the normalized Rabi frequency.

We have obtained an analytical expression of the absorption coefficient in the linear response approximation of the Rabi frequency by using a very low driving field as following:

$$\frac{\alpha}{\alpha_0} = \frac{A+B}{C-D} \tag{3.17a}$$

where

$$A = (1 + a_1(\alpha_{cb} - \alpha_{ca}) + a_2(\alpha_{ca} - \alpha_{cb}))\,(a_3 + a_4) \tag{3.18a}$$

$$B = (a_4(\alpha_{ca} - \alpha_{cb}) - a_3(\alpha_{ba} + \alpha_{cb}) + 1)\,(a_2 + a_1) \tag{3.18b}$$

$$C = (1 - a_1\alpha_{ca} - a_2\alpha_{cb})(1 - a_3\alpha_{ba} - a_4\alpha_{cb}) \tag{3.18c}$$

$$D = (a_4\alpha_{ca} + a_3\alpha_{cb})(a_2\alpha_{ba} + a_1\alpha_{cb}) \tag{3.18d}$$

The other parameters are defined as:

$$a_1 = i\left[\frac{d_{ba}d_{cb}(\rho^0_{aa}-\rho^0_{cc})-P^2(\rho^0_{cc}+\rho^0_{bb})}{d_{cb}(d_{ba}d_{ca}-P^2)}\right] \tag{3.19a}$$

$$a_2 = iP\left[\frac{d_{ba}(\rho^0_{cc}+\rho^0_{bb})-d_{cb}(\rho^0_{aa}-\rho^0_{bb})}{d_{cb}(d_{ba}d_{ca}-P^2)}\right] \tag{3.19b}$$

$$a_3 = i\left[\frac{d_{cb}d_{ca}(\rho^0_{aa}-\rho^0_{bb})-P^2(\rho^0_{cc}+\rho^0_{bb})}{d_{cb}(d_{ba}d_{ca}-P^2)}\right] \tag{3.19c}$$

$$a_4 = -iP\left[\frac{d_{cb}(\rho^0_{aa}-\rho^0_{bb})+d_{ca}(\rho^0_{cc}+\rho^0_{bb})}{d_{cb}(d_{ba}d_{ca}-P^2)}\right] \tag{3.19d}$$

In Eqns. 3.17a to 3.19d and ρ^0_{ij} denotes the elements of the density matrix at $t = 0$.

In the second configuration, a probe laser field of normalized Rabi frequency Ω_{0c} sweeps the $|c\rangle \leftrightarrow |a\rangle$ transition in order to study the absorption coefficient of the quantum dots. Here the $|b\rangle \leftrightarrow |a\rangle$ transition is driven by a strong control laser field of normalized Rabi frequency Ω_{0b}, which manipulates the absorption coefficient. In this case to make sure that the probe and pump fields are driving the desired transitions we consider that $\boldsymbol{\mu}_{ca}.\mathbf{E}_{0b} = 0$ and $\boldsymbol{\mu}_{ba}.\mathbf{E}_{0c} = 0$. In Fig. 3-2 the orientations of electric fields and dipole moments are illustrated. This configuration is one the most famous utilized models that study quantum coherence and interference effects in three- or multi-level atoms [87][88][70]. In this case the absorption coefficient is obtained as [76]:

$$\alpha = \alpha_0\left[\frac{\mathrm{Im}(\rho_{ac}(\Omega_c)-\rho_{ac}(\Omega_c=0))}{\Omega_c}\right]$$

where the normalized Rabi frequencies related to each transition are defined as [76][88].

$$\Omega_b = \frac{\boldsymbol{\mu}_{ba}.\mathbf{E}_{0b}}{\hbar\Gamma_0} = \Omega_{0b}\sqrt{1-P_0^2} \tag{3.20a}$$

$$\Omega_c = \frac{\boldsymbol{\mu}_{ca}.\mathbf{E}_{0c}}{\hbar\Gamma_0} = \Omega_{0c}\sqrt{1-P_0^2} \tag{3.20b}$$

In this configuration, we are not able to obtain the analytical expression for the absorption coefficient. Here the normalized detuning parameter represents the difference between the probe laser resonance and the excited level $|c\rangle$ (i.e. $\delta_k = 2\Delta_c/\Gamma_0$).

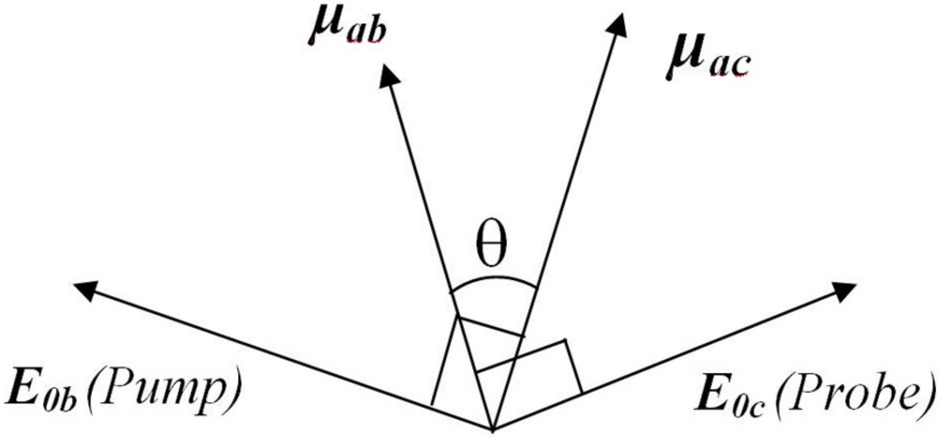

Figure 3-2: The pump field ($\mathbf{E}_{0b}$) drives the $|b\rangle \leftrightarrow |a\rangle$ transition where $\boldsymbol{\mu}_{ca}.\mathbf{E}_{0b} = 0$ and similarly the probe field ($\mathbf{E}_{0c}$) drives the $|c\rangle \leftrightarrow |a\rangle$ transition where $\boldsymbol{\mu}_{ba}.\mathbf{E}_{0c} = 0$. The quantum interference parameter $P_0 = \cos(\theta)$.

3.3 Results and Discussion

Our main focus in this section is to vary the plasma energy and then observe its effects this on the absorption coefficient profile, for both quantum dot-field configurations. Here our MPC is made from silver spheres embedded in MgF_2 ($n_b = 1.5$). The radius of the metallic spheres and lattice constant of the PC in reduced units are chosen as $r_s = 0.25\ \hbar c/\varepsilon_p$ and $L = 10.5\ \hbar c/\varepsilon_p$, respectively. The energies of the lower and upper photonic band edges are calculated as $\varepsilon_l = 1.81$eV and $\varepsilon_u = 2.49$ eV, respectively for silver spheres with $\varepsilon_p = 9$ eV. For the first configuration, the normalized absorption coefficient (α/α_0) is plotted in Fig. 3-3 as a function of the normalized detuning parameter ($\delta_k = (\Delta_b + \Delta_c)/\Gamma_0$), using the analytical expression obtained in Eqn. 3.17a. The energy levels $\varepsilon_{ba} = 2.6$ eV and $\varepsilon_{ca} = 2.6001$ eV are located very close to each other, as the energy difference between $|b\rangle$ and $|c\rangle$ is taken as $\varepsilon_{cb} = 0.1$ meV.

In our calculation the normalized energy factor is defined as $\Gamma_0 = 1.5751\gamma_0$, which gives a decay rate with energy $\varepsilon_m = 2.92$ eV. The quantity γ_0 is taken as $\gamma_0 = 1meV/\hbar$, from reference [85]. All dipole-dipole interaction parameters are considered equal (i.e. $\alpha_{ca} = \alpha_{cb} = \alpha_{cb} = \alpha$), and the maximum quantum interference strength is applied, (i.e. $P_0 = 1$).

In Fig. 3-3, the solid and dotted curves show the normalized absorption coefficients the

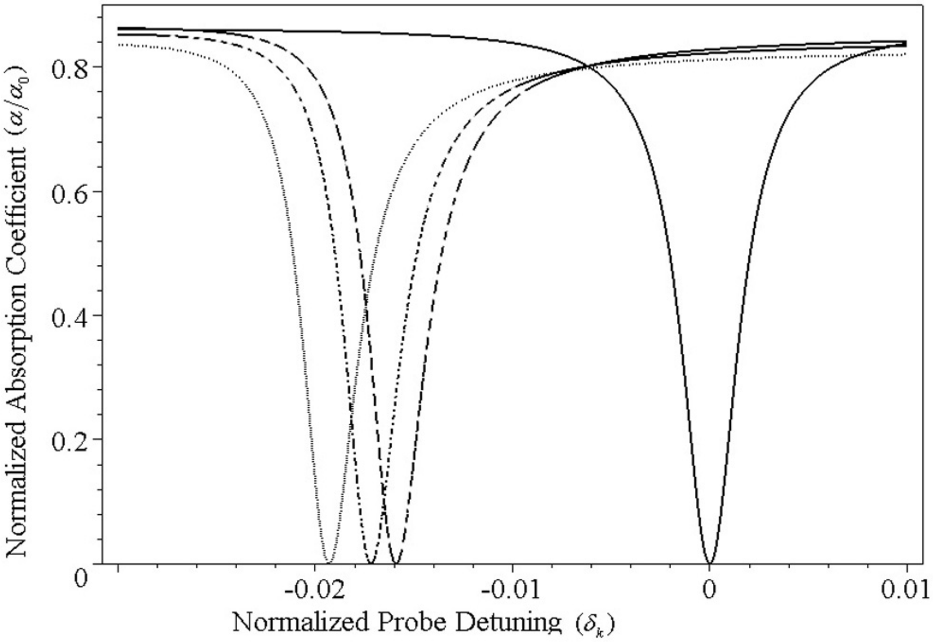

Figure 3-3: Steady state results for the normalized absorption spectrum(α/α_0), given in arbitrary units (a.u.), as a function of the normalized probe field detuning (δ_k), which given in Eq. (23). The solid curve corresponds to $\alpha = 0$ and $\epsilon_p = 9$ eV. For the dotted, dash-dotted and dashed curves we have α=0.1, while the plasma energy is varied as $\epsilon_p = 9$ eV (dotted curve), 8.97 eV (dash-dotted curve) and 8.95 eV (dashed curve).

dipole-dipole interaction parameters $\alpha = 0$ and $\alpha = 0.1$, respectively, while the plasma energy in both cases is taken as $\varepsilon_p = 9$ eV. We note that the absorption spectrum has one sharp dip and two peaks. However, the two peaks are not shown in Fig. 3-3 because the detuning parameter is taken to lie very close the dip. The dip in absorption corresponds to a transparent resonance, and is due to the cancellation of the spontaneous emission through quantum interference. Note that in the presence of dipole-dipole interaction the sharp dip in the absorption profile shifts to the left side of the zero detuning $\delta_k = -0.019$, as indicated by the dotted curve in Fig. 3-3. This shift in the dip is due the presence of dipole-dipole interaction, which causes a change in the detuning parameter, as the energy difference between levels $|b\rangle$ and $|c\rangle$ changes (See Eqn. 3.4).

Interesting results are obtained when the plasma energy of the MPC is changed while

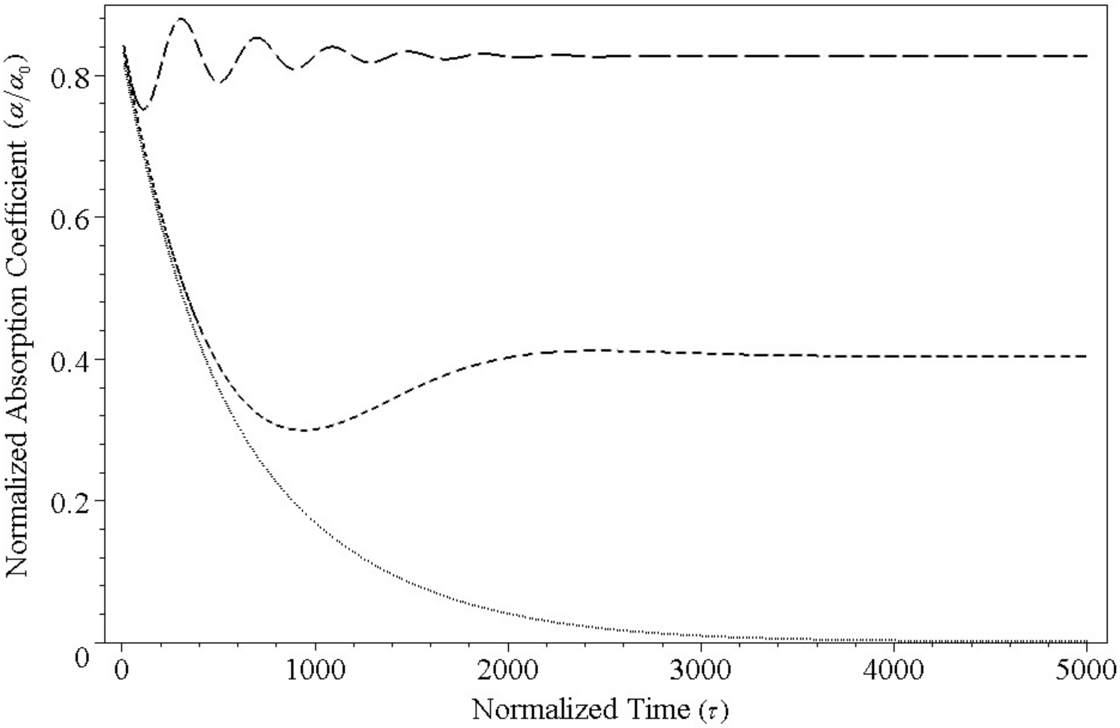

Figure 3-4: The normalized absorption coefficient versus normalized time τ for plasma frequency $\epsilon_p = 9$ eV (dotted curve), $\epsilon_p = 8.97$ eV (dashed curve) and $\epsilon_p = 8.95$ eV (long dashed curve). Here Γ_0(2.92 eV)=1.5751γ_0 for ϵ_{bc}=0.1 meV, Ω=0.01 and P$_0$=1.

considering the dipole-dipole interaction($\alpha = 0.1$). The dotted, dash-dotted and dashed curves are plotted for $\varepsilon_p = 9$ eV, $\varepsilon_p = 8.97$ eV and $\varepsilon_p = 8.95$ eV, respectively. When the plasma energy decreases, the dip shifts to new locations at $\delta_k = -0.017$ and $\delta_k = -0.016$. Consequently, the transparency at $\delta_k = -0.019$ disappears, and is replaced with strong absorption. This phenomenon occurs because the locations of band edges of the MPC changes when the plasma energy is modified. This change in the photonic band gap affects the linewidths Γ_b and Γ_c through the form factor (See Eqns. 2.15a and 2.17a). In summary, these results demonstrated that the system can be switched from an absorbing state to a transparent state by changing the plasma energy in the presence of dipole-dipole interaction.

To understand the physical behavior of the system at $\delta_k = -0.019$ due to the plasma energy, we have studied the time evolution of the absorption spectrum. Here, the differential equations for the density matrix elements given in Eqns. 3.6 to 3.10 in the presence of dipole-dipole interaction for a weak laser probe field ($\Omega = \Omega_c = \Omega_b = 0.01$) are solved numerically. We have used the dverk78 method (seventh-eighth order continuous Runge–Kutta) provided by Maple.

Our results show that the dverk78 method has a rather higher precision in comparison to other available methods. As an initial condition, we assume that $\rho_{aa}^{(0)} = 1$, $\rho_{bb}^{(0)} = \rho_{cc}^{(0)} = 0$ and $\rho_{ij}^{(0)} = 0$. This result is plotted in Fig. 3-4, where the dotted, dashed and long-dashed curves are plotted for plasma energies $\varepsilon_p = 9$ eV, $\varepsilon_p = 8.97$ eV and $\varepsilon_p = 8.95$ eV, respectively. Our calculations show that for $\varepsilon_p = 8.95$ eV, the absorption profile exhibits oscillations and eventually reaches a steady state. However, when we change the plasma energy to $\varepsilon_p = 9$ eV, the oscillatory behaviour of the absorption profile disappears, and the system becomes transparent, reaching its steady state exponentially.

Note that the achieved results have a reasonable explanation based on the derived theory associated with the temporal behaviour of the absorption profile. It is well-known that the number of oscillations during the temporal evolution of quantum coherence is proportional to the value of the decay rate for related energy transitions. As the linewidths increase, the number of oscillations decreases.

To show the variation of the linewidths (Γ_b and Γ_c) as a function of plasma energy, the form factor squared ($Z^2(\varepsilon_p)$) is plotted in Fig. 3-5 for different photon energies (ε_k), lying just above the upper photonic band edge. In this figure, the solid, dashed and dash-dotted curves correspond to photon energies of $\varepsilon_k = 2.6$ eV, $\varepsilon_k = 2.61$ eV and $\varepsilon_k = 2.62$ eV, respectively. From these results, it is seen that the linewidths increase when the plasma energy increases. Note that in Fig. 3-5, the lattice constant of the MPC and the radius of the metallic spheres are given as functions of the plasma energy, which is done in order to simplify our numerical simulations. For the range of plasma energies considered, the variation in these parameters is negligibly small and thus can be ignored.

We have again calculated the absorption coefficient using Eqns. 3.6 to 3.10 to investigate the accuracy of the derived analytical expression for the first configuration. We found that there is a good agreement between analytical and exact calculations, for small values of dipole-dipole interaction parameters. These results are not plotted because they give the same curves as in Fig. 3-3. This means that the analytical expression obtained in this paper gives excellent results for small values of dipole-dipole interaction parameters, and can be used by experimentalists

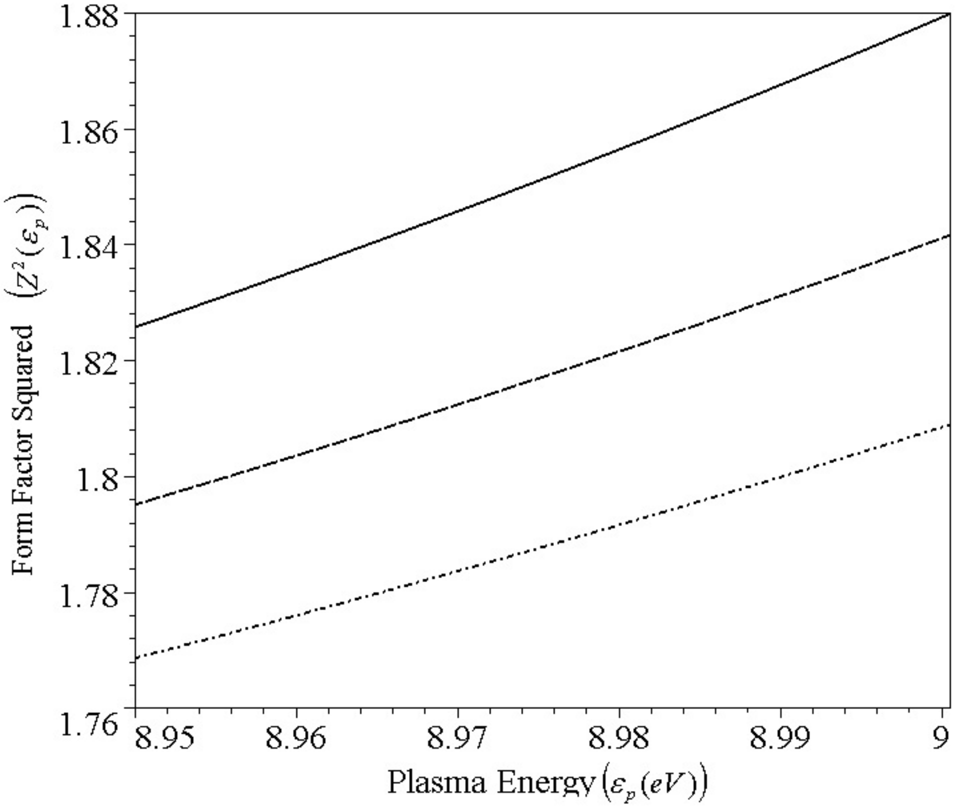

Figure 3-5: Plot of the form factor squared $Z^2(\epsilon_p)$ just above the upper photonic band edge versus the plasma energy for a MPC with $n_m(\epsilon_k) = \sqrt{1 - \epsilon_p^2/\epsilon_k^2}$, n$_b$ = 1.5, $r_s = 0.25\hbar c/\epsilon_p$ and $L = 10.5\hbar c/\epsilon_p$, for ϵ_k= 2.6 eV (solid curve), ϵ_k = 2.61 eV (dashed curve) and ϵ_k = 2.62 eV (dash-dotted curve).

to compare their results with the present theory. However, the analytical expression does not agree with the exact expression for large values of α.

In Fig. 3-6, the dashed and solid curves show results from the numerical calculation and analytical expression, respectively. As one can see for $\alpha = 0.1$, these curves are closely matched around $\delta_k = -0.02$. As the dipole-dipole interaction parameter increases to $\alpha = 0.5$, both curves shift to the left but they are no longer closely matched.

For the second configuration the normalized absorption coefficient in calculated by numerically solving Eqns. 3.6 to 3.10, with the same set of initial conditions. The pump laser field is considered to be resonant with $|b\rangle \leftrightarrow |a\rangle$ transition, (i.e. $\Delta_b = 0$). The resonance energies

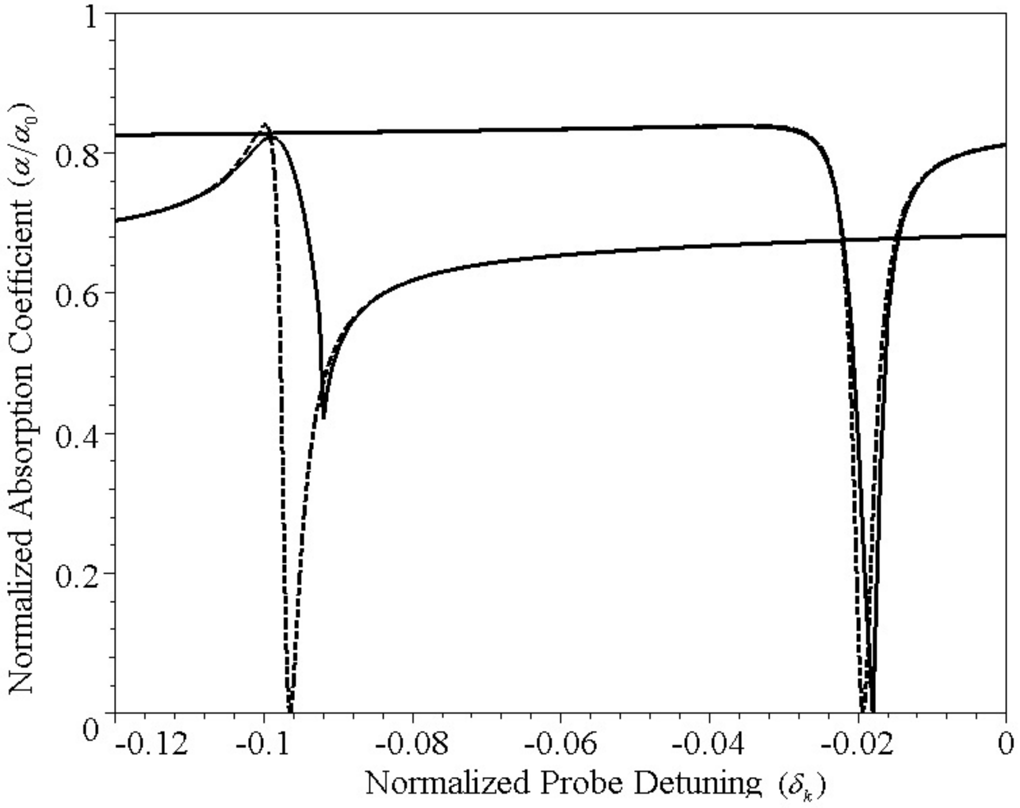

Figure 3-6: Steady state results for normalized absorption spectrum (α/α_0) in arbitrary units (a.u.) as a function of the normalized probe field detuning (δ_k). Here the dashed curves show the results obtained from the derived analytical expression given in Eq. 3.17a, while the solid curves are obtained by numerically solving Eqs. 3.6-3.10. Parameters for this figure are taken as ϵ_p= 9 eV, α=0.1 and α=0.5.

are located at $\varepsilon_{ac} = 2.4857$ eV and $\varepsilon_{ab} = 2.9$ eV. Note that in this configuration, the resonance energies are not close to each other. The normalized Rabi frequencies of the pump and probe fields are taken as $\Omega_{0c} = 1$ and $\Omega_{0b} = 20$. Here the strength of the quantum interference, P_0, is taken as 0.99 [76].

Fig. 3-7 shows the steady state of the absorption profile versus the normalized probe laser detuning ($\delta_k = 2\Delta_c/\Gamma_0$), while considering the dipole-dipole interaction ($\alpha = 1$). The solid, dashed and dash-doted curves correspond to plasma energies of $\varepsilon_p = 9.00$ eV, $\varepsilon_p = 8.999$ eV and $\varepsilon_p = 8.995$ eV, respectively. Note that the absorption coefficient has only one peak for $\varepsilon_p = 9.00$ eV, which splits into two peaks for plasma energies $\varepsilon_p = 8.999$ eV and $\varepsilon_p = 8.995$ eV.

This splitting, which is well-known as the induced Autler-Townes splitting [89], is due to the splitting of the ground state because of the presence of the strong pump field. This splitting disappears for $\varepsilon_p = 9.00$ eV because of the broadening of dressed states which are larger than the energy splitting. These results show that the system can be switched from one absorption peak to two due by changing the plasma frequency. In Fig. 3-7, the dipole-dipole interaction causes the observed asymmetry and the small amount of gain with inversion, which corresponds to the negative values of absorption.

Another remarkable result is shown in Figs. 3-8 and 3-9, where the positions of energy transitions are roughly switched with one another. Here the resonant energies are $\varepsilon_{ac} = 2.9$ eV and $\varepsilon_{ab} = 2.487$ eV. As it seen in Fig. 3-8, the peak in the absorption coefficient for $\varepsilon_p = 9.00$ eV (solid curve) is almost below zero, lying near the zero detuning parameter ($\delta_k = 0$). If we decrease ε_p, the solid peak moves above the zero line and starts splitting into two peaks due to the Autler-Townes splitting, as shown by the dashed and dotted curves. Thus, we find that the system changes from gain to absorption around the zero detuning parameter. This effect is also known as population inversion. To show the population inversion we have also plotted the population difference ($\rho_{cc} - \rho_{aa}$) in Fig. 3-9. One can see clearly that for $\varepsilon_p = 8.97$ eV and $\varepsilon_p = 8.95$ eV, there is no population inversion near the zero detuning parameter. For $\varepsilon_p = 9.00$ eV, the curve moves to positive region and population inversion occurs. This means that population inversion in the system can be achieved by changing the plasma energy.The gain state in the system is due to the quantum coherences in the $|b\rangle \leftrightarrow |a\rangle$ and $|c\rangle \leftrightarrow |a\rangle$ transitions (i.e.Im(ρ_{ba}) and Im(ρ_{ca})) and quantum interference P [90]. When the plasma energy lies, for example, at $\varepsilon_p = 8.95$ eV, Γ_b is greater than Γ_c, and so the electrons in state |b⟩ have a smaller lifetime than electrons in state |c⟩. Due to quantum coherence, more electrons move from state $|b\rangle$ to state $|c\rangle$ via state $|a\rangle$ than the electrons from state $|c\rangle$ to $|b\rangle$, but for this case we do not get $\rho_{cc} > \rho_{aa}$. However, when we change the plasma energy to $\varepsilon_p = 8.97$ eV, the linewidth for transition$|b\rangle \leftrightarrow |a\rangle$ (Γ_b) becomes very large compared to the transition $|c\rangle \leftrightarrow |a\rangle$ (Γ_c). In this case a large number of electrons move from state $|b\rangle$ to $|c\rangle$ because the lifetime of state $|b\rangle$ is very small compared to the lifetime of state $|c\rangle$; thus we observe gain.

Finally, we comment on a possible switching nanoscale device made by using the physics of the present paper. We have found that three-level quantum dots doped in metallic photonic

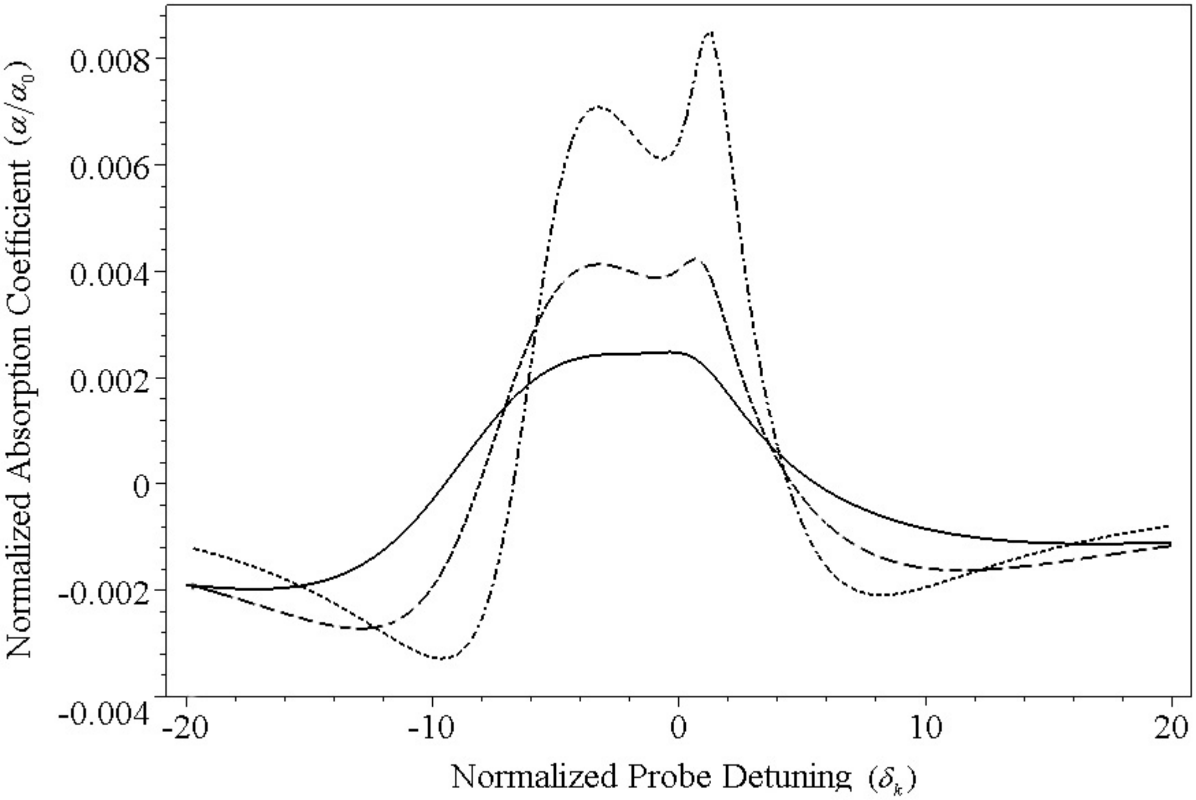

Figure 3-7: Steady state results for normalized absorption spectrum (α/α_0), in arbitrary units (a.u.), as a function of the normalized probe field detuning ($\delta_k = 2\Delta_c/\Gamma_0$) for a fixed value of DDI parameter ($\alpha = 1$) and different plasma energies. The $|c\rangle \leftrightarrow |a\rangle$ transition decay rate $\Gamma_c(\epsilon_{ac} = 2.4857$ eV) is 41.28 γ_0 for ϵ_p=9.00 eV (solid curves), 23.33 γ_0 for ϵ_p=8.999 eV (dashed curves) and 12.13 γ_0 for ϵ_p=8.995 eV (dash-dotted curves). The $|b\rangle \leftrightarrow |a\rangle$ transition decay rate $\Gamma_b(\epsilon_{ab} = 2.9eV)$ is 1.575 γ_0. The other parameters are Δ_b=0 (The pump laser field detuning), $P_0 = 0.99$ (quantum interference), Ω_{0c}=1 and Ω_{0b}=20 (normalized Rabi frequencies).

crystals can be switched from a transparent state to an absorbing state by changing the plasma energy. The plasma energy of metals can be changed by applying a pulsed magnetic field, as pointed out in Ref. [48]. By applying such a field, the photonic device formed from nano size quantum dots doped in a metallic photonic crystal can be switched from the ON position to the OFF position. For example, with a certain plasma energy the system will be in its transparent state. Therefore, in this case the probe laser will propagate through the system, and the optical switch can be considered to be in an OFF position. On the other hand, due to the application of the pulsed magnetic field, the plasma energy can be changed in such a way so that the system switches to the absorbing state. Then the laser beam will be completely reflected by the system, and in this case the switch is ON.

3.4 Conclusion

In this chapter we have studied the effect of a changing plasma frequency on the absorption profile of quantum dots. We consider that the quantum dots are doped in a metallic photonic crystal fabricated from metallic spheres embedded in a background dielectric material. These quantum dots are considered as an ensemble of three-level energy systems, containing two excited states and a ground state. The quantum dots are interacting with each other via the dipole-dipole interaction, and they are coupled with plasma-photon modes present the system. We also consider quantum interference between the two decay channels from the excited levels to the ground state. We consider that a probe laser field is applied to the system in order to study the absorption coefficient for two possible field configurations. Absorption occurs due to the transitions from the ground state to an excited state, and it is calculated by using the density matrix method. In the first configuration, the probe field couples with the ground state and the two excited states, which have energies lying very close to one another. In the dipole approximation, the transition between excited states is forbidden. In this case it is found that the position of the transparent peak is moved, due to a slight change in the plasma energy. This means that the transparent state becomes an absorbing state. In the second configuration, a pump field couples with only one excited state, while the probe field couples to the other. In this case, we found that a peak in the absorption profile appears due to plasmon coupling, and this peak splits into two peaks when the plasma energy is decreased. This change in plasma energy can also take the system from the absorption region to the gain region. These are very interesting results and can be useful for developing nanoscale plasmonic devices.

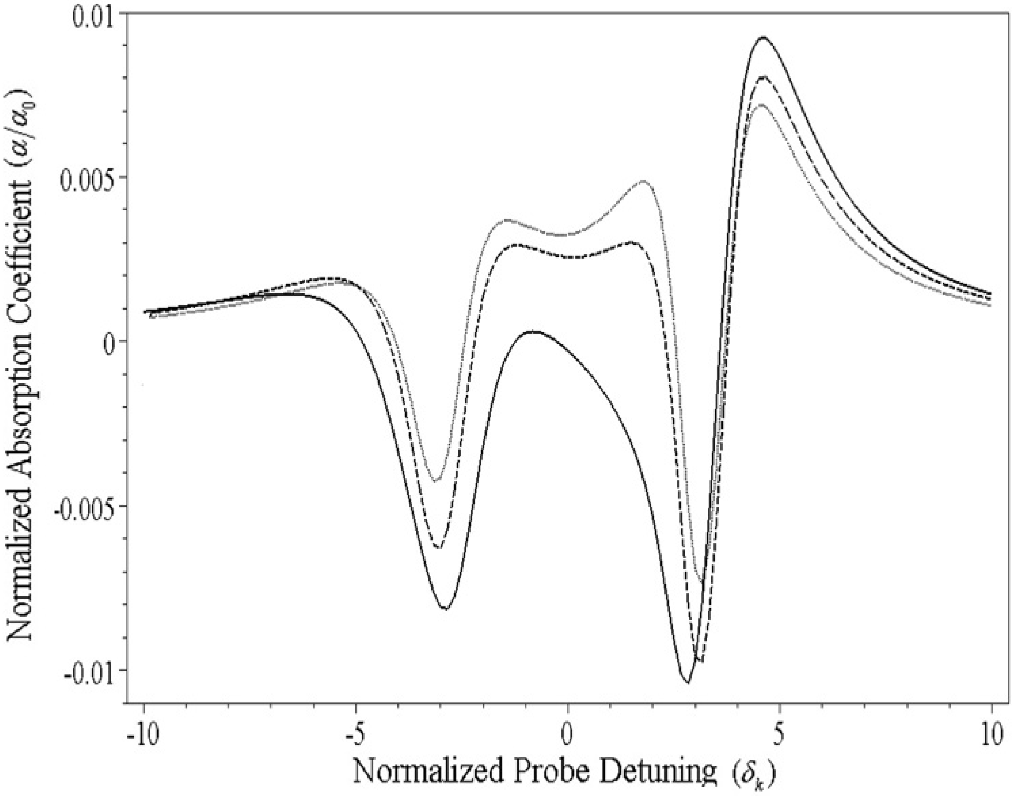

Figure 3-8: Steady state results for normalized absorption spectrum (α/α_0) in arbitrary units (a.u.) as a function of the normalized probe field detuning ($\delta_k = 2\Delta_c/\Gamma_0$) for a fixed and different value of DDI parameter and plasma energy, respectively. The $|b\rangle \leftrightarrow |a\rangle$ transition decay rate $\Gamma_b(\epsilon_{ab} = 2.487eV)$ is 12.46 γ_0 for ϵ_p=9.00 eV (solid curves), 4.90 γ_0, for ϵ_p=8.97 eV (dashed curves) and 3.98 γ_0 for ϵ_p=8.95 eV (dotted curves). The $|c\rangle \leftrightarrow |a\rangle$ transition decay rate $\Gamma_c(\epsilon_{ac} = 2.9eV)$ is 1.575 γ_0. The other parameters Δ_b=0 (The pump laser field detuning), P_0=0.99 (quantum interference), Ω_{0c}=1 and Ω_{0b}=20 (normalized Rabi frequencies).

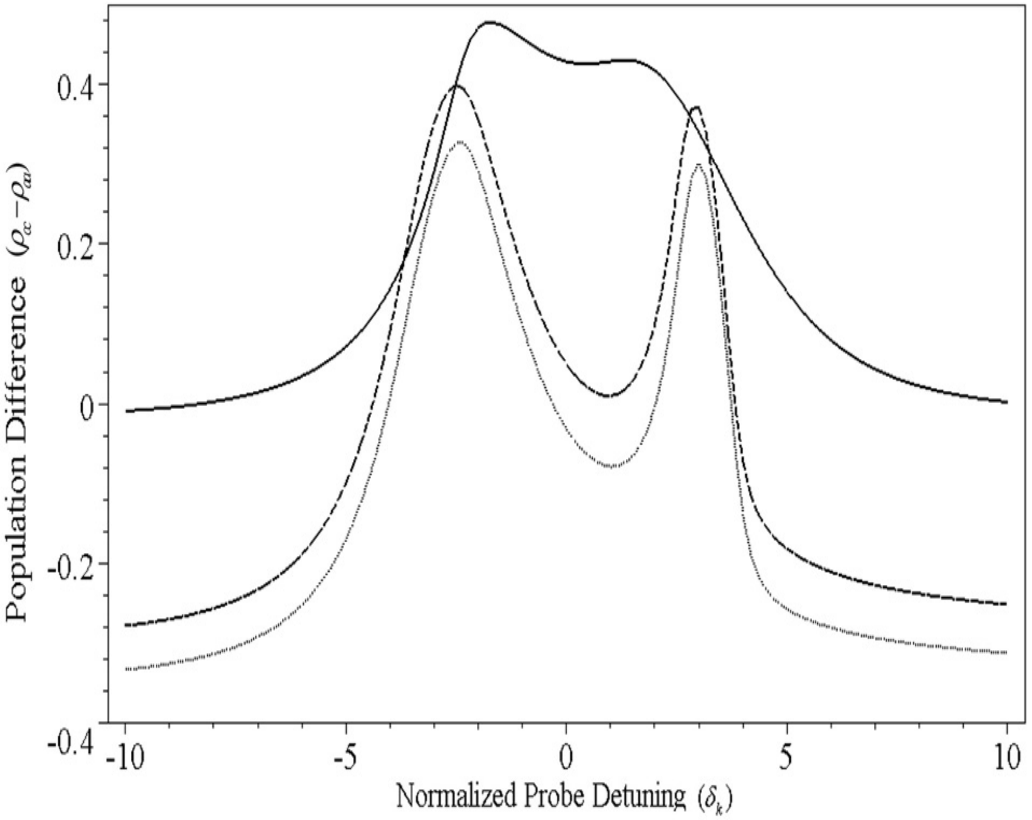

Figure 3-9: Population difference $(\rho_{cc}-\rho_{aa})$ as a function of the normalized probe field detuning $(\delta_k = 2\Delta_c/\Gamma_0)$ for a fixed and different value of DDI parameter and plasma energy, respectively. The $|b\rangle \leftrightarrow |a\rangle$ transition decay rate $\Gamma_b(\epsilon_{ab} = 2.487eV)$ is 12.46 γ_0 for ϵ_p=9.00 eV (solid curves), 4.90 γ_0, for ϵ_p=8.97 eV (dashed curves) and 3.98 γ_0 for ϵ_p=8.95 eV (dotted curves). The $|c\rangle \leftrightarrow |a\rangle$ transition decay rate $\Gamma_c(\epsilon_{ac} = 2.9eV)$ is 1.575 γ_0. The other parameters are Δ_b=0 (The pump laser field detuning), P$_0$=0.99 (quantum interference), Ω_{0c}=1 and Ω_{0b}=20 (normalized Rabi frequencies).

Chapter 4

Decay of a quantum dot in two-dimensional metallic photonic crystals

4.1 Introduction

There is a great deal of interest in two-dimensional (2-D) photonic crystals due to their relative ease of fabrication as well as the underlying idea that two-dimensional (2-D) photonic crystals can be used to develop a direct continuation of planar integrated optics [91]. Recently, 2-D MPCs have been fabricated by using various methods[92][93][94]. For example, Katsarakis *et al.* [92] reported the fabrication of 2-D MPCs consisting of square and triangular lattices of nickel pillars using deep X-ray lithography. They showed that the photonic band structures of these crystals exhibited high-pass filter characteristics with a cutoff in the far-infrared energy regime. Puscasu *et al.* [93] used a 2-D metallodielectric photonic crystal to investigate narrow-band infrared sources and spectroscopic sensors. Zhang *et al.* [94] fabricated 2-D MPC waveguides using solution-processible gold nanoparticles.

For device applications it is critical to accurately calculate higher-order photonic band gaps. Typically, the band structures of 2-D MPCs are determined with numerical approaches such as the plane wave method (PWM) [95], transfer matrix method (TMM) [96], finite-difference time-domain method (FDTD) [97] [98] and multiple multipole method (MMP) [99]. For example, Ustyantsev *et al.* [98] investigated the effect of different dielectric backgrounds on the band structure of MPCs composed of circular metallic pillars in a square lattice. They used the PWM and FDTD method to determine the photonic dispersion bands and the TMM to determine the reflectivity characteristics. Takayma and Cada [100] reported theoretical results of photonic band gaps based on the TMM for a MPC in the form of a hexagonal lattice consisting of silver pillars in anodic porous alumina. However, it is very complicated to use numerical band structure methods in studying the absorption and emission of light in these structures. On the other hand, analytical expressions are very useful for experimentalists so that they can analyze their data easily. There are also many useful applications for analytical expressions of photonic dispersion relations. For example, these expressions allow for an accurate determination of band gaps in all crystal directions. Determination of very narrow photonic band gaps is important for the design of oversized single-mode photonic cavities or waveguides. They are also very useful for rigorous error analysis and help establish error tolerance in numerical simulation techniques. Finding an analytical formulation of band structures in photonic crystals represents a major mathematical challenge because analytical expressions for the band structure are generally limited to one-dimensional structures [101]. Recently, some effort has been devoted towards developing analytical models [102][103][104][105] for 2-D photonic crystals in order to understand and predict the physical properties of these photonic crystals without the need for heavy and time consuming calculations.

Some efforts have also been placed towards obtaining analytical expressions for photonic dispersion relations in 2-D MPCs. For example, Pokrovsky *et al.* [106] presented an analytical theory for low-energy EM waves in MPCs with a small volume fraction of metal. Wang *et al.* [107] developed an analytical expression for the effective velocity of EM waves at low energies for 2-D dielectric photonic crystals and MPCs.

In this chapter we study the quantum optics and band structure of the 2-D MPC crystals. We consider 2-D MPCs made from rectangular metallic pillars arranged periodically in a 2-D plane, where air is taken as the background medium[1]. The advantage of choosing two metals

---

[1] A. Hatef and M. Singh, "Decay of a quantum dot in two-dimensional metallic photonic crystals" Optics Communications 284, 2363-2369, (2011).

lies in the fact that one can easily control the size and location of crystal's photonic band gap by manipulating the plasma frequencies of two metals rather than one. This structure has another advantage in that one can obtain analytical expressions for the band structure, density of states, linewidth and absorption coefficients. These expressions can be very useful for experimental studies and device design involving metallic photonic crystals.

We have used the TMM to derive an analytical expression of the photonic dispersion relation in our 2-D MPC. The photonic band structure is obtained by using the dispersion relation. An analytical expression of the photonic density of states has also been derived. We have investigated the effect of modifying the plasma energy of the metals in the MPC on the spontaneous emission in these structures. To study spontaneous emission, we consider the situation where a two-level quantum dot is doped in our MPC. The quantum dot is interacting with the photonic states of the crystal via the electron-photon interaction. Analytical expressions of the linewidth and spectral function of the quantum dot due to spontaneous emission have been calculated by using the Schrödinger equation method. Numerical simulations have been performed on the band structure and density of states in all 2-D crystal directions. We consider a MPC consisting of aluminum (Al) with zinc (Zn) in an air background. This structure gives a complete 2-D photonic band gap. The density of states of photons has also been calculated in all crystal directions. It is found that density of states has singularities near the band edges. This agrees with the findings of other researchers in the literature [98]. Finally we have calculated the effect of the plasma energy on the spectral function for spontaneous emission, which contains information about the linewidths of the energy levels of the quantum dot. It is found that manipulating the normalized plasma energy of the metal changes the width of the absorption peak. This means that by changing the plasma energy one can control spontaneous emission in these structures.

4.2 Two Dimensional Metallic Photonic Crystals

As is schematically depicted in Fig. 4-1, we consider a 2-D MPC made from two rectangular metallic pillars B and C with dielectric constants ϵ_b and ϵ_c, infinite in the z-direction. The unit cell is arranged in a simple tetragonal lattice. In each unit cell the opening domain (A) has a square shape, and is empty (i.e. an air space) with a dielectric constant ϵ_a. The structure is homogeneous in the z-direction and periodic in the x and y directions with period L; therefore the unit cell for this crystal is a square. The metallic pillars used in the MPC are conductors in which electrons are free to move. When an EM field is propagating in a metal, the conductivity of the metal is energy dependant. According to the Lorentz model, the dielectric constants of a metal is obtained as

$$\epsilon_{b,c}(\varepsilon_k) = 1 - \frac{\varepsilon_p^2}{\varepsilon_k\left(\varepsilon_k + i\gamma\right)} \tag{4.21}$$

where ε_p is called the plasma energy and is obtained as

$$\varepsilon_p^2 = \frac{n\hbar^2 e^2}{m\epsilon_0}. \tag{4.22}$$

The plasma energy is the natural energy of oscillation for the electron gas in the metal pillars. In the above equations, n is the electron concentration, e is the electron charge, m is the mass of an electron and γ is the relaxation energy of the electrons in a pillar.

Kady *et al.* [108] utilized the energy dependency of the real and imaginary parts of the dielectric constant for noble metals (i.e. Al, Ag, Au, and Cu). They showed that the imaginary part of dielectric constant (i.e. loss) is negligible in the range of optical and ultraviolet frequencies. Here the value of the relaxation energy is on the order of few meV and can be ignored without any significant variation in our calculations [109].

4.3 Spontaneous Emission Decay Rate

The 2-D MPC is doped with a two-level quantum dot. Energy levels of the quantum dot are denoted as $|a\rangle$ and $|b\rangle$, where the former is the ground state (see Fig. 4-2). We consider that the quantum dot decays spontaneously from the excited state to the ground state via the electron-photon (EP) interaction. The Hamiltonian of the system is written as:

$$H = \left[\begin{array}{c} \varepsilon_{ba}(\sigma_{ba}^z + \frac{1}{2}) + \int_C \frac{d\varepsilon_k}{2\pi}\varepsilon_k p^+(\varepsilon_k)p(\varepsilon_k) \\ -\int_C \frac{d\varepsilon_k}{2\pi} z(\varepsilon_k)[p(\varepsilon_k)\sigma_{ba}^+ + \sigma_{ba}^- p^+(\varepsilon_k)] \end{array}\right] \tag{4.23}$$

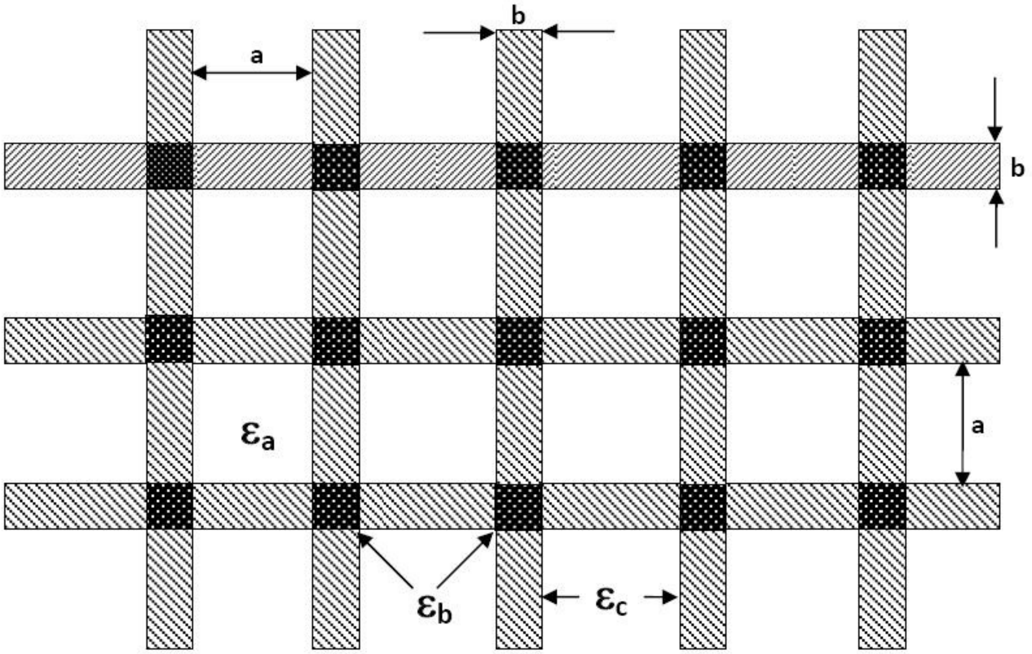

Figure 4-1: Schematic of the dielectric function in the 2-D separable rectangular MPC. The large white square region has a dielectric constant $\epsilon_a = 2n_1^2$, while the small dark square and rectangular regions have $\epsilon_b = 2n_2^2$ and $\epsilon_c = n_1^2 + n_2^2$, respectively. The parameters a and b give the thicknesses of the layers and $L = a + b$ is the lattice constant in both the x and y directions.

Here $\sigma_{ba}^{+} = |b\rangle\langle a|$, $\sigma_{ba}^{-} = |a\rangle\langle b|$ and σ_{ba}^{z}=$|b\rangle\langle b| - |a\rangle\langle a|$. The $p(\varepsilon_k)$ and $p^{+}(\varepsilon_k)$ operators denote the annihilation and creation of photons, respectively. The first and second terms correspond to the Hamiltonians of the quantum dot and photons in the photonic crystal, respectively. The third term describes the coupling between a quantum dot and photons. The integration contour C consists of two intervals: $-\infty < \varepsilon_k \leq \varepsilon_v$ and $\varepsilon_c \leq \varepsilon_k < \infty$. Here ε_v and ε_c are the lower and the upper band edges of photonic band gap, respectively, such that the photonic band gap of the the MPC lies between ε_v and ε_c. Note that there is no integration between energies ε_v and ε_c. In Eqn. 4.23 ε_k is photon energy which is obtained from the band structure of 2-D MPC. The band structure is calculated by using the separable model [102][103][104][105]. We consider transverse electric (TE) plane waves propagating in the x-y plane (i.e. $k_z = 0$) on 2-D crystal. The length and width of pillar B are taken the same, and are denoted as b. Similarly

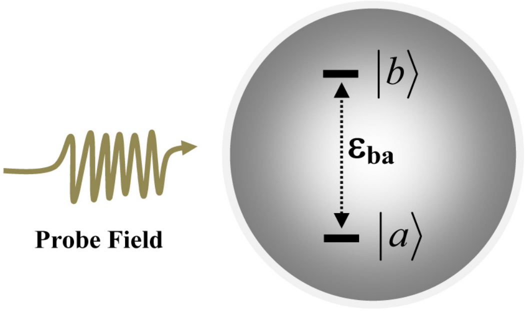

Figure 4-2: A schematic diagram of a two-level quantum dot where the levels are denoted by $|a\rangle$ and $|b\rangle$. When the quantum dot is in the excited state is decays to the ground state spontaneously.

the length and width of pillar C is taken as a and b, respectively. The periodicity of the crystal along x and y directions is given as $L = a + b$. The dispersion relation is obtained as

$$\cos\left(K_x L\right) = F_x(\varepsilon_k, \eta) \tag{4.24a}$$

$$\cos\left(K_y L\right) = F_y(\varepsilon_k, \eta) \tag{4.24b}$$

where

$$F_x(\varepsilon_k, \eta) = \phi_+ - \nu_- \varphi \tag{4.25a}$$

$$F_y(\varepsilon_k, \eta) = \phi_- \left(1 - \nu_+\right) \tag{4.25b}$$

$$\phi_\pm = \cos\left(\sqrt{\left(\frac{\varepsilon_k n_1}{\hbar c}\right)^2 \mp \eta^2} a\right) \cos\left(\sqrt{\left(\frac{\varepsilon_k n_2}{\hbar c}\right)^2 \mp \eta^2} b\right) \tag{4.26a}$$

$$\nu_\pm = \frac{\left(\frac{\varepsilon_k n_1}{\hbar c}\right)^2 + \left(\frac{\varepsilon_k n_2}{\hbar c}\right)^2 \pm 2\eta^2}{2\sqrt{\left(\frac{\varepsilon_k n_1}{\hbar c}\right)^2 - \eta^2}\sqrt{\left(\frac{\varepsilon_k n_2}{\hbar c}\right)^2 \pm \eta^2}} \tag{4.26b}$$

$$\varphi = \sin\left(\sqrt{\left(\frac{\varepsilon_k n_1}{\hbar c}\right)^2 - \eta^2} a\right) \sin\left(\sqrt{\left(\frac{\varepsilon_k n_2}{\hbar c}\right)^2 - \eta^2} b\right) \tag{4.26c}$$

where η is separation constant , n_1^2 and n_2^2 are related to ϵ_a, ϵ_b and ϵ_c as $\epsilon_a = 2n_1^2$, $\epsilon_b = 2n_2^2$ and $\epsilon_c = n_1^2 + n_2^2$. Generally, the band structure of a square lattice is plotted in symmetric directions in the Brillioiun zone. The centre of the Brillioiun zone is located at $(K_x = 0, K_y = 0)$ and is denoted as Γ. The other symmetric points are called X and M and are at $(K_x = \pi/L, K_y = 0)$ and $(K_x = 0, K_y = \pi/L)$, respectively. The band structure is then plotted along three major directions $\Gamma - X$, $\Gamma - M$ and $X - M$.

In Eqn. 4.23, $z(\varepsilon_k)$ is called the coupling constant and is obtained as

$$z(\varepsilon_k) = \sqrt{\gamma_0}\sqrt{\frac{3\pi^2\hbar^3 c^3}{d_x d_y d_z \varepsilon_k^2} D(\varepsilon_k)} \tag{4.27}$$

$$\gamma_0 = \frac{\mu^2 \varepsilon_{ba}^3}{3\pi\epsilon_0 \hbar^4 c^3} \tag{4.28}$$

where γ_0 is the linewidth for an energy level of the quantum dot when it is located in a vacuum. The coupling constant controls the coupling between photons and electrons and depends on the photon density of states function $D(\varepsilon_k)$ (density of states) in the 2-D MPC . This function is calculated from the dispersion relation (Eqns. 4.24a and 4.24b) as follows.

We consider that d_x, d_y and d_z are the dimensions of 2-D MPC along x, y and z direction, respectively. By using the concept of the density of states the summation over and K_x and K_y can be replaced by integration over photon energy ε_k as

$$\sum_{K_x}\sum_{K_y} = \int D(\varepsilon_k) d\varepsilon_k \tag{4.29}$$

where $D(\varepsilon_k)$ is obtained as

$$D(\varepsilon_k) = \frac{d_x d_y}{\pi} k_\perp \frac{dk_\perp}{d\varepsilon_k} \tag{4.30}$$

where

$$k_\perp = \frac{1}{L}\sqrt{\left[\arccos F_x(\varepsilon_k, \eta)\right]^2 + \left[\arccos F_y(\varepsilon_k, \eta)\right]^2} \tag{4.31}$$

with the help of the above equation the density of states is then evaluated as

$$D(\varepsilon_k) = \frac{d_x d_y}{\pi L}\left[\frac{G_x(\varepsilon)\xi_x\left(\varepsilon_k\right)}{\sqrt{1 - F_x^2\left(\varepsilon_k\right)}} + \frac{G_y(\varepsilon)\xi_y\left(\varepsilon_k\right)}{\sqrt{1 - F_y^2\left(\varepsilon_k\right)}}\right] \tag{4.32}$$

where

$$\xi_\pm\left(\varepsilon_k\right) = \xi_1^\pm\left(\varepsilon_k\right) + \xi_2^\pm\left(\varepsilon_k\right) + \xi_3^\pm\left(\varepsilon_k\right) \tag{4.33}$$

where

$$\xi_1^{\pm}\left(\varepsilon_k\right) = -\cos\left(k_{1\pm}a\right)\sin\left(k_{2\pm}a\right)\left(\frac{n_{2d}n_2\varepsilon_k a}{\left(\hbar c\right)^2 k_{2\pm}}\right) \tag{4.34a}$$

$$-\cos\left(k_{2\pm}a\right)\sin\left(k_{1\pm}a\right)\left(\frac{a n_1^2\varepsilon_k}{k_{1\pm}\left(\hbar c\right)^2}\right) \tag{4.34b}$$

$$\xi_1^{\pm}\left(\varepsilon_k\right) = -\cos\left(k_{1\pm}a\right)\sin\left(k_{2\pm}a\right)\left(\frac{n_{2d}n_2\varepsilon_k a}{\left(\hbar c\right)^2 k_{2\pm}}\right) \tag{4.34c}$$

$$-\cos\left(k_{2\pm}a\right)\sin\left(k_{1\pm}a\right)\left(\frac{a n_1^2\varepsilon_k}{k_{1\pm}\left(\hbar c\right)^2}\right) \tag{4.34d}$$

$$\xi_2^{\pm}\left(\varepsilon_k\right) = \sin\left(k_{1\pm}a\right)\sin\left(k_{2\pm}b\right)\times \tag{4.34e}$$

$$\left[\frac{n_{2d}n_2\varepsilon_k k_{1\pm}}{\left(\hbar c\right)^2 k_{2\pm}^3} - \frac{n_1^2\varepsilon_k}{\left(\hbar c\right)^2 k_{2\pm}k_{1\pm}} + \frac{n_1^2\varepsilon_k k_{2\pm}}{\left(\hbar c\right)^2 k_{1\pm}^3} - \frac{n_{2d}n_2\varepsilon_k}{\left(\hbar c\right)^2 k_{1\pm}k_{2\pm}}\right] \tag{4.34f}$$

$$\xi_3^{\pm}\left(\varepsilon_k\right) = \sin\left(k_{1\pm}a\right)\cos\left(k_{2\pm}a\right)\left[\frac{2n_{2d}n_2\varepsilon_k a}{\left(\hbar c\right)^2 k_{2\pm}}\right] \tag{4.34g}$$

$$+\sin\left(k_{2\pm}a\right)\cos\left(k_{1\pm}a\right)\left(\frac{a n_1^2\varepsilon_k}{k_{1\pm}\left(\hbar c\right)^2}\right) \tag{4.34h}$$

where $+$ and $-$ stand for y and x, respectively. Other terms are defined as

$$n_{2d} = \frac{\left(1+\varepsilon_p^2\varepsilon_k^{-2}\right)}{\sqrt{\left(1-\varepsilon_p^2/\varepsilon_k^2\right)}} \tag{4.35a}$$

$$k_{1-} = \sqrt{\left(\frac{\varepsilon_k n_1}{\hbar c}\right)^2 - \eta^2}, k_{1+} = \sqrt{\left(\frac{\varepsilon_k n_1}{\hbar c}\right)^2 + \eta^2} \tag{4.35b}$$

$$k_{2-} = \sqrt{\left(\frac{\varepsilon_k n_2}{\hbar c}\right)^2 - \eta^2}, k_{2+} = \sqrt{\left(\frac{\varepsilon_k n_2}{\hbar c}\right)^2 + \eta^2} \tag{4.35c}$$

To find the decay rate of the quantum dot we use the Schrödinger equation method. The Schrödinger equation is written as

$$(H-\varepsilon_k)|\psi_k\rangle = 0 \tag{4.36}$$

The eigenstate of system can be written as a single particle eigenket in the form

$$|\psi_k\rangle = g_k\ \sigma^+|0\rangle + \int_C \frac{d\varepsilon_k}{2\pi} f_k(\varepsilon_k)p^+(\varepsilon_k)|0\rangle, \tag{4.37}$$

where the vacuum state of the system is denoted as $|0\rangle$. Putting Eqn. 4.37 into Eqn. 4.36 the

Schrödinger equation takes the form

$$(\varepsilon' - \varepsilon_k) f_k(\varepsilon_k) = C\sqrt{D(\varepsilon_k)}\, g_k \tag{4.38a}$$

$$(\varepsilon_{ba} - \varepsilon_k) g_k = C \int_C \frac{d\varepsilon_k}{2\pi} \sqrt{D(\varepsilon_k)} f_k(\varepsilon_k), \tag{4.38b}$$

where C is a constant, given as

$$C = \left(\frac{3\pi^2 \hbar^3 c^3 \gamma_0}{d_x d_y d_z \varepsilon_{ba}^2} \right)^{1/2} \tag{4.39}$$

When the eigenvalue ε_k lies outside the photonic band gap the solution of the first equation can be written as

$$f_k(\varepsilon_k) = 2\pi\delta(\varepsilon' - \varepsilon_k) + \lim_{s\to 0^+} \frac{C\sqrt{D(\varepsilon_k)}}{\varepsilon' - \varepsilon_k - is} g_k. \tag{4.40}$$

Putting $f_k(\varepsilon_k)$ into Eqn. 4.38b we obtain

$$(\varepsilon_{ba} - \varepsilon_k) g_k = C\sqrt{D(\varepsilon_k)} + \lim_{s\to 0^+} \int_C \frac{d\varepsilon_k}{2\pi} \frac{C^2 D(\varepsilon_k)}{\varepsilon' - \varepsilon_k - is} g_k. \tag{4.41}$$

Let us define a quantity called self-energy $\Xi_{ba}(\varepsilon_k)$ as

$$\Xi_{ba}(\varepsilon_k) = \lim_{s\to 0^+} \int_C \frac{d\varepsilon_k}{2\pi} \frac{C^2 D(\varepsilon_k)}{\varepsilon' - \varepsilon_k - is} \tag{4.42}$$

Putting this into Eqn. 4.38b we get the expression for g_k as

$$g_k(\varepsilon_k) = \frac{C\sqrt{D(\varepsilon_k)}}{\varepsilon_{ba} - \varepsilon_k - \Xi_{ba}(\varepsilon_k)} \tag{4.43}$$

Note that Ξ_{ba} is a complex quantity. The real part of the self-energy gives the energy shift and the imaginary part gives the decay rate or linewidth:

$$\Xi_{ba} = \Delta_{ba} + i\Gamma_{ba}, \tag{4.44}$$

where

$$\Delta_{ba} = P \int_C \frac{d\varepsilon_k}{2\pi} \left(\frac{C^2 D(\varepsilon_k)}{\varepsilon' - \varepsilon_k} \right), \tag{4.45}$$

and P stands for the principal part. The expression for the linewidth is calculated as

$$\Gamma_{ba} = \gamma_0 \left(\frac{3\pi^2 \hbar^3 c^3}{d_x d_y d_z \varepsilon_{ab}^2} \right) D(\varepsilon_{ab}). \tag{4.46}$$

Note that the linewidth has a very large value when the resonance energy ε_{ba} lies near the photonic band edges but outside the photonic band gap. Putting the expression of density of states into the above expression, we find

$$\Gamma_{ba} = \gamma_0 \left(\frac{3\pi \hbar^3 c^3}{d_z \varepsilon_{ab}^2} \right) \left[\frac{G_x(\varepsilon_k) \xi_x(\varepsilon_k)}{L_x \sqrt{1 - F_x^2(\varepsilon_k)}} + \frac{G_y(\varepsilon_k) \xi_y(\varepsilon_k)}{L_y \sqrt{1 - F_y^2(\varepsilon_k)}} \right]. \tag{4.47}$$

The probability of finding the quantum dot in the excited state is then found as

$$I(\varepsilon_k) = |g_k|^2 . \tag{4.48}$$

This quantity is called the spectral density of the radiation due to spontaneous emission and is found as

$$I(\varepsilon_k) = \frac{C^2 D(\varepsilon_{ab})}{\left(\varepsilon_k - \varepsilon_{ba} + \Delta_{ba}^2\right)^2 + C^4 D^2(\varepsilon_{ab})}. \tag{4.49}$$

Note that in empty space, $I(\varepsilon_k)$ reduces into the standard Wigner-Weisskopf expression for a natural radiation line width.

4.4 Results and Discussions

For our numerical simulations of the 2-D MPC we choose a dielectric-metal composite. The structure is homogeneous in the z-direction and periodic in the x and y directions. We consider that the crystal is made from square and rectangular metallic pillars embedded in a background dielectric material. The rectangular pillars are connected to the sides of square pillars. In our simulation the background dielectric material is air. The dielectric functions in Eqns. 4.26a and 4.26c can be written as following:

$$\epsilon_a = 2n_1^2 = n_a^2 = 1 \tag{4.50a}$$

$$\epsilon_b = 2n_2^2 = n_b^2 = 1 - \frac{\varepsilon_{pb}^2}{\varepsilon^2} \tag{4.50b}$$

$$\epsilon_c = n_1^2 + n_2^2 = n_c^2 = 1 - \frac{\varepsilon_{pc}^2}{\varepsilon^2} \tag{4.50c}$$

where the ε_{bp} and ε_{cp} are the plasma energy of pillars A and B, respectively. Substituting the values of $n_1^2 = \frac{1}{2}$ and $n_2^2 = \frac{1}{2}(1 - \frac{\varepsilon_{pb}^2}{\varepsilon^2})$ into Eqns. 4.50a to 4.50c we get the following relation between the plasma frequencies of the metallic pillars.

$$\varepsilon_{pc} = \frac{\varepsilon_{pb}}{\sqrt{2}} \tag{4.51}$$

This shows that our calculation is valid for any metallic pillars which satisfy this relation. Several options are available for different metals whose plasma energies satisfy Eqn. 4.51. For instance, options for pillars B and C include aluminium (Al) and zinc (Zn), with plasma energies $\varepsilon_{p(Al)} = 15.1$ eV [110] and $\varepsilon_{p(Zn)} = 10.1$ eV [111] or copper (Cu) and platinum (Pt) with plasma energies of $\varepsilon_{p(Cu)} = 7.4$ eV and $\varepsilon_{p(Pt)} = 5.1$ eV [112]. In our simulations, ε_{pb} is chosen to satisfy the relation $\frac{\varepsilon_{pb} L}{2\pi\hbar c} = \lambda$ in order to study the effect of changing plasma energy, and we take $n_1^2 = 0.5$ and $n_2^2 = 0.5 - \frac{1}{\varepsilon_n^2}$, where $\varepsilon_n = \frac{\sqrt{2}}{\lambda} \frac{L\varepsilon_k}{2\pi\hbar c} = \sqrt{2}\frac{\varepsilon_k}{\varepsilon_{pb}}$ is defined as the normalized energy.

In order to visualize and analyze the direction and propagation behavior of incident EM waves inside the MPC, we employ constant-energy contour diagrams in wave vector space (K) whose gradient vectors give the group velocities of the photonic modes. To plot constant-energy contours of the crystal we eliminate η in Eqns. 4.24a and 4.24b using MAPLE code for plotting a parametric system of real nonlinear equations.

Fig. 4-3 illustrate several constant-energy contours, which are the projections of the photonic bands in the (K_x, K_y) plane, for various normalized energy in the reduced Brillouin zone ($-1 < K_x L/\pi < 1$, $-1 < K_y L/\pi < 1$). For the given parameters ($a = 0.5L$ and $b = 0.5L$) and $\lambda = 1$, our calculations show there is a low-energy complete photonic band gap from zero up to a normalized cut-off energy ($\varepsilon_n = 0.9$), and below that the normal surface is an exact square which means no EM modes can propagate through the crystal, and hence the MCP

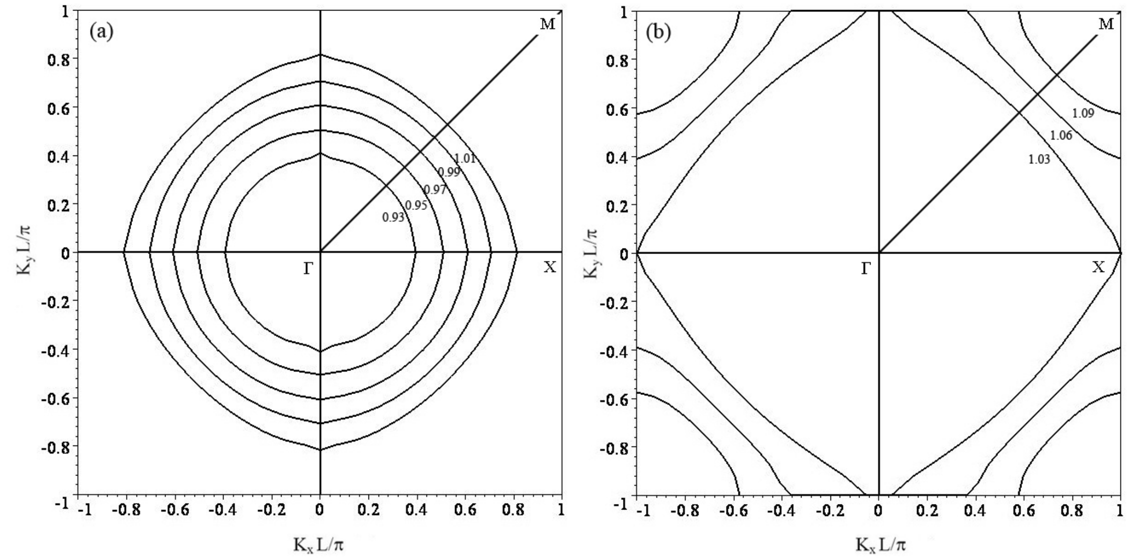

Figure 4-3: Normal surface in the (K_x, K_y) plane of the 2-D MPC at different normalized energies. The normal surfaces plotted in the reduced Brillouin zone exhibit a fourfold symmetry. The parameters are $n_1^2 = 0.5$, $n_2^2 = 0.5 - 1/\varepsilon_n^2$, $a = 0.5L$ and $b = 0.5L$.

behaves like a perfect reflector. However, a high-energy complete photonic band gap appears in the normalized energy region between (1.15, 1.30) where the normal surfaces on this range of energy are all exactly square (see Fig. 4-3). Above the normalized cut-off energy between (0.93, 1.01) the contours are in the form of circles, meaning that the MPC behaves like a isotropic homogenous medium. By increasing the normalized energy the contours are no longer circular, showing the effect of the periodic structure of MPC. For example, at the normalized energy of $\varepsilon_n = 1.03$, a partial photonic band gap occurs at $K_x L/\pi = 1$. However, at the normalized energy of $\varepsilon_n = 1.06$ a partial photonic band gap occurs at $K_x L/\pi = 1$ and $K_y L/\pi = 1$.

We also studied the effect of an increase in the plasma energy on the photonic band gap; our calculations show that by increasing the value of plasma energy the photonic band gap shifts towards the smaller energies. For example for 5% ($\lambda = 1.05$) and 10% ($\lambda = 1.10$) increases in plasma energy, the normalized full photonic band gap lies between (1.10, 1.28) and (1.00, 1.27), respectively. Using the relation between normalized energy and real energy one can easily calculate the range of the energies of the photonic band gap. For example for $\varepsilon_{pb} = 15.1$ eV the photonic band gap for $\lambda = 1.0$ lies in the ultraviolet region of the electromagnetic spectrum between (12.28 eV, 13.89 eV).

Fig. 4-4 shows the numerical result of the band structure for TE waves with the electric

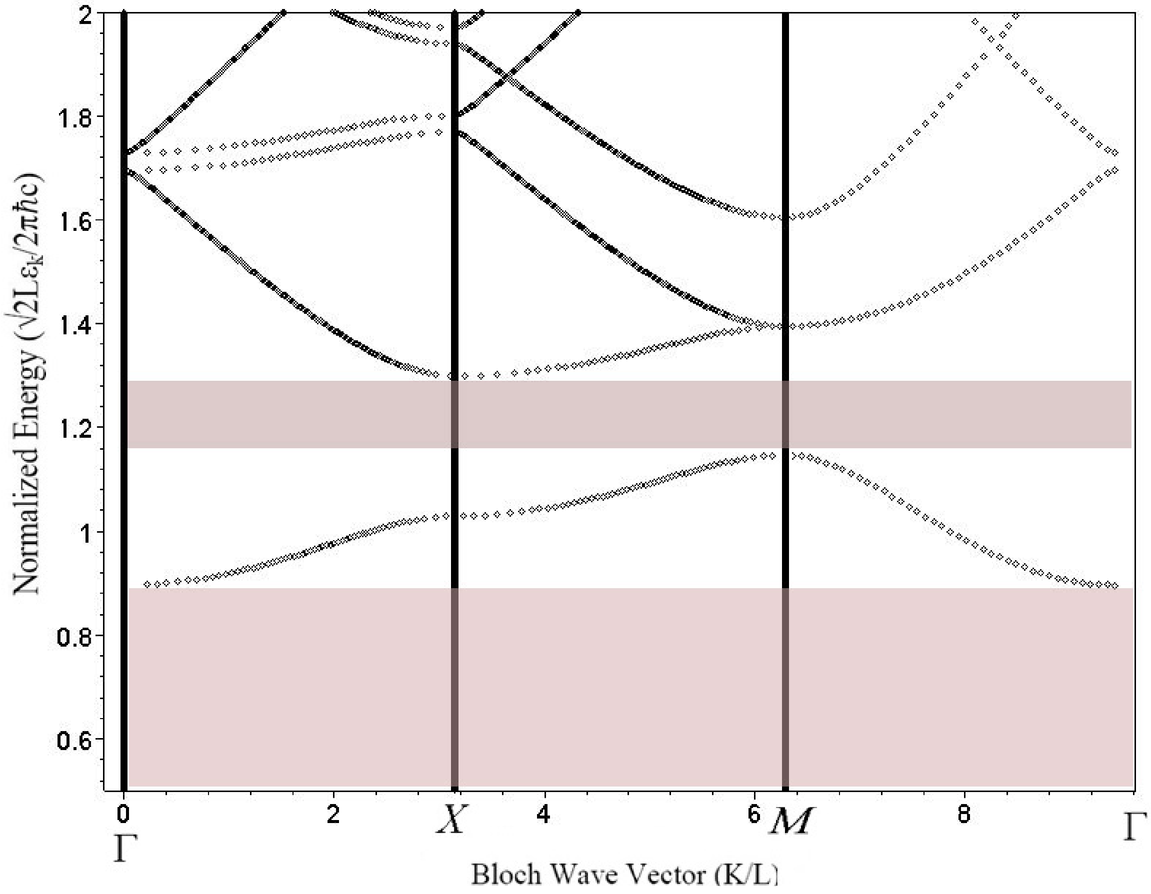

Figure 4-4: Band structure of the 2-D MPC with parameters $n_1^2 = 0.5$, $n_2^2 = 0.5 - 1/\varepsilon_n^2$, $a = 0.5L$ and $b = 0.5L$. The vertical axis is the normalized energy (ε_n) and the horizontal axis is normalized wave vector (K/L). Special points Γ, M, X correspond to $K = 0$, $K = (\pi/L)i$, $K = (\pi/L)i+ (\pi/L)j$ and $K = (\pi/L)j$ respectively. The second complete PBG occupies the normalized energy region between (1.15, 1.30).

field vector lying perpendicular to the plane of propagation (K_x, K_y plane) along the paths connected by the symmetry wave vector points of Γ, X and M. These points are located at ($K_x = 0, K_y = 0$), ($K_x = \pi/L$, $K_y = 0$) and ($K_x = \pi/L, K_y = \pi/L$), respectively. To calculate the band structure of rectangular MPC we have developed MAPLE code for solving the system of real nonlinear equations given in Eqns. 4.24a and 4.24b using the function FSOLVE. To plot the band structure along the $\Gamma - X$ direction, we set $K_y = 0$ in Eqn. 4.24b and divide the normalized energy into 600 intervals ($[\varepsilon_{n_i}, \varepsilon_{n_{i+1}}]$, $i = 0,\ 1,\ 2...600$). Substituting a given value of normalized energy (ε_n) we are able to determine the values of η, and using these values with their correspondent normalized energy in Eqn. 4.24a, we obtain the corresponding value of K_x between $(0,\ \pi/L)$. In this direction we have the largest photonic band gap, which lies between (1.03, 1.3). In the $X - M$ direction we put $K_x = \pi/L$ in Eqn. 4.24a and perform the same calculation to find all the possible values of K_y between $(0,\ \pi/L)$. In this direction the photonic band gap lies between (1.15, 1.3). For the $M - \Gamma$ direction we divide the ($K = 0$, $K = \pi/L$) interval into 40 intervals ($[K_i, K_{i+1}]$, $i = 0,\ 1,\ 2...40$) and use the same K_i instead of K_x and K_y in Eqns. 4.24a and 4.24b. We simultaneously solve these equations for η and normalized energy. In this direction the first photonic band gap occurs at the normalized energy between (1.15, 1.4). Our results are approximately consistent with results found by Ustyantsev *et al.* [98], especially in first and second bands, where they used the FDTD method combined with auxiliary differential equations. Their photonic crystal was composed of circular metallic rods arranged in a square lattice and embedded in an air background.

The existence of photonic band gaps in each direction is confirmed in the density of states calculation. We show that the density of states vanishes for energies lying within the photonic band gap. To calculate the spectral density of the radiation due to spontaneous emission, one needs to find the total density of states by adding up all the values of density of states in each direction for a given energy.

To calculate this parameter we used Eqns. 4.33 to 4.34g and the developed MAPLE code which uses the FSOLVE function. We divide the ($K = 0, K = \pi/L$) interval into 40 intervals ($[K_i, K_{i+1}]$, $i = 0,\ 1,\ 2...40$). Substituting each K_i instead of K_x and K_y in Eqns. 4.25a to 4.26c for each direction gives all the possible solutions for η and normalized energy. We substituted these solutions in Eqn. 4.32 and calculate the total density of states value. The results of the calculation for $\lambda = 1.0$ is shown in Fig. 4-5, where we show that the density of states vanishes in the region of the photonic band gap. Note that at the band edges the value of density of states approaches infinity. To show the detailed features of the of density of states behavior, we omit values greater than 150.

The normalized spectral function $I(\varepsilon)/I(0)$ has also been calculated as a function of energy, where the results are shown in Fig. 4-6. The peak of the spectrum is located at zero detuning.

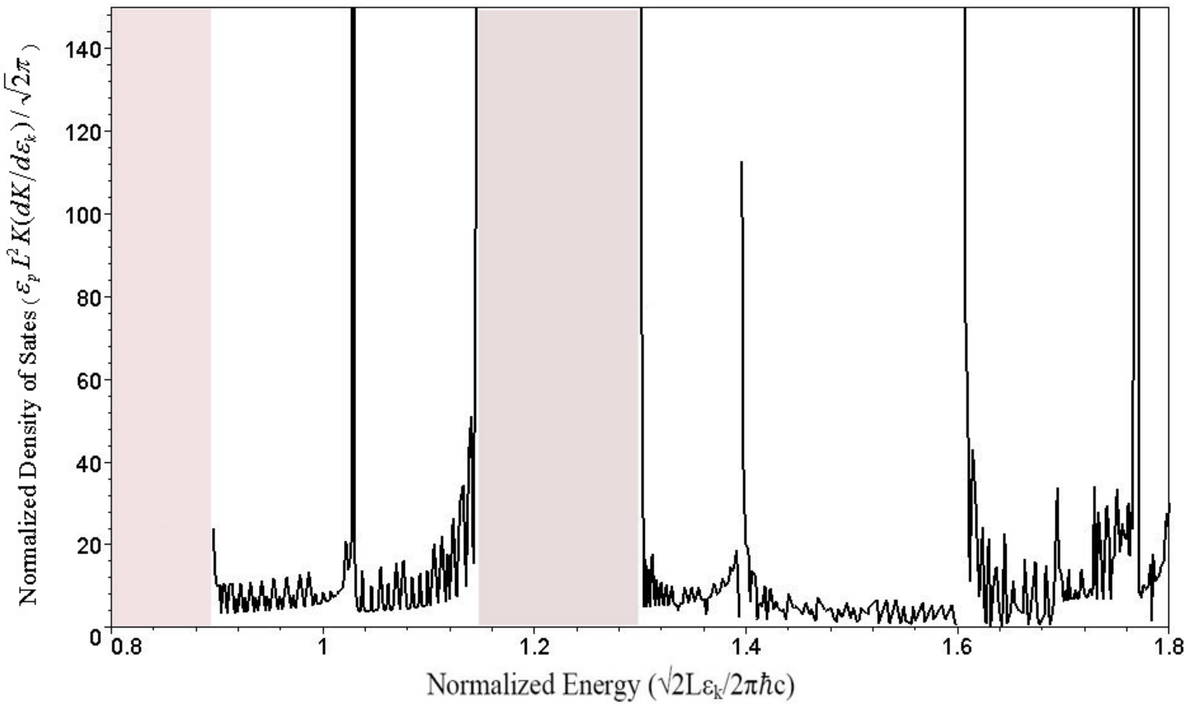

Figure 4-5: Plot of the normalized density of states $D(\varepsilon_n)$ of the MPC versus the normalized energy $\left(\frac{\sqrt{2}L\varepsilon_k}{2\pi\hbar c}\right)$ with parameters $n_1^2 = 0.5$, $n_2^2 = 0.5 - 1/\varepsilon_n^2$, $a = 0.5L$ and $b = 0.5L$.

We know that the width of the peak at half maximum gives the linewidth. It can be proved as follows: The height of the maximum is $I(0) = 2I_0/\Gamma$. Then the half maximum has value I_0/Γ. Putting this into Eqn. 4.49 we get

$$\frac{I_0}{\Gamma} = I_0 \frac{\Gamma/2}{\left(\varepsilon_k - \varepsilon_{ba}\right)^2 + [\Gamma/2]^2}. \tag{4.52}$$

Solving this equation we get

$$\varepsilon_{\pm} = \varepsilon_{ba} \pm \Gamma/2. \tag{4.53}$$

This proves that the energy width $(\varepsilon_+ - \varepsilon_-)$ of the half maxima is equal to Γ.

To calculate the linewidth for different excitation energies (ε_{ba}) we use Eqn. 4.47, where the height of the 2-D MPC and the plasma energy is 200 nm and $\varepsilon_{p(Al)} = 15.1$ eV, respectively. We choose three excitation energies energies which are far away from ($\varepsilon_{ba} = 10.7$ eV), close to ($\varepsilon_{ba} = 11.75$ eV) and very close to ($\varepsilon_{ba} = 12.1$ eV) the lower-energy photonic band gap. The values of the linewidth for these three energies are $3.1\gamma_0$, $2.8\gamma_0$ and $12.1\gamma_0$, respectively. The results from our simulation of the normalized spectral function are shown in Fig. 4-7. Note that the dotted curve has the greatest width because of the maximum linewidth near the edge of the photonic band gap. We also studied the normalized spectral function's variation due to modification of the plasma energy. Fig. 4-7 shows the behavior of the spectral function for a fixed energy, $\varepsilon_{ba} = 10.8$ eV, where the solid, dashed and dotted curves correspond to $\lambda = 1.00$, 1.05 and 1.10, respectively. The values of the linewidth energies are $5.70\gamma_0$ ($\lambda = 1.0$), $3.99\gamma_0$ ($\lambda = 1.05$) and $7.09\gamma_0$ ($\lambda = 1.10$). Note when the plasma energy is changed, the linewidth is also changed. This occurs due to the linewidth dependency on the density of states, as pointed out by Eqn. 4.47.

4.5 Conclusions

We have developed an analytical theory for the photonic band structure and density of states of two-dimensional rectangular metallic photonic crystals. The transfer matrix method is used to derive analytical expressions for the dispersion relation of the metallic photonic crystal, which

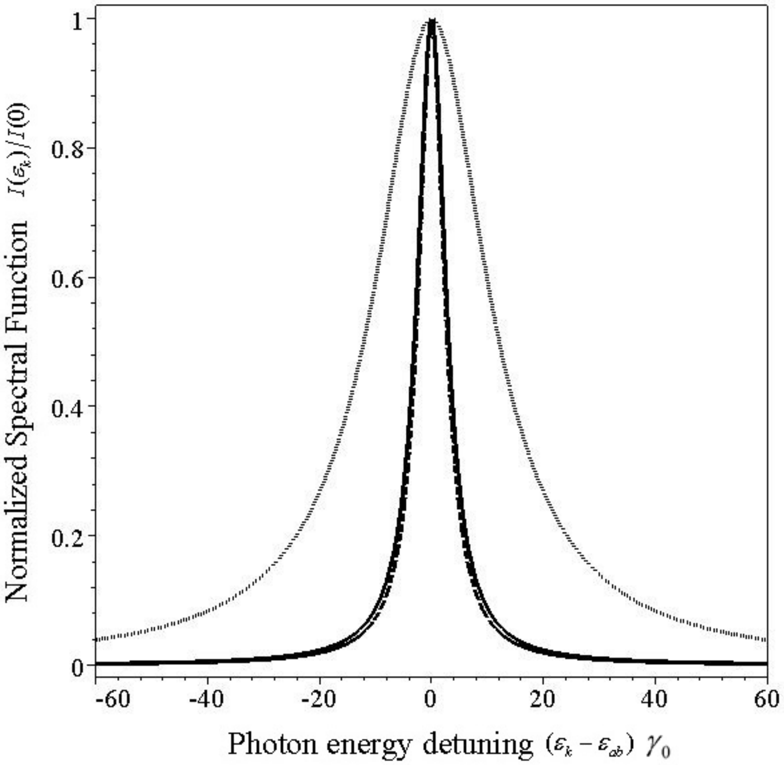

Figure 4-6: Plot of the normalized spectral function as a function of photon energy detuning for different resonance energies (ε_{ba}) and a fixed normalized plasma energy ($\lambda = 1.0$). Here, the height of the 2-D MPC is 200 nm and the plasma energy is $\varepsilon_{p(Al)} = 15.1$ eV. The excitation energies are $\varepsilon_{ba} = 10.7$ eV , $\varepsilon_{ba} = 11.75$ eV and $\varepsilon_{ba} = 12.1$ eV. The values of the linewidth for these three energies are $\Gamma = 3.1\gamma_0$ (dashed line), $2.8\gamma_0$ (solid line) and $12.1\gamma_0$ (dotted line), respectively.

are used to obtain its photonic band structure. Our band structure calculations show that the metallic photonic crystal considered here forms a complete two-dimensional photonic band gap. We found that the location of the photonic band gap can be controlled by modifying the plasma energy of either metal. For example, by increasing the plasma energy the band gap shifts towards lower energies. In the case of aluminum (Al) and zinc (Zn) the photonic band gap lies in the ultraviolet region. An analytical expression of the photonic density of states has been derived from the dispersion relation. It is found that the photonic density of states has singularities near the edges of the photonic band gaps. We have considered the case where

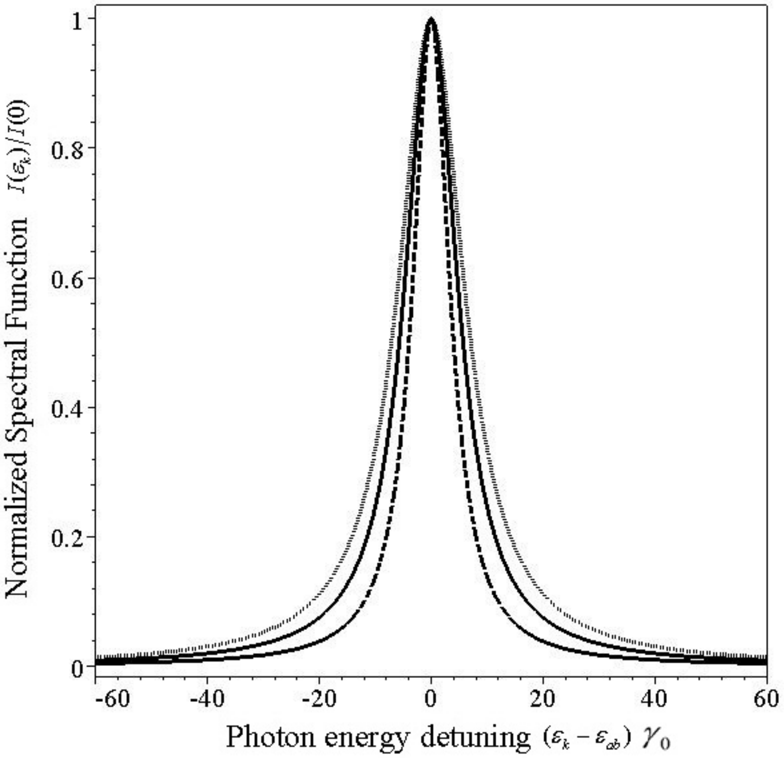

Figure 4-7: Plot of the normalized spectral function as a function of the photon energy detuning for a fixed resonance energy ($\varepsilon_{ba} = 10.8$ eV) and diffrent normalized plasma energies ($\lambda = 1.0, 1.05$ and 1.10). Here, the excition energy is $\varepsilon_{ba} = 10.8$ eV. The solid, dashed and dotted curves correspond to $\lambda = 1.00$, 1.05 and 1.10, respectively. The values of the linewidth energies are $5.70\gamma_0$ for $\lambda = 1.0$, $3.99\gamma_0$ for $\lambda = 1.05$ and $7.09\gamma_0$ for $\lambda = 1.10$.

a two-level quantum dot is doped in the metallic photonic crystal, and have calculated the linewidth and spectral function due to spontaneous emission using our analytical expression for the photonic density of states. The linewidth and spectral function of the quantum dot due to spontaneous emission were calculated by using the Schrödinger equation method. Finally, we showed that by changing the plasma energy one can control the spontaneous emission in the metallic photonic crystal.

Chapter 5

Plasmonic electromagnetically induced transparency in metallic nanoparticle-quantum dot hybrid systems

5.1 Introduction

Recently, significant attention has been paid to the investigation of the hybrid nanostructures combining different types of nanoparticles such as nanowires, semiconductor quantum dots (QDs), metal nanoparticles (MPs), etc. A significant amount of this research has been focused on hybrid QD-MP systems. It is well understood that when the plasmon resonances in MPs match the excitonic transitions of QDs many diverse optical effects can appear. Hybrid QD-MP systems have been used in the investigation of DNA sensors [113][114], laser systems without cavities [115], manipulation of heat generation in MPs [116][31], nanothermometers [117], etc.

In the majority of these studies, the QDs were taken as two level localized quantum systems. Recently, however, several interesting results have been reported where QDs were instead treated as multi-level systems. For example, Yannopapas et al. [118] showed that the quantum interference between two spontaneous emission channels can be greatly enhanced when a three-

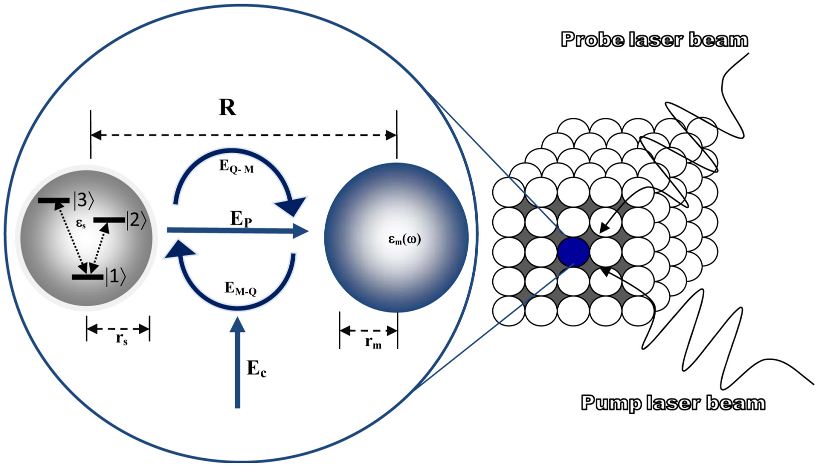

Figure 5-1: Schematic illustration of the QD–MP hybrid system embedded into a photonic crystal background. Two probe (E_p) and control (E_c) external fields are applied on the system. The curved arrows show the dipole-dipole QD-MP interaction. The MP has radius a and dielectric function $\epsilon_m(\omega)$. The QD is considered as a three-level V-configuration with dielectric constants of ϵ_s.

level V-type atom is placed near plasmonic nanostructures such as metallic slabs, nanospheres, or periodic arrays of metal-coated spheres. Sadeghi et al. [31] studied the application of an infrared laser to control heat dissipation in a MP when it is in the vicinity of a three-level ladder-type QD. They showed that the infrared laser causes a transparency window to appear in the absorption rate spectrum of the MP, making it non-dissipative at a frequency which has maximum absorption in the absence of the infrared laser.

In previous investigations the background media of the QD-MP systems were mostly isotropic with uniform refractive indices. In this chapter for the first time, to our knowledge, we theoretically investigate the MP energy absorption rate of a hybrid QD-MP system when the system is embedded in a three-dimensional photonic crystal. Photonic crystals are periodic dielectric structures that possess one or more global photonic band gaps, and have been widely used to manipulate light on the nanoscale to strongly enhance light-matter interactions [2][3]. Photonic crystals can act as a background material or a modified quantum electrodynamic vacuum for active media such as atoms, molecules, semiconductor quantum dots and hybrid nanostructure systems. The quantum optical and the nonlinear optical responses of such active media are noticeably altered from their behaviour in free space. This modification manifests as an inhibition or strong alteration of spontaneous emission of the excited states in such systems [37][38]. These abilities have led to the design of novel photonic devices such as nano-optical switching elements [119], laser systems with very low thresholds [120], quantum buffers [121], etc. The QD has three excitonic states which form a V-type atomic configuration. Two laser fields are applied, each of which drives one of the two transitions in the QD (see Fig. 5-1). In this chapter[1], we first investigate the impact of a QD with a V-configuration on the energy dissipation of the MP, and then study the role of the photonic crystal. We independently consider both the excitonic resonance frequencies ($|2\rangle \leftrightarrow |1\rangle$ and $|3\rangle \leftrightarrow |1\rangle$ transitions) to be close to the upper edge of the photonic band gap.

We perform all the calculations in strong-coupling (nonlinear) regime, wherein an exciton-induced transparency (EIT) appears in the absorbed energy rate spectrum of the MP. Here EIT occurs due to destructive interference between the applied electric field and the field from the QD acting on the MP. In this situation the coupling between the QD and MP is strong enough that the induced local field at the MP becomes larger than the applied external field with frequency close to the QD exciton resonance. We demonstrate that the photonic crystal allows us to switch the absorption of the MP at a given frequency range when the excitonic frequencies lie near the band edge. Our results also show that when the hybrid system is probed around the frequency of the $|2\rangle \leftrightarrow |1\rangle$ transition, three exciton-induced transparencies may appear. These results show the significant impact of the control field, which is in resonant with the $|1\rangle \leftrightarrow |3\rangle$ transition, and configuration of QDs in the heat dissipation of MPs.

5.2 Formalism

We consider three excitonic states of a QD where $|1\rangle$ refers to the excitonic ground state and $|2\rangle$ and $|3\rangle$ are two upper excitonic excited states (see Fig. 5-2). The frequencies of the transitions between $|1\rangle \leftrightarrow |2\rangle$ and $|1\rangle \leftrightarrow |3\rangle$ are denoted as ω_{21} and ω_{31}, respectively. The entire system is subjected to two applied electric fields $E_c = \frac{E_c^0}{2}e^{-i\omega_c t}$ (control field) and $E_p = \frac{E_p^0}{2}e^{-i\omega_p t}$ (probe field). The probe (E_p) and control fields (E_c) drive the exciton transitions $|1\rangle \leftrightarrow |2\rangle$

---

[1] A. Hatef, Seyed M. Sadeghi and M. Singh, "Plasmonic electromagnetically induced transparency in metallic nanoparticle-quantum dot hybrid systems", Nanotechnology- NANO/403136/PAP, (Accepted 12/2011).

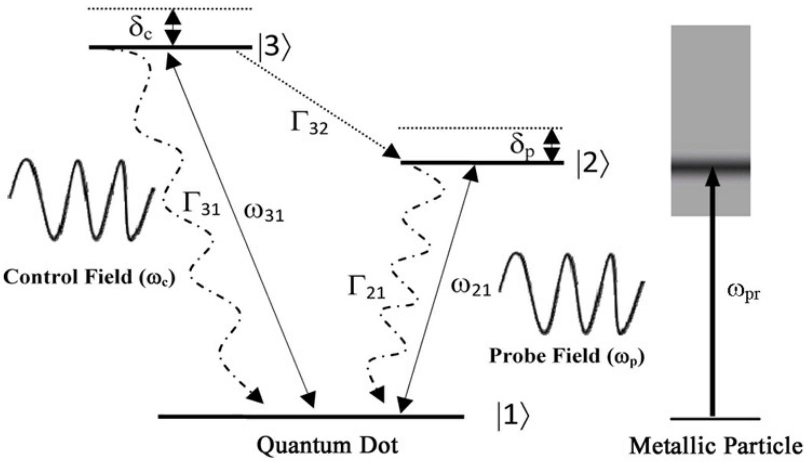

Figure 5-2: Schematic illustration of the three-level V configuration QD (left) with two upper excitonic states $|3\rangle$ and $|2\rangle$ and ground sate $|1\rangle$. The frequency difference between transitions $|2\rangle \longrightarrow |1\rangle$ and $|3\rangle \longrightarrow |1\rangle$ are denoted as ω_{21} and ω_{31}, respectively. Γ_{21} and Γ_{31} are the decay rates from the upper excitonic states to ground state. Γ_{32} is the non-radiative decay rate for state transition $|3\rangle \rightarrow |2\rangle$ .The three-level quantum dot driven by a probe laser field with energy ω_2 and ω_1, respectively. $\delta_c = \omega_{31} - \omega_c$, and $\delta_p = \omega_{21} - \omega_p$, are the detunings of the excitonic transitions. The shaded area shows the energy band of the MP (right) where the dark strip shows the plasmon resonance energy which is the same as the frequency of excitonic transition $|1\rangle \leftrightarrow |2\rangle$.

and $|1\rangle \leftrightarrow |3\rangle$, respectively. The induced dipole moments for transitions $|1\rangle \leftrightarrow |2\rangle$ (μ_{12}) and $|1\rangle \leftrightarrow |3\rangle$ (μ_{13}) are considered to be perpendicular to each other [122][123]. The QD is also interacting with the plasmonic excitations of the MP, where it is considered that the exciton transition frequency ω_{21} lies near the plasmon resonance energy ω_{pr} (see Fig. 5-2). On the other hand, the exciton transition frequency ω_{31} lies far away from the plasmon resonance frequency of the MP. Furthermore, we assume that the control field is at resonance with the excitonic transition $|1\rangle \leftrightarrow |3\rangle$. Here the QD and MP are both spherical with radii r_s and r_m, respectively, and the center-to-center distance between the QD and the MP is denoted as R. We consider that the whole system is embedded in a 3-D photonic band gap (PBG) structure. As a result, the QD is influenced by both the near field of the MP [116] and the modified electromagnetic vacuum reservoir of the photonic crystal.

To study this system we first consider the interaction of the QD with the MP alone, and then introduce the effect of the surrounding photonic crystal. Here we consider that the frequency of the control laser field (ω_c) is larger than the exciton transition frequency ω_{21} and plasmon frequency ω_{pr}, and that $\omega_{21} \approx \omega_{pr}$. As a result, the absorption of the control laser field by the MP and by the $|1\rangle \leftrightarrow |2\rangle$ excitonic transition is ignored. Therefore, the net electric field seen by the QD is given from [33]

$$E_Q = \frac{E_c}{2\epsilon_{dr}} + \frac{E_p}{2\epsilon_{dr}} + \frac{gP_m}{(4\pi\epsilon_B\epsilon_0)\,\epsilon_{dr}R^3} \tag{5.1}$$

where $\epsilon_{dr} = (2\epsilon_B + \epsilon_s)/3\epsilon_B$. Here ϵ_B, ϵ_s and ϵ_0 are the dielectric constant of the background material, dielectric constant of the QD and permittivity of free space, respectively. The factor g is the polarization parameter and has value of $g = 2\ (-1)$ when the external fields are parallel (perpendicular) to the major axis of the hybrid system. In Eqn. 5.1 the first two terms are represent the effect of the probe and control fields while the last term is the dipolar electric field created by the MP, where the dipole P_m is generated by the charge induced on the surface of the MP.

The dipole moment P_m is influenced by the direct interaction of the external laser field with the MP and by the electric dipole field generated by the QD due to transition $|1\rangle \leftrightarrow |2\rangle$. It is obtained as [124]:

$$P_m = (4\pi\epsilon_B\epsilon_0)\,r_m^3 \left(E_p + \frac{g\mu_{12}(\widetilde{\rho}_{12} + \widetilde{\rho}_{21})}{(4\pi\epsilon_B\epsilon_0)\,\epsilon_{dr}R^3}\right) \tag{5.2}$$

where $\gamma = [\epsilon_m(\omega) - \epsilon_B] / [2\epsilon_B + \epsilon_m(\omega)]$. We describe the MP with the local dynamic of dielecteric function $\epsilon_m(\omega) = \epsilon_{IB}(\omega) + \epsilon_D(\omega)$, which is a combination of the contribution of d electrons ($\epsilon_{IB}(\omega)$) and s electrons ($\epsilon_D(\omega)$) in the MP. The dielectric function $\epsilon_D(\omega)$ is obtained from the Drude model as [125].

$$\epsilon_D(\omega) = 1 - \frac{\omega_p^2}{\omega^2 + i\omega\left(\gamma_{bulk} + \frac{Av_F}{r_m}\right)} \tag{5.3}$$

where γ_{bulk} is the bulk damping constant, v_F is the velocity of the electrons at Fermi energy and A is a model-dependent parameter. In Eqn. 5.2 μ_{12} and $\widetilde{\rho}_{12} = \rho_{12}e^{-i\omega_p t}$ are the dipole moment and density matrix element (coherence term) of the QD in the hybrid system for the transition $|1\rangle \leftrightarrow |2\rangle$, respectively. Putting Eqn. 5.2 into Eqn. 5.1 we get

$$E_Q = \frac{E_c^0}{2\epsilon_{dr}} e^{-i\omega_c t} + \left(\frac{E_p^0}{2\epsilon_{dr}} + \frac{E_p^0}{2\epsilon_{dr}} \frac{\gamma g r_m^3}{R^3} + \frac{\gamma r_m^3 g^2 \mu_{12}}{(4\pi\epsilon_B\epsilon_0)\,\epsilon_{dr}^2 R^6} \rho_{12} \right) e^{-i\omega_p t} + C.C. \tag{5.4}$$

Note that Eqn. 5.4 shows the contributions of different electric fields experienced by the QD when the hybrid system is placed under the influence of the external probe and control fields. The first and the second terms are the contribution from the external fields, the third term is due to the field generated by the plasmons directly excited by the external field and the fourth term represents the indirect self-action contribution of the QD via the MP, which shows the dependency of the field inside the QD on its own dipole moment.

The probe field energy absorbed by the QD-MP system is due to the absorption of energy required to create excitons in the QD followed by a nonradiative decay and energy absorbed by the MP. The total absorbed energy rate by the QD-MP hybrid system is [124]:

$$Q_T = Q_{QD} + Q_{MP} = \hbar\omega_{21}\rho_{22}\Gamma_2 + 2\pi\varepsilon_0\omega_{21}r_m^3\,\mathrm{Im}(\gamma)(E_r^2 + E_i^2) \tag{5.5}$$

where the first and second terms show the absorption energy rates in the QD and MP, respectively. In the above expression, E_r and E_i are the components of the total electric field applied on the MP due to the external probe field and the polarization of the QD. E_r and E_i are in and 90° out of the phase with the applied field, respectively. These components are obtained as [33]:

$$E_r = E_p^0 + \left(\frac{g\mu_{12}}{2\pi\varepsilon_0\varepsilon_{effs}R^3}\right)\mathrm{Re}(\rho_{21}) \tag{5.6}$$

$$E_i = \left(\frac{g\mu_{12}}{2\pi\varepsilon_0\varepsilon_{effs}R^3}\right)\mathrm{Im}(\rho_{21}) \tag{5.7}$$

Note that in the strong regime E_i is several orders of magnitude smaller than E_r. Therefore, the role of E_i can be ignored and E_r^2 is the dominant factor in Q_{MP} [33].

To calculate the absorption energy rate we use the density matrix method to find the coherence terms of the QD in the hybrid system. The Hamiltonian of the QD interacting with the applied laser fields and induced electric field from the MP can be expressed in the interaction picture as

$$
\begin{aligned}
H_{QD} = \hbar\omega_{21}\sigma_{21} + \hbar\omega_{31}\sigma_{31} - \Omega_p e^{-i(\omega_p-\omega_{21})t}\sigma_{21}^{+} - \Omega_c e^{-i(\omega_c-\omega_{31})t}\sigma_{31}^{+} \\
- \Lambda_p \rho_{21} e^{-i(\omega_p-\omega_{21})t}\sigma_{21}^{+} + H.C.
\end{aligned}
\tag{5.8}
$$

where $\sigma_{ij} = |i\rangle\langle j|$ and $\sigma_{ij}^{+} = |j\rangle\langle i|$ (i, $j = 1$, 2 or 3) are called the exciton raising and lowering operators, respectively. The other quantities are defined as:

$$
\Omega_p = \frac{\mu_{12}E_p^0}{2\hbar\epsilon_{dr}} + \frac{\mu_{12}E_p^0}{2\hbar\epsilon_{dr}}\frac{\gamma g r_m^3}{R^3}, \tag{5.9a}
$$

$$
\Omega_c = \frac{\mu_{13}E_c^0}{2\hbar\epsilon_{dr}} \tag{5.9b}
$$

$$
\Lambda_p = \frac{\gamma r_m^3 g^2 \mu_{12}^2}{(4\pi\epsilon_B\epsilon_0)\,\hbar\epsilon_{dr}^2 R^6} \tag{5.9c}
$$

In above equations, Ω_p is the normalized Rabi frequency associated with external probe field and the field produced by the induced dipole moment P_m of the MP and Ω_c is the Rabi frequency associated with external control field. As mentioned before, Λ_p (Eqn. 5.9c) shows the self-interaction factor (interaction between polarized QD and MP). The imaginary part of Λ_p shows the Forster energy transfer rate between the QD and MP. Since we consider the excitonic resonance frequency $|1\rangle \leftrightarrow |2\rangle$ to be the same as that of the plasmonic resonance the Forster energy transfer is maximum.

We consider that a three-dimensional photonic crystal with an isotropic geometry acts as reservoir for the hybrid system. This photonic crystal consists of air spheres periodically arranged in a dielectric background material. The excited states $|2\rangle$ and $|3\rangle$ spontaneously decay to the ground state $|1\rangle$ due to coupling between excitons and the photonic crystal reservoir. To calculate the radiative decay rate the interaction Hamiltonian of the system in the interaction picture is considered as:

$$
H_{QD-PBG} = -\hbar\sum_k \left[g_{21}(\omega_k)\right] p_k \sigma_{21}^{+} e^{i(\omega_{21}-\omega_k)t} - \hbar\sum_k \left[g_{31}(\omega_k)\right] p_k \sigma_{31}^{+} e^{i(\omega_{31}-\omega_k)t} \tag{5.10}
$$

Here p_k and p_k^{+} are called the photon annihilation and creation operators, respectively, and

$g(\omega_k)$ is the coupling constant written as

$$g_{ij}(\omega_k) = \sqrt{\left(\frac{\omega_k}{2\hbar\epsilon_0 V}\right)}\mathbf{e}_k.\boldsymbol{\mu}_{ij} \tag{5.11}$$

Here V is the mode volume of the reservoir field, $\boldsymbol{\mu}_{ij}$ is the electronic dipole moment induced by the transition $|i\rangle \leftrightarrow |j\rangle$ and $\mathbf{e}_k$ is the unit polarization vector of the field, while ω_k and k are the frequency and wave vector of photons, respectively.

The photonic crystal structure consists of a periodical arrangement of air spheres in a dielectric background material where the dispersion relation of the photonic structures is calculated by John's group in ref. [58] as:

$$\cos(kL) = F(\omega_k) \tag{5.12}$$

where

$$F(\omega_k) = \sum_{\pm}\left[\pm\left(\frac{[n_a \pm n_b]^2}{4n_a n_b}\right)\cos\left(\frac{2\omega_k[n_a a \pm n_b b]}{c}\right)\right] \tag{5.13}$$

in the above equation, $L = 2a + 2b$ is the photonic crystal lattice constant, $2b$ is the spacing between the spheres and a is the radius of the dielectric spheres. Here, n_a and n_b are the refractive index of of dielectric spheres and the background dielectric material, respectively.

From Eqn. 5.8 and 5.10 we obtained the following equations of motion for the density matrix elements in an appropriate rotating frame of the QD in the hybrid system in the usual rotating-wave and dipole approximations:

$$\frac{d\rho_{22}}{dt} = -\Gamma_{21}\rho_{22} + i(\Omega_p + \Lambda_p\rho_{21})\rho_{12} - i(\Omega_p^* + \Lambda_p^*\rho_{21})\rho_{21} \tag{5.14a}$$

$$\frac{d\rho_{33}}{dt} = -\Gamma_{32}\rho_{33} - \Gamma_{31}\rho_{33} + i\Omega_c\rho_{13} - i\Omega_c^*\rho_{31} \tag{5.14b}$$

$$\frac{d\rho_{32}}{dt} = -\left(\frac{\Gamma_{31}+\Gamma_{32}+\Gamma_{21}}{2} + i(\delta_c - \delta_p)\right)\rho_{23} - i(\Omega_p^* + \Lambda_p^*\rho_{12})\rho_{31} + i\Omega_c\rho_{12} \tag{5.14c}$$

$$\frac{d\rho_{21}}{dt} = -\left(\frac{\Gamma_{21}}{2} + i\delta_p\right)\rho_{21} + i(\Omega_p + \Lambda_p\rho_{21})(\rho_{11} - \rho_{22}) - i\Omega_c\rho_{23} \tag{5.14d}$$

$$\frac{d\rho_{31}}{dt} = -\left(\frac{\Gamma_{32}+\Gamma_{31}}{2} + i\delta_c\right)\rho_{31} - i(\Omega_p + \Lambda_p\rho_{21})\rho_{32} - i\Omega_c(\rho_{33} - \rho_{11}) \tag{5.14e}$$

In the above equations, $\delta_c = \omega_{31} - \omega_c$ and $\delta_p = \omega_{21} - \omega_p$ are the detunings of the control and the probe field, respectively, Γ_{32} is the non-radiative decay rate for the transition $|3\rangle \rightarrow |2\rangle$

and Γ_{21} and Γ_{31} are the radiative decay rates of excitonic states $|2\rangle$ and $|3\rangle$ due to spontaneous emission, respectively.

The background photonic crystal modifies the electromagnetic density of states, and therefore influences the radiative decay rates of the QDs (Γ_{21} and Γ_{31}) as [126]

$$\Gamma_{21} = \Gamma_0 Z^2(\omega_{21}) \tag{5.15a}$$

$$\Gamma_{31} = \Gamma_0 Z^2(\omega_{31}) \tag{5.15b}$$

Here, Γ_0 is the exciton radiative decay rate in the absence of the photonic crystal, which includes the effect of the plasmonic field enhancement from the MP [30], and $Z^2(\varepsilon_k)$ is called the form factor, which is obtained from Eqn. 5.12 as

$$Z(\omega_k) = \left[\frac{c^3}{3L^3\omega_k^2} \frac{(\arccos[F(\omega_k)])^2}{\sqrt{1 - F^2(\omega_k)}} \xi(\omega_k) \right]^{1/2} \tag{5.16}$$

where

$$\xi(\omega_k) = \sum_{\pm} \left[\pm \left(\frac{[n_a \pm n_b]^2 \, [n_a a \pm n_b b]}{2cn_a n_b} \right) \sin\left(\frac{2\omega_k \, [n_a a \pm n_b b]}{c} \right) \right] \tag{5.17}$$

The form factor given in Eqn. 5.16 depends on the density of states which is obtained from the dispersion relation of the photonic crystal.

5.3 Results and Discussions

In this chapter we consider the large field limit, which means that both probe and control fields are strong ($I_c = I_p = 1$ kW/cm^2). We assume that probe and control fields are perpendicular to each other and the probe field is parallel to the axis of the QD-MP hybrid system, i.e. $g = 2$ and $\omega_{21} = \omega_{pr} = 2.5$ eV. The control laser field (E_C) is resonant with the excitonic transition $|1\rangle \leftrightarrow |3\rangle$ and so $\delta_3 = 0$. The QD consists of a CdSe/ZnS core coated by ZnSe. As shown recently [127], in such a structure the relaxation rate of the intersubband transition (Γ_{32}) can increase significantly, reaching one nanosecond or longer. In the absence of the shell, which delocalizes the whole wavefunction, this rate can be very large [128]. Taking this into account, we use parameters $\Gamma_{21} = 1/0.8\ \Gamma_0$ [31], $\Gamma_{31} = 1.0\ \Gamma_0$ and $\Gamma_{32} = 1/1.7\ \Gamma_0$. The MP is a gold nanoparticle with dielectric function $\epsilon_m(\omega) = \epsilon_{IB}(\omega) + \epsilon_D(\omega)$ [129]. For a small, spherical, gold MP, $\epsilon_{IB}(\omega) = 1.15 + i10.5$ at $\omega = 2.5$ eV. The parameter $\epsilon_D(\omega)$ is obtained from Eqn. 5.3 where we take $\gamma_{bulk} = 0.1$ eV, $v_F = 1.40 \times 10^6$ m/s and $A = 1$. Note that although $\epsilon_m(\omega)$ is a function of frequency, it is approximately constant over the range of frequencies that we are interested in due to the broad Plasmon peak. The radius of the MP is taken as 3 nm.

The dielectric constant of the background is taken as $\epsilon_B = 1$ (air) and $\epsilon_B = \frac{n_a^2+n_b^2}{2}$ in the absence and presence of photonic crystal, respectively, where $n_a = 1$ and $n_b = 4$. In our calculations we consider an inverse opal photonic crystal made of air spheres with radius $a = 58$ nm and a background with dielectric constant $n_b = 4$. The lattice constant of the photonic crystal is $L = 295$ nm. With these parameters, a photonic band gap appears between 1.95 and 2.50 eV. The induced dipole moment of the QD is taken as $4e$ nm [33] and its dielectric constant $\epsilon_s = 6$.

To calculate the energy absorption rate variations in the MP (Q_{MP}) the coherence terms ρ_{21} and ρ_{12} are obtained via solving Eqns. 5.14a - 5.14e numerically using the dverk78 method (seventh-eighth order continuous Runge–Kutta) provided by the software package Maple. Our results show that the dverk78 method has a rather higher precision in comparison to other available methods. The following initial conditions are considered: $\rho_{11}(0) = 1$, $\rho_{22}(0) = \rho_{33}(0) = 0$ and $\rho_{ij}(0) = 0$ $(i \neq j)$. These initial conditions imply that the electron is in the ground state at $t = 0$.

To show the distinctive features of the results for the V-configuration we begin by investigating the case where the QD is taken as a two-level excitonic system. Fig. 5-3 illustrates the Q_{MP} spectrum as a function of the probe detuning δ_p for different values of inter-particle distances R when $I_c = 0$ and $I_p = 1$ kw/cm^2. The results show the formation of a dip, i.e., transparency window, in the Q_{MP} spectrum. Furthermore, the amplitudes of the two peaks become smaller by increasing the value of R. In other words, the energy absorption rate is suppressed at zero detuning and the hybrid system shows an exciton-induced transparency state. This behavior can be explained by the total external electric field applied on the MP which consists of two main terms due to the applied probe field (E_p) and the field due to the polarization of the QD. The total field can be written in the form of two components which are in phase (E_r) and 90° out of phase (E_i) with the applied probe field (see Eqn. 5.6 and Eqn. 5.7) [33]. As one can see

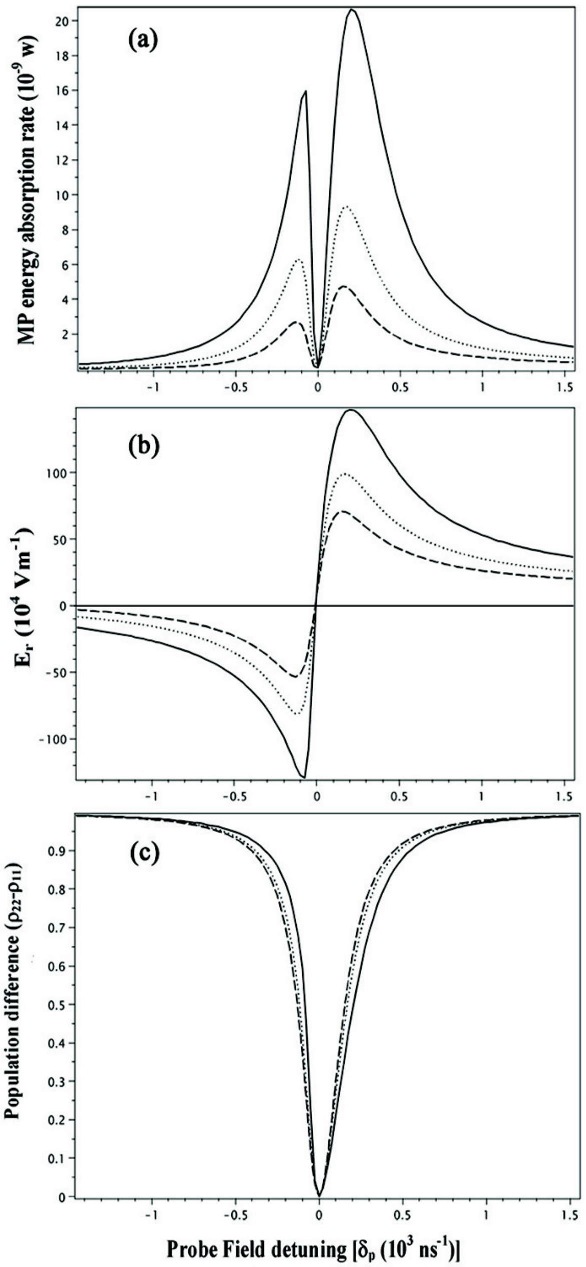

Figure 5-3: MP energy absorption rate spectra (Q_{MP}) as a function of the detuning probe frequency (δ_p) in the strong field regime for different inter-particle distances in the absence of control field. Here the QD is considered as a two-level system when $I_c = 0$ and $I_p = 1$ kw/cm^2. Here the solid, dotted and dashed curves show the Q_{MP} for $R = 13$ nm , 15 nm and 17 nm, respectively. (b) shows the component of total electric incident on the MP that is in phase with the applied probe field (E_r). (c) shows the dip in the population difference at resonance ($\rho_{22} - \rho_{11}$).

in Eqn. 5.5, Q_{MP} is controlled directly by the variation of E_r and E_i. In the strong-coupling regime, the dominant component of the field acting on the MP is E_r, and E_i is two orders of magnitude smaller, suggesting that the contribution from E_i is negligible. The variation of E_r as a function of the probe detuning δ_p is plotted in Fig. 5-3b. As it is shown in this figure the sign of E_r changes at zero detuning (i.e. $\delta_p = 0$) which means that at this location the local field due to the polarization of the QD is out of phase with applied electric filed (E_{0p}) and its magnitude becomes even greater. In this location the interference between the applied filed and the induced field produced by the QD at the MP changes from constructive to destructive.In Fig. 5-4 we show the role of the strong control field (I_c) on Q_{MP} for different values of R when the QD is taken as a three-level system with V-configuration. Our results show that when the strong control field is applied each peak splits to into two peaks, and three exciton-induced transparencies appear in the Q_{MP} spectrum. As one can see in Fig. 5-4b for $R = 13$ nm the sign of the E_r changes three times for three values of probe detuning. The amplitudes of the peaks can be easily controlled by the value of R.

To study the control of Q_{MP} by the laser field intensities, we consider the case where $R = 13$ nm and investigate how Q_{MP} is changed as the control and probe laser field intensities are varied. The results in Fig. 5-5 show that as the intensity of control field I_c is increased the spectrum of Q_{MP} changes dramatically. Increasing the value of I_c leads to shifts of the exciton-induced transparency locations, and therefore the hybrid system can be switched between complete annihilation and absorption of MP heat dissipation by varying the intensity of the control field.We also study the variations of Q_{MP} when the probe field intensity I_p is changed. The results in Fig. 5-6 show that as I_p is increased the amplitudes of the peaks are changed and the amount of heat dissipation rate in the MP can be controlled by changing the probe field intensity. One interesting feature here is the disappearance of the central peak in Q_{MP} when the ratio I_p/I_c increases (dashed line). This process can be understood in terms of the dressed state picture. When I_p and I_c are comparable ($I_p/I_c \sim 1$) the V-system supports one- and two-photon coupling processes [130]. When this ratio is far from unity the two-photon process is suppressed and the one-photon dressing becomes dominant. In this sense, the system becomes similar to that studied in Fig. 5-3. In this part of the chapter we investigate how Q_{MP} is changed when the hybrid system is embedded in an isotropic photonic crystal. For any

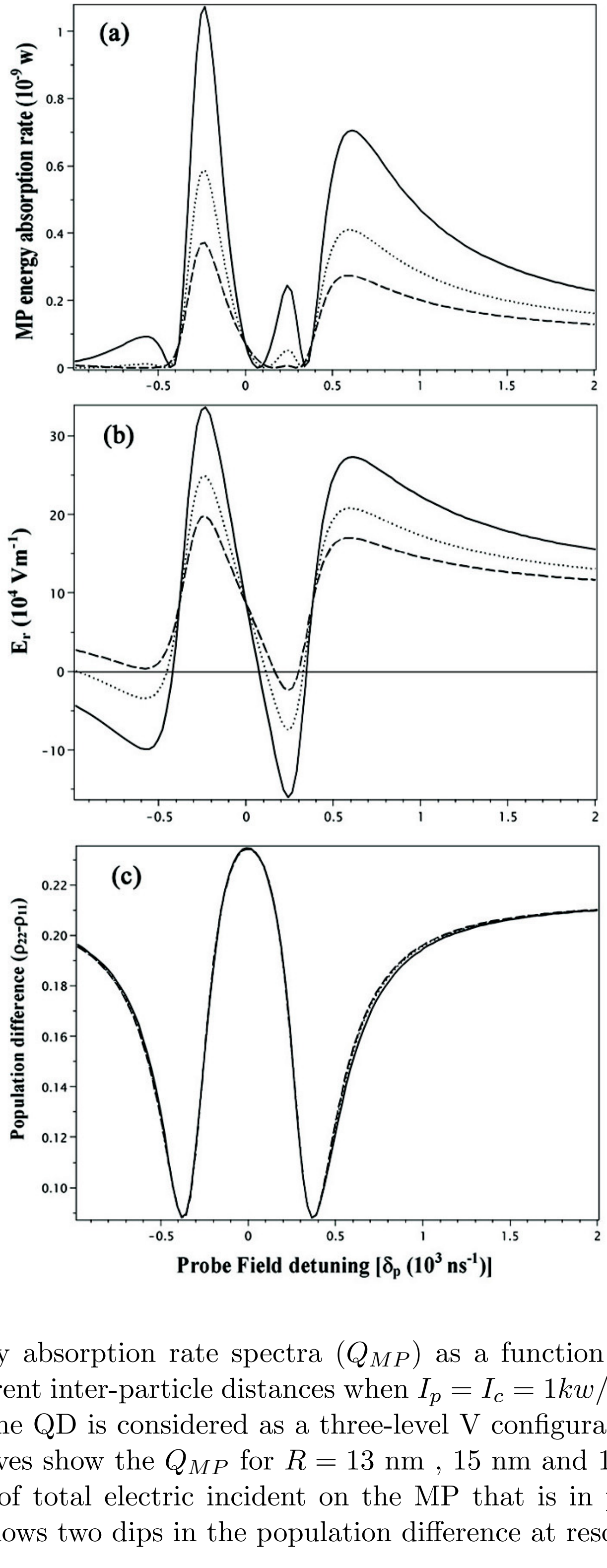

Figure 5-4: MP energy absorption rate spectra (Q_{MP}) as a function of the detuning probe frequency (δ_p) for different inter-particle distances when $I_p = I_c = 1kw/cm^2$ (probe and control field intensity). Here the QD is considered as a three-level V configuration system. The solid, dotted and dashed curves show the Q_{MP} for $R = 13$ nm , 15 nm and 17 nm, respectively. (b) shows the component of total electric incident on the MP that is in phase with the applied probe field (E_r). (c) shows two dips in the population difference at resonance ($\rho_{22} - \rho_{11}$).

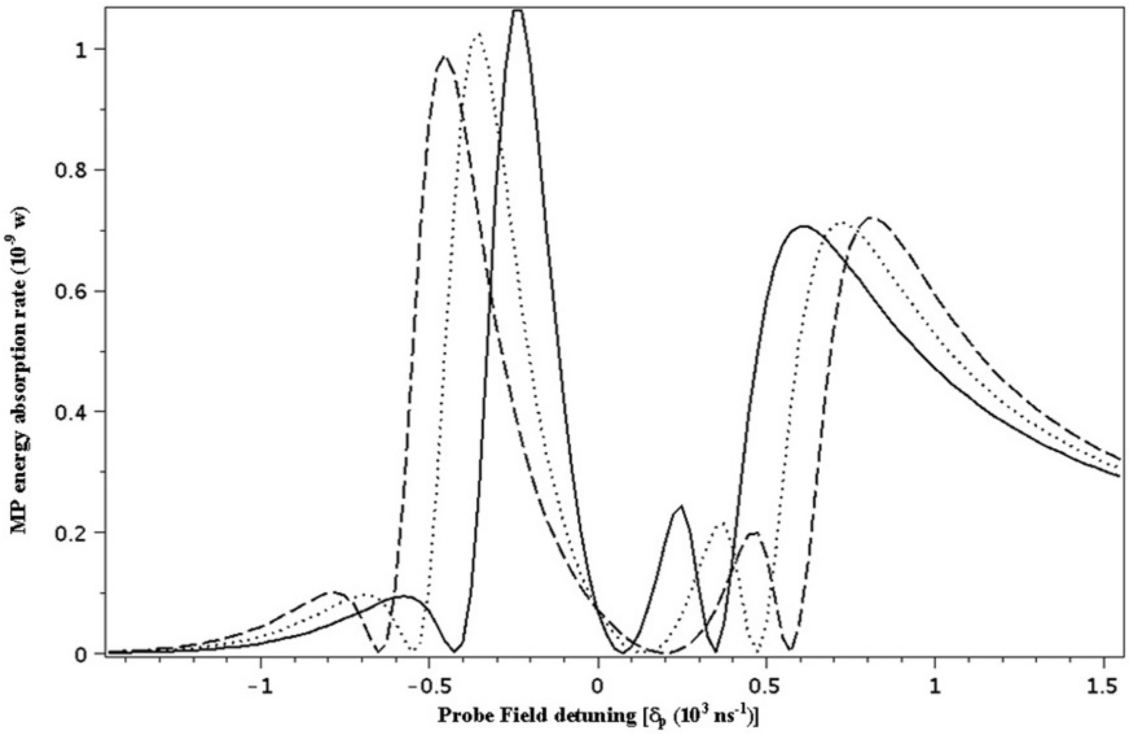

Figure 5-5: MP energy absorption rate spectra (Q_{MP}) as a function of the detuning probe frequency (δ_p) in the strong field regime for different control field intensity (I_c). $r_m = 3$ nm (radius of MP), $\mu_{12} = 4e$ nm (the induced dipole moment) and $I_p = 1kw/cm^2$ (probe intensity). Here the solid, dotted and dashed curves show the Q_{MP} for $I_c = 1$, 2 and 3 kw/cm^2, respectively.

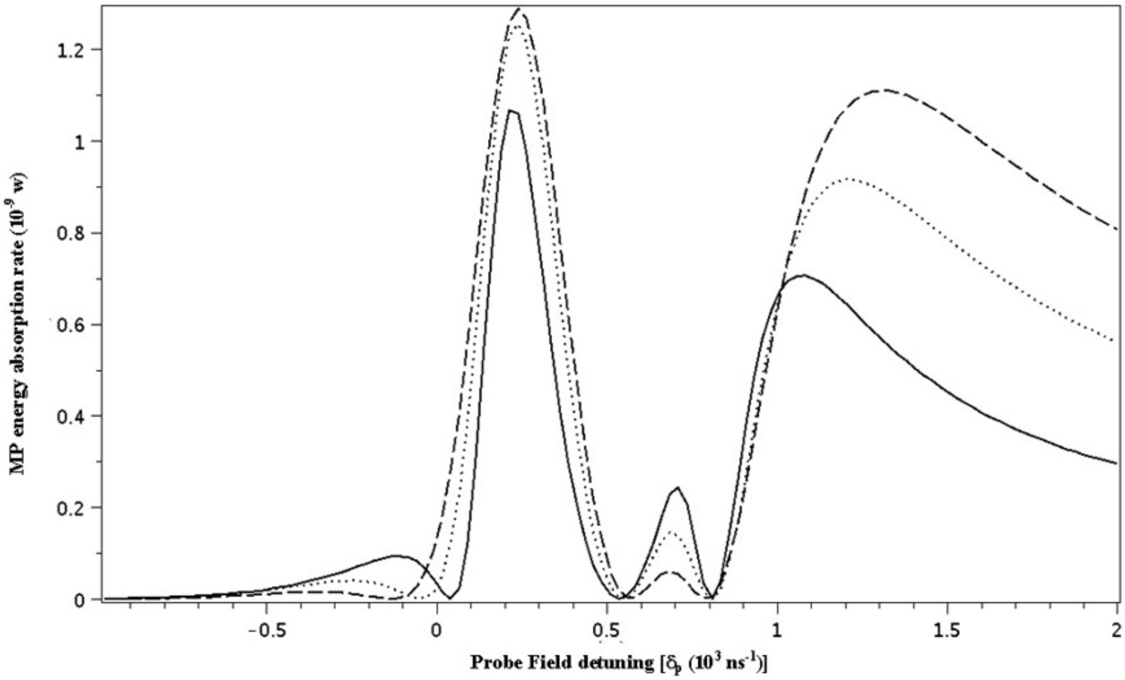

Figure 5-6: MP energy absorption rate spectra (Q_{MP}) as a function of the detuning probe frequency (δ_p) in the strong field regime for different probe field intensity (I_p). $r_m = 3$ nm (radius of MP), $\mu_{12} = 4e$ nm (the induced dipole moment) and $I_c = 1kw/cm^2$ (Probe intensity). Here the solid, dotted and dashed curves show the Q_{MP} for $I_p = 1$, 2 and 3 kw/cm^2, respectively.

photonic crystal, the location of the photonic band gap is controlled by the lattice constant and the refractive indices of the dielectric components. In terms of fabrication both opal and inverse opal photonic crystals can be used. Manipulation of the radiative decay rate can be achieved if the photonic crystal has a band gap near the excitonic resonance frequencies of the QD (See Fig.5-7).

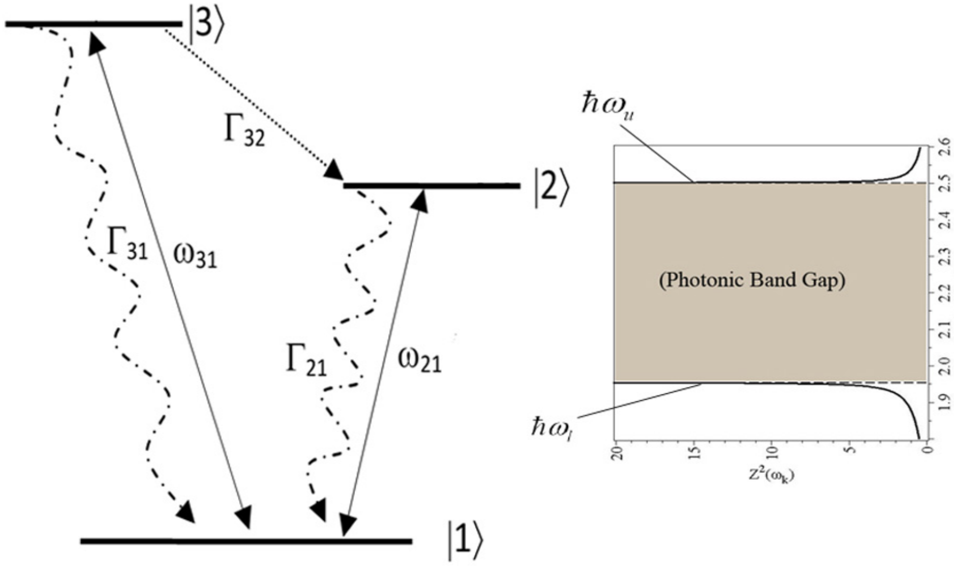

Figure 5-7: Plots of the form factor squared $Z^2(\omega_k)$ (right panel) of the photonic crystal with refractive indices $n_a = 1$ and $n_b = 4$. The lattice constant $L = 295$ nm the radius of air spheres is $a = 0.2$ L, where k denotes the wave vector. The quantities $\hbar\omega_u = 2.50$ eV and $\hbar\omega_l = 1.95$ eV are the maximum energy of the upper band and the minimum energy of the lower band, respectively. In this figure the resonance excitonic frequency $|1\rangle \leftrightarrow |2\rangle$ is assumed to be near the upper photonic band edge ($\hbar\omega_u$).

Fig. 5-8 shows the variation of energy absorption rate in the MP (Q_{MP}) for several values of the decay rate of excitonic transition $|1\rangle \leftrightarrow |2\rangle$ which is close to the plasmon frequency of the MP. In this figure the solid line shows the behavior of Q_{MP} when both excitonic transitions $|1\rangle \leftrightarrow |3\rangle$ and $|1\rangle \leftrightarrow |2\rangle$ are far from the band gap edge. In this situation we consider the radiative decay rate of excitonic transition $|1\rangle \leftrightarrow |2\rangle$ and $|1\rangle \leftrightarrow |3\rangle$ to be the same as Fig. 5-4a where $\Gamma_{21} = 1/0.8\ \Gamma_0$ and $\Gamma_{31} = 1.0\ \Gamma_0$, respectively. However, when the band gap of the photonic crystal is shifted towards the excitonic transition $|1\rangle \leftrightarrow |2\rangle$ by changing the excitonic

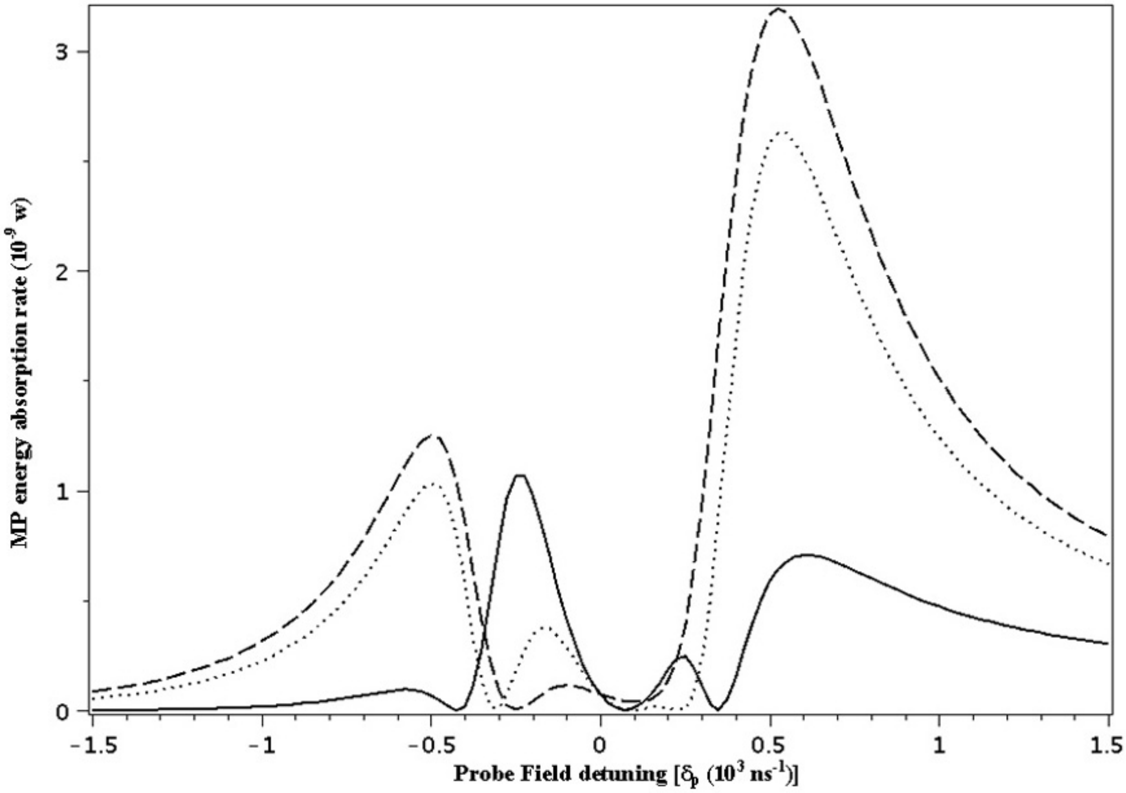

Figure 5-8: MP energy absorption rate spectra (Q_{MP}) as a function of the detuning probe frequency (δ_p) in the strong field regime for different values of transition $|2\rangle \leftrightarrow |1\rangle$ decay rate (Γ_{21}). Here the solid, dotted and dashed curves show the Q_{MP} for $\Gamma_{21} = 1/0.8\ \Gamma_0$, $4.0\ \Gamma_0$ and $8.0\ \Gamma_0$, respectively.

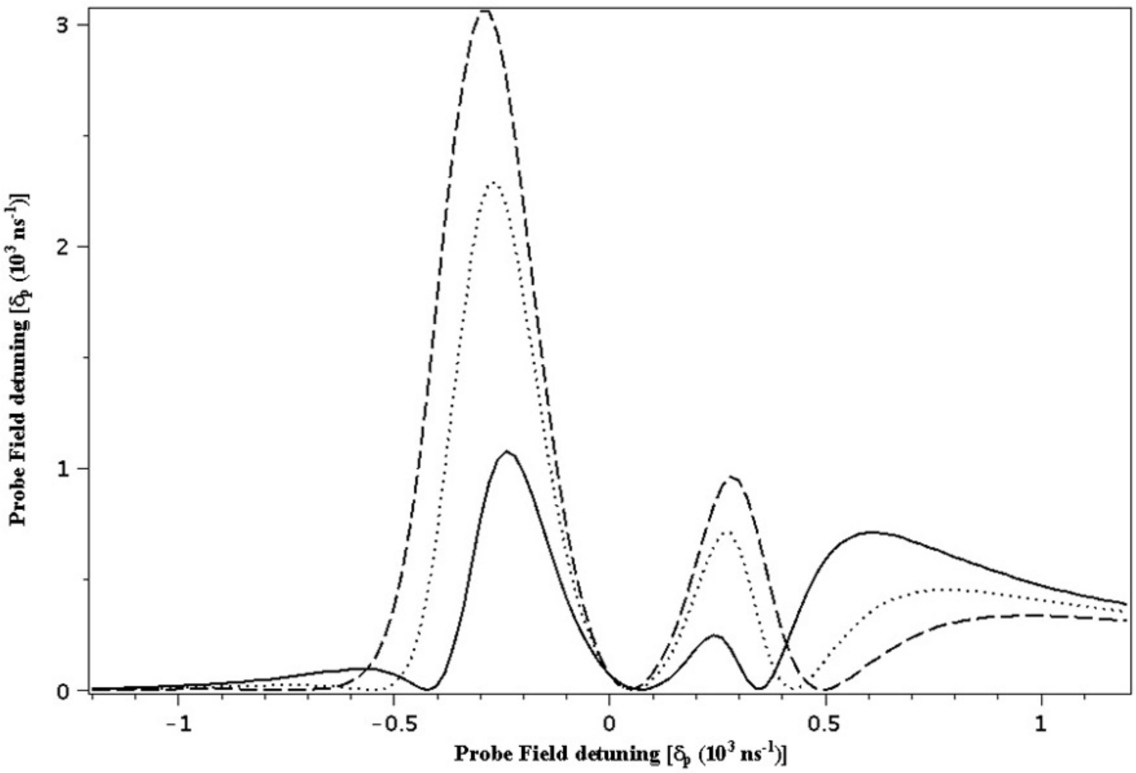

Figure 5-9: MP energy absorption rate spectra (Q_{MP}) as a function of the detuning probe frequency (δ_p) in the strong field regime for different values of transition $|3\rangle \leftrightarrow |1\rangle$ decay rate (Γ_{31}). Here the solid, dotted and dashed curves show the Q_{MP} for $\Gamma_{31} = 1.0\ \Gamma_0$, $4.0\ \Gamma_0$ and $8.0\ \Gamma_0$, respectively.

transition frequency ω_{12}, the decay rate Γ_{21} becomes greater. This is because of the significant increase of density of states near the edge of the photonic band gap. For this situation we plotted Q_{MP} for two values of decay rates $\Gamma_{21} = 4.0\ \Gamma_0$ (dotted line) and $\Gamma_{21} = 8.0\ \Gamma_0$ (dashed line). As one can see by increasing the decay rate the amplitudes of the side peaks rise dramatically and the middle peak disappears. This process leads to complete annihilation of the MP heat dissipation at a broad frequency range around the zero detuning parameter and the system exhibits a large excitonic induced transparency.

We also illustrate the effect of the radiative decay rate modification of excitonic transition $|1\rangle \leftrightarrow |3\rangle$ (Γ_{31}) on Q_{MP}. In this case, we take the upper edge of the photonic band gap to be close to ω_{31}. Depending on the value of ω_{31} one can change the photonic crystal parameters in such a way so that a band gap appears in the desired frequency range. In Fig. 5-9 the solid, dotted and dashed lines show Q_{MP} for $\Gamma_{31} = 1.0\ \Gamma_0$, $4.0\ \Gamma_0$ and $8.0\ \Gamma_0$, respectively. Our calculation shows that by increasing Γ_{31} the amplitude of the two middle and side peaks increase and decrease, respectively. This implies that by increasing Γ_{31} the nature of Q_{MP} becomes similar to the case where the QD was considered as a two-level system.

5.4 Conclusion

We have studied the manipulation of the exciton induced transparency mechanism in a hybrid nanostructure composed of a MP and a three-level V-configuration QD in the strong-coupling regime. Here external probe and control fields are applied to the system, each of which is coupled to a transition in the QD. Using the density matrix method, we have investigated the energy absorption rate of the MP (Q_{MP}) when it is coupled with the QD. In the absence of a background photonic crystal we have shown first the role of inter-particle distance and the intensities of the applied fields on Q_{MP}. In this situation three transparent states can be seen in the Q_{MN} spectrum, and the location of these states can be controlled by changing the intensities of probe and control fields. We found that the amplitudes of the absorption peaks can be controlled by varying the inter-particle distance between the QD and MP. In the second case we include the effect of a background photonic crystal, which modifies the radiative excitonic decay rate of the QD. We have shown the effect of the radiative excitonic decay rates on Q_{MP} when the excitonic resonance frequencies are close to the upper edge of the photonic band gap. Our calculation shows that if the excitonic resonance frequency of the QD ω_{21}, which is coupled with the plasmon resonance frequency of MP ω_{pr}, is tuned around upper edge of the photonic band gap, one absorbing mode disappears and the system exhibits transparency for a broad range of probe field detuning values. On the other hand, when the other excitonic resonance frequency of the QD ω_{31}, which is far away from the plasmon resonance frequency of MP, is close to and tuned around the frequency of the upper edge of the photonic band gap, only the amplitude of the peaks in the Q_{MP} spectrum are changed, and the amount of heat dissipation can be easily controlled.

Chapter 6

Concluding Remarks

The time evolution of the absorption coefficient in metallic photonic crystals has been studied numerically in this chapter. The refractive index of the metallic spheres depends on the plasma frequency. Probe and pump fields are applied to monitor the absorption process. First we consider that nanoparticles are embedded lightly so that they should not interact with each other. It is found that when the resonance states lie away from the band edges system goes to transparent sate. In the second situation we consider that quantum dots are doped densily so that they will interact with each other via the dipole-dipole interaction effect. The time evolution of the spontaneous emission cancellation is studied in the presence of dipole-dipole interaction.

It is found when the detuning parameter between electron resonance energy and probe laser field is zero the system reaches the steady states exponentially. However, when the detuning parameter is not zero the absorption coefficient and the populations of upper two levels oscillated with time and then reach the steady state.

In this paper we have studied the effect of a changing plasma frequency on the absorption profile of quantum dots. We consider that the quantum dots are doped in a metallic photonic crystal fabricated from metallic spheres embedded in a background dielectric material. These quantum dots are considered as an ensemble of three-level energy systems, containing two excited states and a ground state.

The quantum dots are interacting with each other via the dipole-dipole interaction, and are coupled with plasma-photon modes present the system. We also consider quantum interference between the two decay channels from the excited levels to the ground state. We consider that a probe laser field is applied to the system in order to study the absorption coefficient for two possible field configurations. Absorption occurs due the transitions from the ground state to an excited state, and is calculated by using the density matrix method. In the first configuration, the probe field couples with the ground state and the two excited states, which have energies lying very close to one another.

Using the dipole approximation, the transition between excited states is forbidden. In this case it is found that the position of the transparent peak is moved, due to a slight change in the plasma energy. This means that the transparent state becomes an absorbing state. In the second configuration, a pump field couples with only one excited state, while the probe field couples to the other. In this case, we found that a peak in the absorption profile appears due to plasmon coupling, and this peak splits into two peaks when the plasma energy is decreased. This change in plasma energy can also take the system from the absorption region to the gain region. These are very interesting results, and can be useful for developing nano-scale plasmonic devices.

We have developed an analytical theory for the photonic band structure and density of states of two-dimensional rectangular metallic photonic crystals. The transfer matrix method is used to derive analytical expressions for the dispersion relation of the metallic photonic crystal, which are used to obtain its photonic band structure. Our band structure calculations show that the metallic photonic crystal considered here forms a complete two-dimensional photonic band gap. We found that the location of the photonic band gap can be controlled by modifying the plasma energy of either metal. For example, by increasing the plasma energy the band gap shifts towards lower energies. In the case of aluminum (Al) and zinc (Zn) the photonic band gap lies in the ultraviolet region.

An analytical expression of the photonic density of states has been derived from the dispersion relation. It is found that the photonic density of states has singularities near the edges of the photonic band gaps. We have considered the case where a two-level quantum dot is doped in the metallic photonic crystal, and have calculated the linewidth and spectral function due to spontaneous emission using our analytical expression for the photonic density of states. The linewidth and spectral function of the quantum dot due to spontaneous emission were calculated by using the Schrödinger equation method. Finally, we showed that by changing the plasma energy one can control the spontaneous emission in the metallic photonic crystal.

In the last chapter, we have studied the manipulation of the plasmonic electromagnetically induced transparency mechanism in a hybrid nanostructure composed of a metallic particle and a three-level V-configuration quantum dot in the strong-coupling regime. Here external probe and control fields are applied to the system, each of which is coupled to a transition in the quantum dot. Using the density matrix method, we have investigated the energy absorption rate of the metallic particle (Q_{MP}) when it is coupled with the quantum dot. In the absence of a background photonic crystal we have shown first the role of inter-particle distance and the intensities of the applied fields on Q_{MP}. In this situation three transparent states can be seen in the Q_{MN} spectrum, and the location of these states can be controlled by changing the intensities of probe and control fields. Here transparent states refer to the energy location of the minima. We found that the amplitudes of the absorption peaks can be controlled by varying the inter-particle distance between the quantum dot and metallic particle. In the second case we include the effect of a background photonic crystal, which modifies the radiative excitonic decay rate of the quantum dot. We have shown the effect of the radiative excitonic decay rates on Q_{MP} when the excitonic resonance frequencies are close to the upper edge of the photonic band gap. Our calculation shows that if the excitonic resonance frequency of the quantum dot ω_{21}, which is coupled with the plasmon resonance frequency of metallic particle ω_{pr}, is tuned around upper edge of the photonic band gap, one absorbing mode disappears and the system exhibits transparency for a broad range of probe field detuning values. On the other hand, when the other excitonic resonance frequency of the quantum dot ω_{31}, which is far away from the plasmon resonance frequency of metallic particle, is close to and tuned around the frequency of the upper edge of the photonic band gap, only the amplitude of the peaks in the Q_{MP} spectrum are changed, and the amount of heat dissipation can be easily controlled.

Bibliography

[1] Kiyotoshi Yasumoto. *Electromagnetic theory and applications for photonic crystals.* CRC Press, 2006.

[2] Eli Yablonovitch. Inhibited spontaneous emission in solid-state physics and electronics. *Phys. Rev. Lett.*, 58(20):2059–2062, May 1987.

[3] Sajeev John. Strong localization of photons in certain disordered dielectric superlattices. *Phys. Rev. Lett.*, 58(23):2486–2489, Jun 1987.

[4] J.D. Joannopoulos, R.D. Meade, and J.N.Winn. *Photonic Crystals: Molding the Flow of Light.* Princeton University Press, 1995.

[5] Sigalas M.M. Subramania G. Ho K.-M. Biswas, R. Photonic band gaps in colloidal systems. *Physical Review B - Condensed Matter and Materials Physics*, 57(7):3701–3705, 1998. cited By (since 1996) 103.

[6] McMahon O.B. Brown, E.R. Large electromagnetic stop bands in metallodielectric photonic crystals. *Applied Physics Letters*, 67:2138, 1995. cited By (since 1996) 111.

[7] Chan C.T. Zhang W. Ming N.-Sheng P. Wang, Z. Three-dimensional self-assembly of metal nanoparticles: Possible photonic crystal with a complete gap below the plasma frequency. *Physical Review B - Condensed Matter and Materials Physics*, 64(11):1131081–1131084, 2001. cited By (since 1996) 70.

[8] Lin S.Y. El-Kady I. Biswas-R. Ho K.M. Fleming, J.G. All-metallic three-dimensional photonic crytal with a large infrared bandgap. *Nature*, 417(6884):52–55, 2002. cited By (since 1996) 296.

[9] Zentgraf T. Kuhl-J. Tikhodeev S.G.-Gippius N.A. Giessen H. Christ, A. Optical properties of planar metallic photonic crystal structures: Experiment and theory. *Physical Review B - Condensed Matter and Materials Physics*, 70(12):125113–1–125113–15, 2004. cited By (since 1996) 52.

[10] Kuhl J. Giessen-H. Linden, S. Controlling the interaction between light and gold nanoparticles: Selective suppression of extinction. *Physical Review Letters*, 86(20):4688–4691, 2001. cited By (since 1996) 126.

[11] Bloemer M.J. Pethel-A.S. Dowling J.P.-Bowden C.M. Manka A.S. Scalora, M. Transparent, metallo-dielectric, one-dimensional, photonic band-gap structures. *Journal of Applied Physics*, 83(5):2377–2383, 1998. cited By (since 1996) 174.

[12] A. Moroz. Three-dimensional complete photonic-band-gap structures in the visible. *Physical Review Letters*, 83(25):5274–5277, 1999. cited By (since 1996) 149.

[13] Chen Y.-S.-Williams H.E. Rumpf-R.C. Kuebler S.M. Tal, A. Fabrication and characterization of three-dimensional copper metallodielectric photonic crystals. *Optics Express*, 15(26):18283–18293, 2007. cited By (since 1996) 7.

[14] Hou-F.-J. Wu S.-C. Huang W.-H. Lai M.-C. Huang Y.-T. Yang, Y.-L. Fabrication and characterization of three-dimensional all metallic photonic crystals for near infrared applications. *Applied Physics Letters*, 94(4), 2009. cited By (since 1996) 0.

[15] He S. Simovski, C.R. Antennas based on modified metallic photonic bandgap structures consisting of capacitively loaded wires. *Microwave and Optical Technology Letters*, 31(3):214–221, 2001. cited By (since 1996) 18.

[16] MartÃŋnez-A.-GarcÃŋa J. Ramos-F. Sanchis P.-Blasco J. MartÃŋ-J. Cuesta-Soto, F. All-optical switching structure based on a photonic crystal directional coupler. *Optics Express*, 12(1):161–167, 2004. cited By (since 1996) 46.

[17] Nien S.Y.-Yu-C. Lee J.H.-Lin C.W. Chiu, N.F. Advanced metal nanostructure design for surface plasmon photonic bandgap biosensor device. *Conference proceedings : ... Annual International Conference of the IEEE Engineering in Medicine and Biology Society. IEEE*

Engineering in Medicine and Biology Society. Conference, Suppl:6521–6524, 2006. cited By (since 1996) 0.

[18] Atienzar P.-Ramiro-Manzano F. Meseguer-F. Corma A.-Garcia H. Rodriguez, I. Photonic crystals for applications in photoelectrochemical processes: Photoelectrochemical solar cells with inverse opal topology. *Photonics and Nanostructures - Fundamentals and Applications*, 3(2-3):148–154, 2005. cited By (since 1996) 18.

[19] A. Christ, S. G. Tikhodeev, N. A. Gippius, J. Kuhl, and H. Giessen. Waveguide-plasmon polaritons: Strong coupling of photonic and electronic resonances in a metallic photonic crystal slab. *Phys. Rev. Lett.*, 91(18):183901, Oct 2003.

[20] Moreno J.-Fleming-J.G. Lin, S.Y. Three-dimensional photonic-crystal emitter for thermal photovoltaic power generation. *Applied Physics Letters*, 83(2):380–382, 2003. cited By (since 1996) 150.

[21] Kim-Y.-S. Constant K.-Ho K.-M. Lee, J.-H. Woodpile metallic photonic crystals fabricated by using soft lithography for tailored thermal emission. *Advanced Materials*, 19(6):791–794, 2007. cited By (since 1996) 19.

[22] Fleming J.G.-Li-Z.Y. El-Kady-I. Biswas-R.-Ho K.M. Lin, S.Y. Origin of absorption enhancement in a tungsten, three-dimensional photonic crystal. *Journal of the Optical Society of America B: Optical Physics*, 20(7):1538–1541, 2003. cited By (since 1996) 35.

[23] Zhi-Yuan Li. Modified thermal radiation in three-dimensional photonic crystals. *Phys. Rev. B*, 66(24):241103, Dec 2002.

[24] Chan C.T.-Ho-K.M. Soukoulis-C.M. Sigalas, M.M. Metallic photonic band-gap materials. *Physical Review B*, 52(16):11744–11751, 1995. cited By (since 1996) 187.

[25] Sigalas M.M.-Tuttle-G. Ho-K.-M. Soukolis-C.M. McCalmont, J.S. A layer-by-layer metallic photonic band-gap structure. *Applied Physics Letters*, 68(19):2759–2761, 1996. cited By (since 1996) 49.

[26] Lu-S.-Y. Kuo, C.-Y. Opaline metallic photonic crystals possessing complete photonic band gaps in optical regime. *Applied Physics Letters*, 92(12), 2008. cited By (since 1996) 2.

[27] Kim Y.S.-Chen-M. Yang-Z.-P. Bur-J.A.-Lin S.-Y.-Ho K.-M. Chang, A.S.P. Visible three-dimensional metallic photonic crystal with non-localized propagating modes beyond waveguide cutoff. *Optics Express*, 15(13):8428–8437, 2007. cited By (since 1996) 11.

[28] Scalora M. Bloemer, M.J. Transmissive properties of ag/mgf2 photonic band gaps. *Applied Physics Letters*, 72(14):1676–1678, 1998. cited By (since 1996) 106.

[29] A. Ridolfo, O. Di Stefano, N. Fina, R. Saija, and S. Savasta. Quantum plasmonics with quantum dot-metal nanoparticle molecules: Influence of the fano effect on photon statistics. *Phys. Rev. Lett.*, 105:263601, Dec 2010.

[30] Bryant G.W.-Zhang-W. Skeini-T.-Lee J.-Kotov-N.A. Slocik-J.M.-Naik R.R. Govorov, A.O. Exciton-plasmon interaction and hybrid excitons in semiconductor-metal nanoparticle assemblies. *Nano Letters*, 6(5):984–994, 2006. cited By (since 1996) 114.

[31] Deng L.-Li-X. Huang-W.-P. Sadeghi, S.M. Plasmonic (thermal) electromagnetically induced transparency in metallic nanoparticle-quantum dot hybrid systems. *Nanotechnology*, 20(36), 2009. cited By (since 1996) 2.

[32] Ryan D. Artuso, Garnett W. Bryant, Aitzol Garcia-Etxarri, and Javier Aizpurua. Using local fields to tailor hybrid quantum-dot/metal nanoparticle systems. *Phys. Rev. B*, 83:235406, Jun 2011.

[33] Ryan D. Artuso and Garnett W. Bryant. Strongly coupled quantum dot-metal nanoparticle systems: Exciton-induced transparency, discontinuous response, and suppression as driven quantum oscillator effects. *Phys. Rev. B*, 82(19):195419, Nov 2010.

[34] Lachaine R.-Meunier-M. Boulais, E. Basic mechanisms of the femtosecond laser interaction with a plasmonic nanostructure in water. volume 7925, 2011. cited By (since 1996) 0.

[35] E. Yablonovitch. Inhibited spontaneous emission in solid-state physics and electronics. *Physical Review Letters*, 58(20):2059–2062, 1987. cited By (since 1996) 6551.

[36] Busch K. John, S. Photonic bandgap formation and tunability in certain self-organizing systems. *Journal of Lightwave Technology*, 17(11):1931–1943, 1999. cited By (since 1996) 78.

[37] Van Driel-A.F.-Nikolaev I.S.-Irman-A. Overgaag-K.-Vanmaekelbergh D.-Vos-W.L. Lodahl, P. Controlling the dynamics of spontaneous emission from quantum dots by photonic crystals. *Nature*, 430(7000):654–657, 2004. cited By (since 1996) 316.

[38] Quang T. John, S. Spontaneous emission near the edge of a photonic band gap. *Physical Review A*, 50(2):1764–1769, 1994. cited By (since 1996) 112.

[39] Chen-H.-Huang H. Zhu, S.-Y. Quantum interference effects in spontaneous emission from an atom embedded in a photonic band gap structure. *Physical Review Letters*, 79(2):205–208, 1997. cited By (since 1996) 167.

[40] Luterova K.-Pelant-I. Honerlage-B.-Astratov V.N. Vlasov, Yu.A. Optical gain of cds quantum dots embedded in 3d photonic crystals. *Thin Solid Films*, 318(1-2):93–95, 1998. cited By (since 1996) 8.

[41] Tsu R. Liu, K. Photoluminescence enhancement of quantum dots with photonic structures. *Microelectronics Journal*, 40(4-5):741–743, 2009. cited By (since 1996) 1.

[42] Sugimoto Y.-Watanabe-Y. Ozaki-N.-Mizutani A.-Takata-Y. Kitagawa-Y.-Ishikawa H.-Ikeda-N. Awazu K. Wang X. Watanabe A. Nakamura S. Ohkouchi S. Inoue K. Kristensen M. Sigmund O. Borel P.I. Baets R. Asakawa, K. Photonic crystal and quantum dot technologies for all-optical switch and logic device. *New Journal of Physics*, 8, 2006. cited By (since 1996) 35.

[43] Sugimoto Y.-Kanamoto-K. Ikeda-N.-Tanaka Y.-Nakamura-Y. Ohkouchi-S.-Watanabe Y.-Inoue-K. Ishikawa H. Asakawa K. Nakamura, H. Ultra-fast photonic crystal/quantum dot all-optical switch for future photonic networks. *Optics Express*, 12(26):6606–6614, 2004. cited By (since 1996) 110.

[44] Scherer A.-Hendrickson-J. Khitrova-G.-Gibbs H.M.-Rupper-G. Ell-C.-Shchekin O.B.-Deppe-D.G. Yoshle, T. Vacuum rabi splitting with a single quantum dot in a photonic crystal nanocavity. *Nature*, 432(7014):200–203, 2004. cited By (since 1996) 671.

[45] Badolato A.-Winger-M. Gerace-D.-AtatÃijre M.-Gulde-S. FÃd'lt-S.-Hu E.L.-ImamoÇğlu-A. Hennessy, K. Quantum nature of a strongly coupled single quantum dot-cavity system. *Nature*, 445(7130):896–899, 2007. cited By (since 1996) 379.

[46] M.R. Singh. Anomalous electromagnetically induced transparency in photonic-band-gap materials. *Physical Review A - Atomic, Molecular, and Optical Physics*, 70(3):033813–1–033813–7, 2004. cited By (since 1996) 27.

[47] John S. Woldeyohannes, M. Coherent control of spontaneous emission near a photonic band edge: A qubit for quantum computation. *Physical Review A - Atomic, Molecular, and Optical Physics*, 60(6):5046–5068, 1999. cited By (since 1996) 94.

[48] Chul-Sik Kee, Jae-Eun Kim, and Hae Yong Park. Heliconic band structure of one-dimensional periodic metallic composites. *Phys. Rev. E*, 57(2):2327–2330, Feb 1998.

[49] Giersig M.-Dunstan-D. Mulvaney-P. Ung, T. Spectroelectrochemistry of colloidal silver. *Langmuir*, 13(6):1773–1782, 1997. cited By (since 1996) 119.

[50] Quinten M. Rostalski, J. Effect of a surface charge on the halfwidth and peak position of cluster plasmons in colloidal metal particles. *Colloid and Polymer Science*, 274(7):648–653, 1996. cited By (since 1996) 4.

[51] Ficek Z.-Swain-S. Akram, U. Effect of quantum interference on a three-level atom driven by two laser fields. *Journal of Modern Optics*, 48(6):1059–1084, 2001. cited By (since 1996) 12.

[52] Swain S. Zhou, P. Quantum interference in resonance fluorescence for a driven v atom. *Physical Review A - Atomic, Molecular, and Optical Physics*, 56(4):3011–3021, 1997. cited By (since 1996) 142.

[53] Scully-M.O. Zhu, S.-Y. Spectral line elimination and spontaneous emission cancellation via quantum interference. *Physical Review Letters*, 76(3):388–391, 1996. cited By (since 1996) 331.

[54] Swain S. Zhou, P. Quantum interference in probe absorption: narrow resonances, transparency, and gain without population inversion. *Physical Review Letters*, 78(5):832–835, 1997. cited By (since 1996) 168.

[55] Li J.-Lv-X.-Y.-Si-L.-G.-Yang-X. Hao, X. Entanglement via tunable fano-type interference in asymmetric semiconductor quantum wells. *Physics Letters, Section A: General, Atomic and Solid State Physics*, 373(42):3827–3832, 2009. cited By (since 1996) 2.

[56] Cardimona D.A. Huang, D. Effects of off-diagonal radiative-decay coupling on electron transitions in resonant double quantum wells. *Physical Review A. Atomic, Molecular, and Optical Physics*, 64(1):138221–1382220, 2001. cited By (since 1996) 12.

[57] Dutton R.W.-Fan-S. Veronis, G. Metallic photonic crystals with strong broadband absorption at optical frequencies over wide angular range. *Journal of Applied Physics*, 97(9):1–4, 2005. cited By (since 1996) 17.

[58] Wang J. John, S. Quantum electrodynamics near a photonic band gap: Photon bound states and dressed atoms. *Physical Review Letters*, 64(20):2418–2421, 1990. cited By (since 1996) 353.

[59] Alexander Moroz. Three-dimensional complete photonic-band-gap structures in the visible. *Phys. Rev. Lett.*, 83(25):5274–5277, Dec 1999.

[60] Liu C.-Pokrovsky-A.L.-Li-C.Y.-Efros-A.L.-Valy Vardeny Z. Kamaev, V. Optical studies of 2d and 3d metallo-dielectric photonic crystals. volume 5927, pages 1–13, 2005. cited By (since 1996) 0.

[61] M. O. Scully and M. S. Zubairy. *Quantum Optics*. Cambridge Univesity Press, 1997.

[62] R. Loudon. *The Quantum Theory of Light*. COxford University Press, 2000.

[63] Wang J. John, S. Quantum optics of localized light in a photonic band gap. *Physical Review B*, 43(16):12772–12789, 1991. cited By (since 1996) 282.

[64] Mahi R. Singh. Photon transparency in metallic photonic crystals doped with an ensemble of nanoparticles. *Phys. Rev. A*, 79(1):013826, Jan 2009.

[65] Ali Hatef and Mahi R. Singh. Plasmonic effect on quantum coherence and interference in metallic photonic crystals doped with quantum dots. *Phys. Rev. A*, 81(6):063816, Jun 2010.

[66] I. Haque and Mahi R. Singh. A study of the ac Stark effect in doped photonic crystals. *Journal of Physics: Condensed Matter*, 19(15):156229, 2007.

[67] Valery I. Rupasov and M. Singh. Quantum gap solitons and many-polariton–atom bound states in dispersive medium and photonic band gap. *Phys. Rev. Lett.*, 77(2):338–341, Jul 1996.

[68] Valery I. Rupasov and M. Singh. Two-atom problem and polariton-impurity band in dispersive media and photonic-band-gap materials. *Phys. Rev. A*, 56(1):898–904, Jul 1997.

[69] Valery I. Rupasov and M. Singh. Quantum gap solitons and soliton pinning in dispersive medium and photonic-band-gap materials: Bethe-ansatz solution. *Phys. Rev. A*, 54(4):3614–3625, Oct 1996.

[70] Yan X.-Wu-J.-H.-Gao-J.-Y. Wang, G. The phase dependent properties of gain and absorption in an er3+-doped yttrium aluminum garnet crystal. *Optics Communications*, 267(1):118–123, 2006. cited By (since 1996) 7.

[71] Keitel C.H.-Knight-P.L.-Marangos-J.P. Petch, J.C. Role of electromagnetically induced transparency in resonant four-wave-mixing schemes. *Physical Review A - Atomic, Molecular, and Optical Physics*, 53(1):543–561, 1996. cited By (since 1996) 80.

[72] Loschialpo P.-Forester-D.-Schelleng-J. Keskinen, M.J. Photonic band gap structure and transmissivity of frequency-dependent metallic-dielectric systems. *Journal of Applied Physics*, 88(10):5785–5790, 2000. cited By (since 1996) 12.

[73] Gong S.-Q.-Knight-P.L. Paspalakis, E. Spontaneous emission-induced coherent effects in absorption and dispersion of a v-type three-level atom. *Optics Communications*, 152(4-6):293–298, 1998. cited By (since 1996) 99.

[74] Mahi R. Singh. Controlling spontaneous emission in photonic-band-gap materials doped with nanoparticles. *Phys. Rev. A*, 75(3):033810, Mar 2007.

[75] M.R. Singh. Controlling spontaneous emission in photonic-band-gap materials doped with nanoparticles. *Physical Review A - Atomic, Molecular, and Optical Physics*, 75(3), 2007. cited By (since 1996) 4.

[76] AntÃşn M.A.-CarreÃśo-F. CalderÃşn, O.G. Near dipole-dipole effects in a v-type medium with vacuum induced coherence. *European Physical Journal D*, 25(1):77–87, 2003. cited By (since 1996) 22.

[77] John S. Florescu, M. Single-atom switching in photonic crystals. *Physical Review A. Atomic, Molecular, and Optical Physics*, 64(3):033801/1–033801/21, 2001. cited By (since 1996) 70.

[78] John S. Florescu, M. Resonance fluorescence in photonic band gap waveguide architectures: Engineering the vacuum for all-optical switching. *Physical Review A - Atomic, Molecular, and Optical Physics*, 69(5 B):053810–1, 2004. cited By (since 1996) 45.

[79] John S. Kaso, A. Nonlinear bloch waves in metallic photonic band-gap filaments. *Physical Review A - Atomic, Molecular, and Optical Physics*, 76(5), 2007. cited By (since 1996) 4.

[80] M.R. Singh. A study of plasmonics in metallic photonic quantum wires. *Journal of Applied Physics*, 106(6), 2009. cited By (since 1996) 1.

[81] Paspalakis E.-Vitanov-N.V. Yannopapas, V. Electromagnetically induced transparency and slow light in an array of metallic nanoparticles. *Physical Review B - Condensed Matter and Materials Physics*, 80(3), 2009. cited By (since 1996) 8.

[82] Singh M. Hatef, A. The study of quantum interference in metallic photonic crystals doped with four-level quantum dots. *Nanoscale Research Letters*, 5(3):464–468, 2010. cited By (since 1996) 1.

[83] A. Moroz. Photonic crystals with small metal inclusions. volume 5036, pages 407–412, 2002. cited By (since 1996) 0.

[84] Vos W.L.-Moroz-A.-Van Blaaderen-A. Velikov, K.P. Reflectivity of metallodielectric photonic glasses. *Physical Review B - Condensed Matter and Materials Physics*, 69(7):751081–751085, 2004. cited By (since 1996) 7.

[85] M.R. Singh. Absorption studies in dipole-dipole interacting nanoparticles doped in nonlinear photonic crystals. *Journal of Modern Optics*, 56(6):758–767, 2009. cited By (since 1996) 1.

[86] Stuart Swain Zbigniew Ficek. *Quantum interference and coherence: theory and experiments*. Springer, 2005.

[87] Ning X.-J.-Zhang-Q. You-J.Q. Li, P. Dressed-state coherent population trapping in a v-type atom. *Journal of Physics B: Atomic, Molecular and Optical Physics*, 41(23), 2008. cited By (since 1996) 1.

[88] Zhang-H.-F.-Gao J.-Y.-Zhang-B. Xu, W.-H. Phase-dependent properties for absorption and dispersion by spontaneously generated coherence in a four-level atomic system. *Journal of the Optical Society of America B: Optical Physics*, 20(11):2377–2382, 2003. cited By (since 1996) 13.

[89] Ian Kenyon. *The light fantastic: a modern introduction to classical and quantum optics*. Oxford University Press, 2008.

[90] Paspalakis-E.-Knight-P.L. Gong, S.-Q. Effects of spontaneous emission interference on population inversions of a v-type atom. *Journal of Modern Optics*, 45(12):2433–2442, 1998. cited By (since 1996) 72.

[91] Dominique Pagnoux Vincent Berger-Jean-Michel Gerard Daniel Maystre Jean-Michel Lourtioz, Henri Benisty. *Photonic crystals: towards nanoscale photonic devices*. Springer, 2005.

[92] Bender M. Singleton L. Kiriakidis G. Soukoulis-C.M. Katsarakis, N. Two-dimensional metallic photonic band-gap crystals fabricated by liga. *Microsystem Technologies*, 8(2-3):74–77, 2002. cited By (since 1996) 11.

[93] Pralle M. McNeal M. Daly J. Greenwald-A.-Johnson E. Biswas R.-Ding C.G. Puscasu, I. Extraordinary emission from two-dimensional plasmonic-photonic crystals. *Journal of Applied Physics*, 98(1):1–6, 2005. cited By (since 1996) 34.

[94] Sun B. Guo H. Tetreault N. Glessen-H.-Friend R.H. Zhang, X. Large-area two-dimensional photonic crystals of metallic nanocylinders based on colloidal gold nanoparticles. *Applied Physics Letters*, 90(13), 2007. cited By (since 1996) 9.

[95] V. Kuzmiak, A. A. Maradudin, and F. Pincemin. Photonic band structures of two-dimensional systems containing metallic components. *Phys. Rev. B*, 50(23):16835–16844, Dec 1994.

[96] J. B. Pendry and A. MacKinnon. Calculation of photon dispersion relations. *Phys. Rev. Lett.*, 69(19):2772–2775, Nov 1992.

[97] Kazuaki Sakoda, Noriko Kawai, Takunori Ito, Alongkarn Chutinan, Susumu Noda, Tsuneo Mitsuyu, and Kazuyuki Hirao. Photonic bands of metallic systems. i. principle of calculation and accuracy. *Phys. Rev. B*, 64(4):045116, Jul 2001.

[98] Marsal L.F. FerrÃľ-Borrull J. PallarÃĺs J. Ustyantsev, M.A. Influence of the dielectric background on the quality factors of metallo-dielectric photonic crystals. *Optics Communications*, 274(2):293–299, 2007. cited By (since 1996) 3.

[99] Esteban Moreno, Daniel Erni, and Christian Hafner. Band structure computations of metallic photonic crystals with the multiple multipole method. *Phys. Rev. B*, 65(15):155120, Apr 2002.

[100] Cada M. Takayama, O. Two-dimensional metallo-dielectric photonic crystals embedded in anodic porous alumina for optical wavelengths. *Applied Physics Letters*, 85(8):1311–1313, 2004. cited By (since 1996) 20.

[101] Sajeev John and Jian Wang. Quantum optics of localized light in a photonic band gap. *Phys. Rev. B*, 43(16):12772–12789, Jun 1991.

[102] Chen C. Qian-B.-L. Samokhvalova, K. Analytical and numerical calculations of the dispersion characteristics of two-dimensional dielectric photonic band gap structures. *Journal of Applied Physics*, 99(6), 2006. cited By (since 1996) 9.

[103] Hardy A.A. Nusinsky, I. Approximate analysis of two-dimensional photonic crystals with rectangular geometry. i.e polarization. *Journal of the Optical Society of America B: Optical Physics*, 25(7):1135–1143, 2008. cited By (since 1996) 7.

[104] S. Kawakami. Analytically solvable model of photonic crystal structures and novel phenomena. *Journal of Lightwave Technology*, 20(8):1644–1650, 2002. cited By (since 1996) 14.

[105] I. Ponomarev. Separation of variables in the computation of spectra in 2-d photonic crystals. *SIAM Journal on Applied Mathematics*, 61(4):1202–1218, 2000. cited By (since 1996) 7.

[106] Efros A.L. Pokrovsky, A.L. Pokrovsky and efros reply to comment on "electrodynamics of metallic photonic crystals and the problem of left-handed material" [2]. *Physical Review Letters*, 92(11):119401–1+i, 2004. cited By (since 1996) 7.

[107] Liu H. Yang-P.-Qiu B. Wang, Y. Study on the cause and countermeasure of the coloring of bohai strait-run distillate during alkali treatment. *Petroleum Processing and Petrochemicals*, 39(5):50–53, 2008. cited By (since 1996) 0.

[108] Sigalas M.M.-Biswas-R. Ho K.M.-Soukoulis-C.M. El-Kady, I. Metallic photonic crystals at optical wavelengths. *Physical Review B - Condensed Matter and Materials Physics*, 62(23):15299–15302, 2000. cited By (since 1996) 97.

[109] Christy R.W. Johnson, P.B. Optical constants of the noble metals. *Physical Review B*, 6(12):4370–4379, 1972. cited By (since 1996) 3151.

[110] C. Kittel. *Introduction to Solid State Physics (7th ed.)*. John Wiley and Sons, 1996.

[111] Schatz G.C. Zeman, E.J. An accurate electromagnetic theory study of surface enhancement factors for ag, au, cu, li, na, al, ga, in, zn, and cd. *Journal of Physical Chemistry*, 91(3):634–643, 1987. cited By (since 1996) 230.

[112] Bell R.J. Alexander Jr.-R.W. Long L.L. Ordal, M.A. *M. R. Query App. Opt.*, 24:24, 1985. cited By (since 1996) 1.

[113] Q. Huo. A perspective on bioconjugated nanoparticles and quantum dots. *Colloids and Surfaces B: Biointerfaces*, 59(1):1–10, 2007. cited By (since 1996) 21.

[114] Xu J.-J. Chen-H.-Y. Shan, Y. Distance-dependent quenching and enhancing of electrochemiluminescence from a cds:mn nanocrystal film by au nanoparticles for highly sensitive detection of dna. *Chemical Communications*, (8):905–907, 2009. cited By (since 1996) 29.

[115] Chiu T.T.-Lin W.-H.-Chen K.L.-Shih-M.H. Lin S.-Y.-Chang Y.-C. Hsu, K.S. Compact microdisk cavity laser with type-ii gasb/gaas quantum dots. *Applied Physics Letters*, 98(5), 2011. cited By (since 1996) 0.

[116] Govorov A.O.-Bryant G.W. Zhang, W. Semiconductor-metal nanoparticle molecules: Hybrid excitons and the nonlinear fano effect. *Physical Review Letters*, 97(14), 2006. cited By (since 1996) 77.

[117] Govorov A.O.-Kotov N.A. Lee, J. Nanoparticle assemblies with molecular springs: A nanoscale thermometer. *Angewandte Chemie - International Edition*, 44(45):7439–7442, 2005. cited By (since 1996) 53.

[118] Vassilios Yannopapas, Emmanuel Paspalakis, and Nikolay V. Vitanov. Plasmon-induced enhancement of quantum interference near metallic nanostructures. *Phys. Rev. Lett.*, 103(6):063602, Aug 2009.

[119] Nihei H.-Okamotol A. Matsuokal, F. Nano-photonic switching in a quantum dot embedded in photonic crystals. 2008. cited By (since 1996) 0.

[120] Bryan Ellis, Marie Mayer, Gary Shambat, Tomas Sarmiento, James S. Harris, Eugene Haller, and Jelena Vuckovic. Ultra-low threshold electrically pumped quantum dot pho-

tonic crystal nanocavity laser. *CLEO:2011 - Laser Applications to Photonic Applications*, page PDPA1, 2011.

[121] Englund D.-Fushman I.-VuÄIJkoviÄĞ-J. Stoltz-N.-Petroff P. Faraon, A. Local quantum dot tuning on photonic crystal chips. *Applied Physics Letters*, 90(21), 2007. cited By (since 1996) 43.

[122] Liu-S.-D.-Wang-Q.-Q. Cheng, M.-T. Modulating emission polarization of semiconductor quantum dots through surface plasmon of metal nanorod. *Applied Physics Letters*, 92(16), 2008. cited By (since 1996) 13.

[123] Alexander O. Govorov. Semiconductor-metal nanoparticle molecules in a magnetic field: Spin-plasmon and exciton-plasmon interactions. *Phys. Rev. B*, 82:155322, Oct 2010.

[124] Bryant G.W. Artuso, R.D. Optical response of strongly coupled quantum dot-metal nanoparticle systems: Double peaked fano structure and bistability. *Nano Letters*, 8(7):2106–2111, 2008. cited By (since 1996) 14.

[125] El-Sayed-M.A. Link, S. Spectral properties and relaxation dynamics of surface plasmon electronic oscillations in gold and silver nanodots and nanorods. *Journal of Physical Chemistry B*, 103(40):8410–8426, 1999. cited By (since 1996) 1330.

[126] Mahi R. Singh. Anomalous electromagnetically induced transparency in photonic-band-gap materials. *Phys. Rev. A*, 70(3):033813, Sep 2004.

[127] Guyot-Sionnest-P. Pandey, A. Slow electron cooling in colloidal quantum dots. *Science*, 322(5903):929–932, 2008. cited By (since 1996) 63.

[128] Victor I. Klimov and Duncan W. McBranch. Femtosecond 1p-to- 1s electron relaxation in strongly confined semiconductor nanocrystals. *Phys. Rev. Lett.*, 80(18):4028–4031, May 1998.

[129] Celep-G.-LermÃl’-J.-Pellarin-M.-Huntzinger-J.R.-Vialle J.L. Broyer-M. Cottancin, E. Optical properties of noble metal clusters as a function of the size: Comparison between experiments and a semi-quantal theory. *Theoretical Chemistry Accounts*, 116(4-5):514–523, 2006. cited By (since 1996) 24.

[130] S. M. Sadeghi and J. Meyer. One- and two-photon-dressed effects in infrared-coupled quantum wells. *Phys. Rev. B*, 53(15):10094–10106, Apr 1996.

Copyright and Reprint Permissions

JOHN WILEY AND SONS LICENSE

TERMS AND CONDITIONS

Dec 15, 2011

This is a License Agreement between Ali Hatef ("You") and John Wiley and Sons ("John Wiley and Sons") provided by Copyright Clearance Center ("CCC"). The license consists of your order details, the terms and conditions provided by John Wiley and Sons, and the payment terms and conditions.

All payments must be made in full to CCC. For payment instructions, please see information listed at the bottom of this form.

License Number	2810270529600
License date	Dec 15, 2011
Licensed content publisher	John Wiley and Sons
Licensed content publication	physica status solidi (c) Current topics in solid state physics
Licensed content title	**Time evolution of absorption process in nonlinear metallic photonic crystals**
Licensed content author	Mahi R. Singh,Ali Hatef
Licensed content date	May 1, 2009
Start page	S158
End page	S161
Type of use	Dissertation/Thesis
Requestor type	Author of this Wiley article
Format	Electronic
Portion	Full article
Will you be translating?	No

ELSEVIER LICENSE TERMS AND CONDITIONS

This is a License Agreement between Ali Hatef ("You") and Elsevier ("Elsevier") provided by Copyright Clearance Center ("CCC"). The license consists of your order details, the terms and conditions provided by Elsevier, and the payment terms and conditions.

All payments must be made in full to CCC. For payment instructions, please see information listed at the bottom of this form.

Customer name Ali Hatef

Customer address Physics and Astronomy Building

London, ON N6A 3K7

License number 2810271171924

License date Dec 15, 2011

Licensed content publisher Elsevier

Licensed content publication Microelectronics Journal

Licensed content title **Quantum interference due to the spontaneous emission in nonlinear metallic photonic crystals**

Licensed content author Mahi R. Singh,A. Hatef

Licensed content date April-May 2009

Licensed content volume number 40

Licensed content issue number 4-5

Number of pages 3

Start Page 854

End Page 856

Type of Use reuse in a thesis/dissertation

Portion full article

Format electronic

Are you the author of this Elsevier article? Yes

Will you be translating? No

Title of your thesis/dissertation Quantum Coherence and Interference in Metallic Photonic Crystal and Hybrid Systems

Expected completion date Dec 2011

Estimated size (number of pages) 130

Nanoscale Research Letter.

Authors of articles published in Nanoscale Research Letters are the copyright holders of their articles and have granted to any third party, in advance and in perpetuity, the right to use, reproduce or disseminate the article, according to the SpringerOpen copyright and license agreement.

SpringerOpen Access license agreement

Brief summary of the agreement

Anyone is free:

- to copy, distribute, and display the work;
- to make derivative works;
- to make commercial use of the work;

Under the following conditions: Attribution

- the original author must be given credit;
- for any reuse or distribution, it must be made clear to others what the license terms of this work are;
- any of these conditions can be waived if the authors gives permission.

Statutory fair use and other rights are in no way affected by the above.

From ELS-PAR

To Ali Hatef

Date Fri, Dec 16, 2011 at 11:53 AM

Subject RE: **Permission to Use Copyrighted Material in a Doctoral Thesis, Optics Communications 284, 2363-2369, (2011).**

Dear Ali Hatef,

We hereby grant you permission to reprint the material detailed below at no charge in your thesis, in print and on the University of Western Ontario web site subject to the following conditions:

1. If any part of the material to be used (for example, figures) has appeared in our publication with credit or acknowledgement to another source, permission must also be sought from that source. If such permission is not obtained then that material may not be included in your publication/copies.

2. Suitable acknowledgment to the source must be made, either as a footnote or in a reference list at the end of your publication, as follows:

"This article was published in Publication title, Vol number, Author(s), Title of article, Page Nos, Copyright Elsevier (or appropriate Society name) (Year)."

3. Your thesis may be submitted to your institution in either print or electronic form.

4. Reproduction of this material is confined to the purpose for which permission is hereby given.

5. This permission is granted for non-exclusive world English rights only. For other languages please reapply separately for each one required. Permission excludes use in an electronic form. Should you have a specific electronic project in mind please reapply for permission.

6. This includes permission for UMI to supply single copies, on demand, of the complete thesis. Should your thesis be published commercially, please reapply for permission.

Yours sincerely,

American Physical Society

From Associate Publisher

To Ali Hatef

Date Fri, Dec 16, 2011 at 3:14 PM

Subject Re: **Permission to Use Copyrighted Material in a Doctoral Thesis, Phys. Rev. A, 81, 063816 (2010).**

Dear Dr. Hatef,

Thank you for your email. As the author, you have the right to use the article or a portion of the article in a thesis or dissertation without requesting permission from APS, provided the bibliographic citation and the APS copyright credit line are given on the appropriate pages.

Best wishes,

Publications Marketing Coordinator

American Physical Society

Subject: Permission to Use Copyrighted Material in a Doctoral Thesis(NANO/403136/PAP)
From: Ali Hatef - Monday 19/12/2011 15:55

Dear Editor,

I am a University of Western Ontario graduate student completing my Doctoral thesis entitled "Quantum Coherence and Interference in Metallic Photonic Crystal and Hybrid Systems". My thesis will be available in full-text on the internet for reference, study and / or copy. Except in situations where a thesis is under embargo or restriction, the electronic version will be accessible through the Western Libraries web pages, the Library's web catalogue, and also through web search engines. I will also be granting Library and Archives Canada and ProQuest/UMI a non-exclusive license to reproduce, loan, distribute, or sell single copies of my thesis by any means and in any form or format. These rights will in no way restrict republication of the material in any other form by you or by others authorized by you.

I would like permission to allow inclusion of the following material in my thesis: **A. Hatef**, S. M. Sadeghi and M. Singh, "Plasmonic electromagnetically induced transparency in metallic nanoparticle-quantum dot hybrid systems", Nanotechnology- NANO/403136/PAP, (Accepted 12/2011).

The material will be attributed through a citation.

Please confirm in writing or by email that these arrangements meet with your approval.

Sincerely Yours
Ali Hatef

PhD student
Department of Physics and Astronomy
University of Western Ontario

PERMISSION TO REPRODUCE AS REQUESTED IS GIVEN PROVIDED THAT:

(b) the source of the material including author, title of article, title of journal, volume number, issue number (if relevant), page range (or first page if this is the only information available), date and publisher is acknowledged.
(c) for material being published electronically, a link back to the original article should be provided (via DOI).

IOP Publishing Ltd
Temple Circus
Temple Way
BRISTOL
BS1 6BE

Curriculum Vitae

Name:	Ali Hatef
Post-secondary Education and Degrees:	Shiraz University Shiraz, Fars, Iran 1994-1998 B.A.
	Shiraz University Shiraz, Fars, Iran 1998-2001 M.A.
Honours and Awards:	Province of Ontario Graduate Scholarship 2011-2012
Related Work Experience	Teaching Assistant The University of Western Ontario 2008-2011

Publications:

M. Singh and **A. Hatef**, “Time Evolution of Absorption Process in Nonlinear Metallic Photonic Crystals”, Phys. Status Solidi C 6, No. S1, S158–S161 (2009).

M. Singh and **A. Hatef**, “Quantum interference due to the spontaneous emission in nonlinear metallic photonic crystals” Microelectronics Journal 40, 854–856, (2009).

A. Hatef and M. Singh, “The Study of Quantum Interference in Metallic Photonic Crystals Doped with Four-Level Quantum Dots” Nanoscale Research Letter 5, 464–468, (2010).

A. Hatef and M. Singh, "Plasmonic effect on quantum coherence and interference in metallic photonic crystals doped with quantum dots", Phys. Rev. A, 81, 063816 (2010).

A. Hatef and M. Singh, “Decay of a quantum dot in two-dimensional metallic photonic crystals” Optics Communications 284, 2363-2369, (2011).

M. R. Singh, D. G. Schindel, and **Ali Hatef**, “The study of exciton-plasmon coupling in a quantum dot and metallic nanowire hybrid system”, Applied Physics Letters- L11-08696, (accepted 10/2011).

A. Hatef, S. M. Sadeghi and M. Singh, “Plasmonic electromagnetically induced transparency in metallic nanoparticle-quantum dot hybrid systems”, Nanotechnology-NANO/403136/PAP, (Accepted 12/2011).